

Transparent boundary condition and its effectively local approximation for the Schrödinger equation on a rectangular computational domain

Samardhi Yadav^a, Vishal Vaibhav^{a,b}

^aDepartment of Physics, Indian Institute of Technology Delhi, Hauz Khas, New Delhi-110016, India

^bOptics and Photonics Center, Indian Institute of Technology Delhi, Hauz Khas, New Delhi-110016, India

Abstract

The transparent boundary condition for the free Schrödinger equation on a rectangular computational domain requires implementation of an operator of the form $\sqrt{\partial_t - i\Delta_\Gamma}$ where Δ_Γ is the Laplace-Beltrami operator. It is known that this operator is nonlocal in time as well as space which poses a significant challenge in developing an efficient numerical method of solution. The computational complexity of the existing methods scale with the number of time-steps which can be attributed to the nonlocal nature of the boundary operator. In this work, we report an effectively local approximation for the boundary operator such that the resulting complexity remains independent of number of time-steps. At the heart of this algorithm is a Padé approximant based rational approximation of certain fractional operators that handles corners of the domain adequately. For the spatial discretization, we use a Legendre-Galerkin spectral method with a new boundary adapted basis which ensures that the resulting linear system is banded. A compatible boundary-lifting procedure is also presented which accommodates the segments as well as the corners on the boundary. The proposed novel scheme can be implemented within the framework of any one-step time marching schemes. In particular, we demonstrate these ideas for two one-step methods, namely, the backward-differentiation formula of order 1 (BDF1) and the trapezoidal rule (TR). For the sake of comparison, we also present a convolution quadrature based scheme conforming to the one-step methods which is computationally expensive but serves as a golden standard. Finally, several numerical tests are presented to demonstrate the effectiveness of our novel method as well as to verify the order of convergence empirically.

Keywords: Transparent Boundary Conditions, Two-dimensional Schrödinger equation, Legendre-Galerkin Spectral Method, Convolution-Quadrature, Padé Approximants

Contents

1	Introduction	2
2	Transparent Boundary Conditions	4
2.1	Fractional operator based approach	6
2.1.1	Corner conditions	8
2.2	Novel-Padé based approach	9
2.2.1	Corner conditions	11
2.3	Difficulty with conventional Padé based approach	12
3	Numerical Implementation	13
3.1	Discretizing the boundary conditions	13
3.1.1	CQ-BDF1	14
3.1.2	CQ-TR	16

Email addresses: Samardhi@physics.iitd.ac.in (Samardhi Yadav), vishal.vaibhav@gmail.com (Vishal Vaibhav)

3.1.3	NP-BDF1	17
3.1.4	NP-TR	20
3.2	Numerical solution of the IBVP	23
3.2.1	Linear system: 1D	23
3.2.2	Linear system: 2D	26
3.3	Algorithmic summary	30
3.3.1	CQ-BDF1	30
3.3.2	NP-BDF1	32
4	Numerical Experiments	33
4.1	Exact solutions	33
4.1.1	Chirped-Gaussian profile	34
4.1.2	Hermite-Gaussian profile	34
4.2	Tests for DtN maps	38
4.3	Tests for evolution error	41
4.4	Tests for convergence	44
5	Conclusion	45
Appendix A	Fractional Operators	51
Appendix B	Boundary Adapted Basis Representation: Useful Results and Identities	51

Notations

The set of non-zero positive real numbers (\mathbb{R}) is denoted by \mathbb{R}_+ . For any complex number ζ , $\text{Re}(\zeta)$ and $\text{Im}(\zeta)$ refer to the real and the imaginary parts of ζ , respectively. The open interval $(-1, 1)$ is denoted by \mathbb{I} .

1. Introduction

This paper is devoted to the numerical solution of the two-dimensional free Schrödinger equation. The free Schrödinger equation and its various generalizations are of significant physical interest because they appear in many areas of application such as quantum mechanics, propagation of electromagnetic waves under paraxial approximation (or slow varying envelope approximation for pulse propagation in optical fibers) [1] and parabolic approximation to one-way propagation equation in underwater acoustics [2].

The initial value problem (IVP) corresponding to the free Schrödinger equation formulated on \mathbb{R}^2 reads as

$$i\partial_t u + \Delta u = 0, \quad (\mathbf{x}, t) \in \mathbb{R}^2 \times \mathbb{R}_+, \quad (1)$$

where the initial condition $u(\mathbf{x}, 0) = u_0(\mathbf{x})$ is assumed to be compactly supported. In order to ensure the uniqueness of the solution, a Sommerfeld-like radiation condition at infinity is imposed [3]. For the numerical solution of this problem, we first need to choose a bounded computational domain, denoted by Ω_i , such that $\text{supp } u_0(\mathbf{x}) \subset \Omega_i$. The next step is to determine appropriate boundary condition at the fictitious boundary ($\partial\Omega_i$) such that the solution of the resulting initial-boundary value problem (IBVP) on Ω_i remains identical to that of original problem which is formulated on an unbounded domain. Such boundary conditions are known as the *transparent boundary conditions* (TBCs) which usually appear as *Dirichlet-to-Neumann* (DtN) or *Neumann-to-Dirichlet* (NtD) maps at the fictitious boundary [3]. In cases where it is possible to obtain these maps in a closed form, they turn out to be nonlocal with respect to space as well as time. The specific form of the transparent or nonreflecting boundary maps depend on the nature of the computational domain chosen. For practical reasons, the rectangular domain happens to be a natural choice for the computational domain. In this work, we address the challenges involved in choosing Ω_i to be a rectangular domain for which an exact nonreflecting boundary condition is known at a continuous level [4, 5]. In particular, we address the problem of designing a numerical scheme which provides a viable trade-off between

computational complexity and accuracy when it comes to dealing with the nonlocal boundary maps at a discrete level. At the outset, let us state that the new algorithm presented in this work circumvents the need to store the entire history of the field on the boundary $\partial\Omega_i$ unlike the existing methods [4] such that the overall complexity turns out to be dominated by that of the linear solver for the interior problem. This effective localization of the DtN maps rely on a *novel* Padé approximant based approach that handles the corners adequately.

Several authors have contributed towards the formulation of exact TBCs for the two-dimensional Schrödinger equation [4–10]. Exact TBCs for the free Schrödinger equation on convex domains with smooth boundary was provided by Schädle [8] in terms of a single and a double layer potential. Han and Huang [9] provided the exact TBCs in terms of Hankel functions for the circular domain. Antoine *et al.* provided asymptotic approximations of a microdifferential TBC for the case of linear Schrödinger equation in \mathbb{R}^2 [11]. Szeftel developed absorbing boundary conditions and showed well posedness of the overall IBVP for the linear Schrödinger equation on convex domains with smooth boundary in \mathbb{R}^d [12]. For more general cases including the nonlinear Schrödinger equation on convex domains, Antoine *et al.* proposed some higher-order absorbing boundary conditions with the use of pseudo-differential operators [13, 14]. The transparent boundary operator for the Schrödinger equation on a rectangular domain has the form $\sqrt{\partial_t - i\Delta_\Gamma}$ where Δ_Γ is the Laplace-Beltrami operator. Note that these operators are nonlocal, both in time as well as space. To the best of our knowledge, an integral representation of this operator first appeared in [6] and more recently derived in [5, 15]. The earliest numerical implementation for the operator $\sqrt{\partial_t - i\Delta_\Gamma}$ was given by Menza [7] who introduced a Padé approximant based rational approximation for the complex square root function to obtain effectively local boundary conditions. However, this method did not address the problems arising at the corners of the rectangular domain properly¹. This issue was first resolved by Feschenko and Popov [4] who derived the exact TBCs for the two-dimensional Schrödinger equation on a rectangular domain by introducing an auxiliary function which satisfies a one-dimensional Schrödinger equation along the boundary. As elaborated in the work of the second author [5], the boundary conditions obtained by Feschenko and Popov can be directly obtained from the operator $\sqrt{\partial_t - i\Delta_\Gamma}$ by reducing it to the time-fractional operator $\sqrt{\partial_t}$ acting on an auxiliary function with the aforementioned properties. The corners are handled by imposing the TBCs for the one dimensional Schrödinger equation at the end points of the segment under consideration. Observe that the nonlocality in space is reduced to solving one-dimensional Schrödinger equations along the boundary segments of the rectangular computational domain but the nonlocality with respect to the temporal variable still poses a serious challenge. The numerical approach presented by Feschenko and Popov becomes computationally expensive on account of the increasing number of linear systems to be solved on the boundary segments with increasing time-steps². The storage requirements also scale linearly with the number of time-steps which makes it a formidable task to carryout the numerical solution with smaller temporal grid parameters (assuming a fixed duration of time).

To remedy this problem, we introduce an effectively local form of these TBCs by inserting a Padé approximant based rational approximation for $\sqrt{\partial_t}$ operator acting on the auxiliary function. The resulting numerical scheme is referred to as the *novel-Padé* (NP) method to contrast it with Padé approximant based approach given by Menza [7]. Let us further emphasize that Menza’s method involved writing an effectively local form for the full transparent boundary operator ($\sqrt{\partial_t - i\Delta_\Gamma}$) via rational approximation as opposed to the temporal fractional operator $\sqrt{\partial_t}$. The NP method ensures that the computational cost and the memory requirement does not grow with increasing time-steps. At the discrete level, the TBCs are formulated as a Robin-type boundary condition at each time-step. For the spatial discretization, we use a Legendre-Galerkin spectral method where we develop a new basis, referred to as the boundary adapted basis [16], in terms of the Legendre polynomials which ensures that the resulting linear system within the framework of Galerkin method is sparse. This approach, however, requires a boundary-lifting procedure in order to homogenize the Robin-type boundary conditions. To demonstrate the effectiveness of our method, we first provide a convolution quadrature (CQ) [17] based implementation of the time-fractional operator $\sqrt{\partial_t}$ followed by the NP method. It must be noted that the former scheme is nonlocal and suffers from the same problems as that of Feschenko and Popov [4] (where the quadrature weights are derived according to [18]) while the latter is effectively local. Further, the CQ scheme considered in this paper ensures that the time-discretization of the interior problem

¹We discuss these issues in Sec. 2.3 of this paper

²The authors in [4] suggested truncating the history of the field at the boundary in the discrete convolution in order to reduce the complexity, however, no estimates for the effective depth of history are available in their work. We have deferred these considerations in this manuscript because such a proposal needs to be first evaluated for the 1D problem before attempting the 2D problem.

remains compatible with that of the boundary conditions unlike that of [18] which was found to suffer from stability issues [19].

Before we conclude this section, we would like to contrast our method with that of perfectly matched layers (PMLs) which introduces an additional layer of finite-thickness outside Ω_i . The method of PMLs introduces inhomogeneous terms which correspond to the spatial derivatives in the PDEs [20, 21]. Therefore, within the spectral-Galerkin method, the resulting linear system necessarily becomes dense. In contrast, our method leads to a banded linear system with TBCs imposed on $\partial\Omega_i$. A thorough comparison with the method of PMLs would require consideration of more general PDEs (such as presence of variable potentials etc.) where spectral methods do not offer any competitive advantage (in the realm of non-iterative solvers). Therefore, this consideration is beyond the scope of this paper. However, let us remark that our numerical scheme will remain competitive with that of PMLs if the TBCs considered in this paper continue to hold for the general system. This conclusion is based on the observation that the one-dimensional Schrödinger equations on the boundary segments have constant coefficients leading to banded linear systems whose cost of computation is significantly smaller than that of the interior problem.

The paper is organized in the following manner: Sec. 2 presents the derivation of TBCs followed by a discussion of numerically tractable forms of the TBCs. This section also addresses the development of corner conditions whose discrete form is useful in developing boundary adapted basis. In Sec. 3, we discuss the time-discretization of TBCs and the numerical solution of the IBVP using Legendre-Galerkin method along a step-by-step analysis of the computational complexity. We confirm the efficiency and stability of our numerical schemes with several numerical tests presented in Sec. 4. Finally, we conclude this paper in Sec. 5.

2. Transparent Boundary Conditions

Consider a rectangular computational domain (Ω_i) with boundary segments parallel to one of the axes (see Fig. 1) with $\Omega_i = (x_l, x_r) \times (x_b, x_t)$ referred to as the *interior* domain. Consider the decomposition of the field $u(\mathbf{x}, t)$ such that $u(\mathbf{x}, t) \in L^2(\mathbb{R}^2) = L^2(\Omega_i) \oplus L^2(\Omega_e)$ where $\Omega_e = \mathbb{R}^2 \setminus \bar{\Omega}_i$ is referred to as the *exterior* domain. An equivalent formulation of the IVP in (1) can be stated as

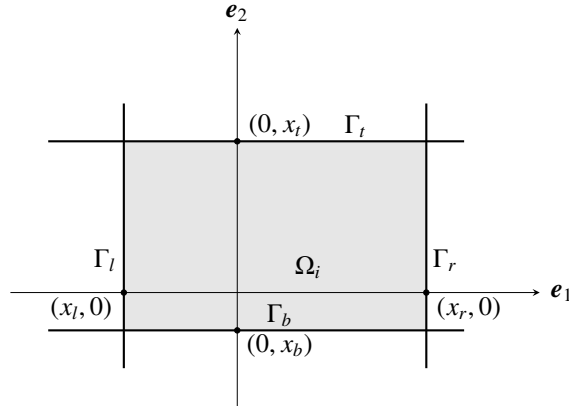


Figure 1: The figure shows a rectangular domain with boundary segments parallel to one of the axes.

$$\begin{aligned}
 \text{interior problem : } & \begin{cases} i\partial_t v + \Delta v = 0, & (\mathbf{x}, t) \in \Omega_i \times \mathbb{R}_+, \\ v(\mathbf{x}, 0) = u_0(\mathbf{x}), & (\mathbf{x}, t) \in \Omega_i, \end{cases} \\
 \text{exterior problem : } & \begin{cases} i\partial_t w + \Delta w = 0, & (\mathbf{x}, t) \in \Omega_e \times \mathbb{R}_+, \\ w(\mathbf{x}, 0) = 0, & \mathbf{x} \in \Omega_e, \\ \lim_{|\mathbf{x}| \rightarrow \infty} \sqrt{|\mathbf{x}|} \left(\nabla w \cdot \frac{\mathbf{x}}{|\mathbf{x}|} + e^{-i\frac{\pi}{4}} \partial_t^{1/2} w \right) = 0; \end{cases} \quad (2) \\
 \text{continuity relations : } & v(\mathbf{x}, t)|_{\Gamma} = w(\mathbf{x}, t)|_{\Gamma}, \quad \partial_n v(\mathbf{x}, t)|_{\Gamma} = \partial_n w(\mathbf{x}, t)|_{\Gamma},
 \end{aligned}$$

where Γ denotes the common boundary of the interior and the exterior domains. Note that the initial data $v(\mathbf{x}, 0) = u_0(\mathbf{x})$ is assumed to be compactly supported³ such that $\text{supp } u_0(\mathbf{x}) \subset \Omega_i$. For the sake of completeness, we would like to present a detailed discussion of the derivation of the TBCs first presented in [5]. To this end, let (ζ_1, ζ_2) be the covariables corresponding to (x_1, x_2) to be used in the two dimensional Fourier transform. Let us denote the one dimensional Fourier transform of $w(x_1, x_2, t)$ with respect to x_2 by $\widetilde{w}(x_1, \zeta_2, t)$:

$$\widetilde{w}(x_1, \zeta_2, t) = \mathcal{F}_{x_2}[w(x_1, x_2, t)] \equiv \int_{\mathbb{R}} w(x_1, x_2, t) e^{-i\zeta_2 x_2} dx_2.$$

Let us denote the Laplace transform of $\widetilde{w}(x_1, \zeta_2, t)$ with respect to t by $\widetilde{W}(x_1, \zeta_2, z)$:

$$\widetilde{W}(x_1, \zeta_2, z) = \mathcal{L}_t[\widetilde{w}(x_1, \zeta_2, t)] \equiv \int_{\mathbb{R}_+} \widetilde{w}(x_1, \zeta_2, t) e^{-zt} dt.$$

First we focus on deriving the TBCs on the segment Γ_r by employing the Fourier transform with respect to x_2 and then taking the Laplace transform of the right exterior problem:

$$(\partial_{x_1}^2 + \alpha^2) \widetilde{W}(x_1, \zeta_2, z) = 0, \quad x_1 \in (x_r, \infty), \quad (3)$$

where $\alpha = \sqrt{iz - \zeta_2^2}$ such that $\sqrt{\cdot}$ denotes the branch with $\text{Im}(\alpha) > 0$. The solution takes the form

$$\widetilde{W}(x_1, \zeta_2, z) = c \exp(+i\alpha x_1) + d \exp(-i\alpha x_1), \quad (4)$$

where c and d are independent of x_1 . In order to have a bounded solution on the right exterior domain, d must be zero. Further, c can be eliminated using the derivative of the field to obtain

$$\partial_{x_1} \widetilde{W}(x_1, \zeta_2, z) = i\alpha \widetilde{W}(x_1, \zeta_2, z). \quad (5)$$

To facilitate the inverse Laplace transform of the equation above, we proceed as follows:

$$\partial_{x_1} \widetilde{w}(x_1, \zeta_2, t) = \mathcal{L}^{-1}[\partial_{x_1} \widetilde{W}(x_1, \zeta_2, z)] = \mathcal{L}^{-1}[i\alpha^{-1}] \star \mathcal{L}^{-1}[\alpha^2 \widetilde{W}(x_1, \zeta_2, z)], \quad (6)$$

where ‘ \star ’ represents the convolution operation with respect t . Let us observe that $\mathcal{L}^{-1}\left[1/\sqrt{z}\right](t) = H(t)/\sqrt{\pi t}$ where $H(t)$ denotes the Heaviside step-function. In the following, we use the fractional operators which are denoted by ∂_t^α , $\alpha \in \mathbb{R}$ (see Miller and Ross [22]). For $\alpha < 0$, we obtain the Riemann-Liouville fractional integral of order $|\alpha|$ while $\alpha > 0$ corresponds to fractional derivatives which are introduced as integral order derivatives of fractional integrals (discussed in Appendix A). Using the shifting property of Laplace transforms and introducing fractional operators of order $1/2$, we can express the result as

$$\partial_{x_1} \widetilde{w}(x_1, \zeta_2, t) = e^{i\pi/4} e^{-i\zeta_2^2 t} \partial_t^{-1/2} e^{i\zeta_2^2 t} \left[i \partial_t \widetilde{w}(x_1, \zeta_2, t) - \zeta_2^2 \widetilde{w}(x_1, \zeta_2, t) \right]. \quad (7)$$

In order to obtain the inverse Fourier transform of the above relations, let us introduce the kernel

$$\mathcal{G}(x_2, t) = \frac{e^{-i\pi/4}}{\sqrt{4\pi t}} \exp\left[i\frac{x_2^2}{4t}\right], \quad (8)$$

defined in a distributional sense with its Fourier transform given by $\widetilde{\mathcal{G}}(\zeta_2, t) = e^{-i\zeta_2^2 t}$. Introducing the integral definition for $1/2$ -order fractional integral and taking inverse Fourier transform of (7) yields

$$\partial_{x_1} w(\mathbf{x}, t) = \frac{e^{i\pi/4}}{\sqrt{\pi}} \int_0^t \int_{\mathbb{R}} \left[i \partial_\tau w(x_1, x'_2, \tau) + \partial_{x'_2}^2 w(x_1, x'_2, \tau) \right] \frac{\mathcal{G}(x_2 - x'_2, t - \tau)}{\sqrt{t - \tau}} dx'_2 d\tau. \quad (9)$$

³This criteria can not be relaxed for our novel Padé approach.

The relationship above is referred to as the *Dirichlet-to-Neumann* (DtN) map relating the Dirichlet data $w(x_1, x_2, t)$ to the Neumann data $\partial_{x_1} w(\mathbf{x}, t)$ on the right segment. Using the following result from calculus of fractional operators

$$\partial_t \left[e^{-i\zeta_2^2 t} \partial_t^{-1/2} e^{i\zeta_2^2 t} \widetilde{w}(x_1, \zeta_2, t) \right] = e^{-i\zeta_2^2 t} \partial_t^{-1/2} e^{i\zeta_2^2 t} \partial_t \widetilde{w}(x_1, \zeta_2, t), \quad (10)$$

we can recast (9) by taking out the operators from square bracketed term as

$$\partial_{x_1} w(\mathbf{x}, t) = -(\partial_t - i\partial_{x_2}^2) \frac{e^{-i\pi/4}}{\sqrt{\pi}} \int_0^t \int_{\mathbb{R}} w(x_1, x'_2, \tau) \frac{\mathcal{G}(x_2 - x'_2, t - \tau)}{\sqrt{t - \tau}} dx'_2 d\tau. \quad (11)$$

In order to express the DtN map compactly, we introduce the notation

$$(\partial_t - i\partial_{x_2}^2)^{-1/2} f(x_2, t) = \frac{1}{\sqrt{\pi}} \int_0^t \int_{\mathbb{R}} f(x'_2, \tau) \frac{\mathcal{G}(x_2 - x'_2, t - \tau)}{\sqrt{t - \tau}} dx'_2 d\tau. \quad (12)$$

so that

$$(\partial_t - i\partial_{x_2}^2)[(\partial_t - i\partial_{x_2}^2)^{-1/2} f] = (\partial_t - i\partial_{x_2}^2)^{1/2} f.$$

Next, invoking the continuity relations defined in (2), the DtN map on the segment Γ_r can now be expressed in the compact form as

$$\partial_{x_1} v(\mathbf{x}, t) + e^{-i\pi/4} (\partial_t - i\partial_{x_2}^2)^{1/2} v(\mathbf{x}, t) = 0. \quad (13)$$

One can obtain the transparent boundary conditions for the rest of the boundary segments of the domain Ω_i in a similar fashion which yields the following equivalent formulation of the IVP corresponding to (1) on the computational domain Ω_i :

$$\begin{cases} i\partial_t u + \Delta u = 0, & (\mathbf{x}, t) \in \Omega_i \times \mathbb{R}_+, \\ u(\mathbf{x}, 0) = u_0(\mathbf{x}) \in L^2(\Omega_i), & \text{supp } u_0 \subset \Omega_i, \\ \partial_n u + e^{-i\pi/4} (\partial_t - i\partial_{x_2}^2)^{1/2} u = 0, & \mathbf{x} \in \Gamma_l \cup \Gamma_r, t > 0, \\ \partial_n u + e^{-i\pi/4} (\partial_t - i\partial_{x_1}^2)^{1/2} u = 0, & \mathbf{x} \in \Gamma_b \cup \Gamma_t, t > 0. \end{cases} \quad (14)$$

Note that the operators present in the DtN maps are non-local both in space and time. For the numerical solution of this IBVP, a suitable numerical implementation needs to be developed. Before we address the numerical aspects, we develop a suitable representation for these operators at the continuous level that is compatible with the rectangular domain. The earliest approach was due to Menza [7] which is discussed in Sec. 2.3. This approach is based on Padé approximant for the square root function, however, the treatment at the corners is inexact. A more recent approach was presented by Feshchenko and Popov [4] who developed a representation in terms of fractional operators. We discuss this approach in Sec. 2.1 where we adopt a more direct way to arrive at the results as presented by the second author [5]. Finally, we present one of the main contributions of this paper in Sec. 2.2 where a novel Padé based approach is described that is capable of handling the corners of the domain in a natural manner.

2.1. Fractional operator based approach

In this section, we focus on expressing the DtN maps in terms of (time-)fractional operators. To this end, let us recall the form of the DtN map given by (7) in terms of the Fourier variables so that

$$\begin{aligned} \partial_{x_1} \widetilde{w}(x_1, \zeta_2, t) &= e^{i\pi/4} e^{-i\zeta_2^2 t} \partial_t^{-1/2} e^{i\zeta_2^2 t} \left[i\partial_t \widetilde{w}(x_1, \zeta_2, t) - \zeta_2^2 \widetilde{w}(x_1, \zeta_2, t) \right] = i e^{i\pi/4} e^{-i\zeta_2^2 t} \partial_t^{1/2} e^{i\zeta_2^2 t} \widetilde{w}(x_1, \zeta_2, t) \\ &= -e^{-i\pi/4} \partial_{t'}^{1/2} e^{-i\zeta_2^2 (t-t')} \widetilde{w}(x_1, \zeta_2, t') \Big|_{t'=t}. \end{aligned} \quad (15)$$

where the last step uses the composition rule for fractional operators. Introducing the auxiliary function $\varphi(x_1, x_2, \tau_1, \tau_2)$ such that

$$\mathcal{F}_{x_2}[\varphi](x_1, x_2, \tau_1, \tau_2) = e^{-i\zeta_2^2 (\tau_2 - \tau_1)} \widetilde{w}(x_1, \zeta_2, \tau_1), \quad (16)$$

we can express the DtN map on the segment Γ_r as:

$$\partial_{x_1} w(x_1, x_2, t) = -e^{-i\pi/4} \partial_{\tau_1}^{1/2} \varphi(x_1, x_2, \tau_1, \tau_2) \Big|_{\tau_1 = \tau_2 = t}. \quad (17)$$

Numerical implementation of this fractional derivative requires the history of the auxiliary function from the start of the computations. In order to compute the history, we introduce ⁴ an IVP for the auxiliary function $\varphi(x_1, x_2, \tau_1, \tau_2)$ by observing the condition in (16):

$$[i\partial_{\tau_2} + \partial_{x_2}^2]\varphi(x_1, x_2, \tau_1, \tau_2) = 0, \quad \tau_2 \in (\tau_1, t], \quad x_1 = x_r, \quad (18)$$

where the diagonal values $\varphi(x_1, x_2, \tau_1, \tau_1) = w(x_1, x_2, \tau_1)$ serve as the initial condition. Note that the history is needed for all $\tau_1 \in [0, t]$ which means that we must solve the IVP for all $\tau_1 \in [0, t]$ over Γ_r . It is interesting to note that the IVP satisfied by the auxiliary function on the segment Γ_r turns out to be a one-dimensional Schrödinger equation. The exact boundary conditions are well-known for this equation when the initial data is compactly supported. The formulation of the TBCs for the IVP (18) requires us to first understand the support (with respect to x_2) of the auxiliary function on the segment Γ_r at $\tau_2 = 0$. From the knowledge of the compact support of the initial field $u_0(\mathbf{x})$, we can establish the support of the auxiliary function at $\tau_2 = 0$. Let $\widetilde{u}_0(\boldsymbol{\zeta}) = \mathcal{F}_{(x_1, x_2)} u_0(\mathbf{x})$, then taking the Fourier transform of the IVP defined by (1), we obtain

$$\partial_t \widetilde{u}(\boldsymbol{\zeta}) + i(\zeta_1^2 + \zeta_2^2) \widetilde{u}(\boldsymbol{\zeta}) = 0. \quad (19)$$

Taking into account the initial condition, the solution to this IVP becomes $\widetilde{u}(\boldsymbol{\zeta}, t) = e^{-i(\zeta_1^2 + \zeta_2^2)t} \widetilde{u}_0(\boldsymbol{\zeta})$ which yields

$$\begin{aligned} \mathcal{F}_{x_1, x_2}[\varphi](x_1, x_2, \tau_1, \tau_2) &= e^{-i\zeta_2^2(\tau_2 - \tau_1)} \widetilde{u}(\zeta_1, \zeta_2, \tau_1) = e^{-i\zeta_2^2(\tau_2 - \tau_1)} e^{-i(\zeta_1^2 + \zeta_2^2)\tau_1} \widetilde{u}_0(\boldsymbol{\zeta}), \\ \varphi(x_1, x_2, \tau_1, \tau_2) &= \frac{1}{(2\pi)^2} \int_{\mathbb{R}^2} e^{i\boldsymbol{\zeta} \cdot \mathbf{x} - i\zeta_1^2 \tau_1 - i\zeta_2^2 \tau_2} \widetilde{u}_0(\boldsymbol{\zeta}) d^2 \boldsymbol{\zeta}. \end{aligned} \quad (20)$$

From the definition of the auxiliary function written above as inverse Fourier transform consisting of $\widetilde{u}_0(\boldsymbol{\zeta})$, we can establish that the $\text{supp}_{x_2} \varphi(x_r, x_2, \tau_1, 0) \subset [x_b, x_r]$ by considering the support of the initial field at $\tau_2 = 0$. It is straightforward to see that the auxiliary function also satisfies the IVP

$$[i\partial_{\tau_1} + \partial_{x_1}^2]\varphi(x_1, x_2, \tau_1, \tau_2) = 0, \quad \tau_1 \in (\tau_2, t], \quad (21)$$

where diagonal values $\varphi(x_1, x_2, \tau_2, \tau_2) = w(x_1, x_2, \tau_2)$ serves as the initial condition. Note that we solve the IVP for all $\tau_2 \in [0, t]$. The transparent boundary condition at the end points of the segment Γ_r becomes:

$$\partial_{x_2} \varphi(x_1, x_2, \tau_1, \tau_2) \pm e^{-i\pi/4} \partial_{\tau_2}^{1/2} \varphi(x_1, x_2, \tau_1, \tau_2) = 0, \quad (22)$$

where the sign is determined by $x_2 \in \{x_r, x_b\}$, respectively. Note that the fractional derivative ($\partial_{\tau_2}^{1/2}$) requires the knowledge of $\varphi(x_1, x_2, \tau_1, \tau_2)$ at the end points of Γ_r from the start of the computation. The DtN map in terms of a time-fractional derivative operator for the IVP (14) can be expressed as

$$\begin{aligned} \partial_{x_1} u(\mathbf{x}, t) &= -e^{-i\pi/4} \partial_{\tau_1}^{1/2} \varphi(x_1, x_2, \tau_1, \tau_2) \Big|_{\tau_1, \tau_2=t}, \quad (x_1, x_2) \in \Gamma_r, \\ \partial_{x_1} u(\mathbf{x}, t) &= +e^{-i\pi/4} \partial_{\tau_1}^{1/2} \varphi(x_1, x_2, \tau_1, \tau_2) \Big|_{\tau_1, \tau_2=t}, \quad (x_1, x_2) \in \Gamma_l, \\ \partial_{x_2} u(\mathbf{x}, t) &= -e^{-i\pi/4} \partial_{\tau_2}^{1/2} \varphi(x_1, x_2, \tau_1, \tau_2) \Big|_{\tau_1, \tau_2=t}, \quad (x_1, x_2) \in \Gamma_t, \\ \partial_{x_2} u(\mathbf{x}, t) &= +e^{-i\pi/4} \partial_{\tau_2}^{1/2} \varphi(x_1, x_2, \tau_1, \tau_2) \Big|_{\tau_1, \tau_2=t}, \quad (x_1, x_2) \in \Gamma_b. \end{aligned} \quad (23)$$

The IVPs for the auxiliary function are summarised below

$$\begin{aligned} [i\partial_{\tau_1} + \partial_{x_1}^2]\varphi(x_1, x_2, \tau_1, \tau_2) &= 0, \quad (x_1, x_2) \in \Gamma_t \cup \Gamma_b, \quad \tau_1 \in (\tau_2, t], \\ [i\partial_{\tau_2} + \partial_{x_2}^2]\varphi(x_1, x_2, \tau_1, \tau_2) &= 0, \quad (x_1, x_2) \in \Gamma_l \cup \Gamma_r, \quad \tau_2 \in (\tau_1, t]. \end{aligned} \quad (24)$$

⁴The idea of introducing an ODE with a solution satisfying the condition instead of writing the condition itself first appeared in the work of Feschenko and Popov [4] and later in [23].

Let us introduce the set of corner points of the computational domain as $\{\Gamma_{rt}, \Gamma_{rb}, \Gamma_{lt}, \Gamma_{lb}\}$ where $\Gamma_{ij} = \Gamma_i \cap \Gamma_j$ with $i, j \in \{r, t, l, b\}$. The transparent boundary conditions at corner points for the IVPs listed in (24) are as follows

$$\begin{aligned} \partial_{x_1} \varphi(x_1, x_2, \tau_1, \tau_2) + e^{-i\pi/4} \partial_{\tau_1}^{1/2} \varphi(x_1, x_2, \tau_1, \tau_2) &= 0, & (x_1, x_2) \in \{\Gamma_{rt}, \Gamma_{rb}\}, \\ \partial_{x_1} \varphi(x_1, x_2, \tau_1, \tau_2) - e^{-i\pi/4} \partial_{\tau_1}^{1/2} \varphi(x_1, x_2, \tau_1, \tau_2) &= 0, & (x_1, x_2) \in \{\Gamma_{lt}, \Gamma_{lb}\}, \\ \partial_{x_2} \varphi(x_1, x_2, \tau_1, \tau_2) + e^{-i\pi/4} \partial_{\tau_2}^{1/2} \varphi(x_1, x_2, \tau_1, \tau_2) &= 0, & (x_1, x_2) \in \{\Gamma_{rt}, \Gamma_{lt}\}, \\ \partial_{x_2} \varphi(x_1, x_2, \tau_1, \tau_2) - e^{-i\pi/4} \partial_{\tau_2}^{1/2} \varphi(x_1, x_2, \tau_1, \tau_2) &= 0. & (x_1, x_2) \in \{\Gamma_{rb}, \Gamma_{lb}\}, \end{aligned} \quad (25)$$

The history required for the fractional derivatives present in the DtN maps can be understood with the help of the schematic shown in Fig. 2. The two IVPs for the auxiliary field $\varphi(x_1, x_2, \tau_1, \tau_2)$ advances the field either above or below the diagonal in the (τ_1, τ_2) -plane starting from the diagonal which also serves as initial conditions for solving IVPs. This is depicted by filled circles where arrows denote the direction of evolution. The TBCs present in (25) to solve the IVPs for the auxiliary functions on the boundary segments require the history of the auxiliary function at corners from the start of the computations which makes the empty circles relevant. Note that these values at the corners can be taken from the adjacent segment of the boundary where it is already being computed. This is depicted by broken lines in Fig. 2.

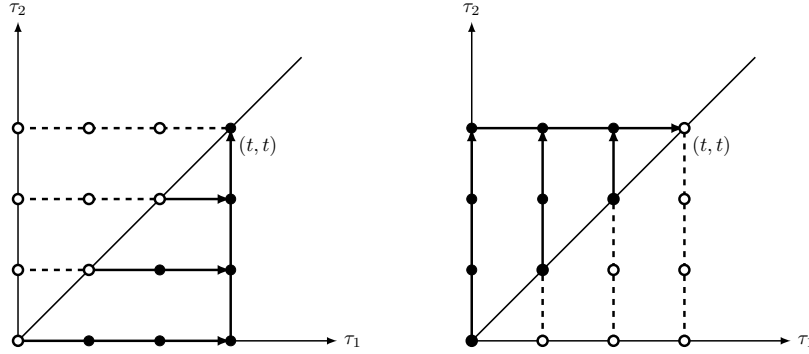


Figure 2: A schematic depiction of the evolution of the auxiliary field $\varphi(x_1, x_2, \tau_1, \tau_2)$ in the (τ_1, τ_2) -plane is provided in this figure where the plot on the right corresponds $\mathbf{x} \in \Gamma_r \cup \Gamma_l$ and the plot on the left corresponds $\mathbf{x} \in \Gamma_t \cup \Gamma_b$. The filled circles depict the evolution of the auxiliary field $\varphi(x_1, x_2, \tau_1, \tau_2)$ either above or below the diagonal in the (τ_1, τ_2) -plane starting from the diagonal which also serves as initial conditions for solving IVPs corresponding to the auxiliary function. The TBCs for the auxiliary field require the history of the auxiliary field at the corner points which makes empty circles relevant. Note that these values at the corners can be taken from the adjacent segment of the boundary where it is already being computed and this is depicted by broken lines. Note that the vertical/horizontal lines where the arrows end corresponds to the history of the auxiliary field needed for the TBCs on $\partial\Omega_i$ in the current time (t).

2.1.1. Corner conditions

Having discussed the boundary conditions satisfied by the field on the four segments of the computational domain (Ω_i) as stated in (23), we turn to the constraints on the field at the corners ($\{\Gamma_{rt}, \Gamma_{rb}, \Gamma_{lt}, \Gamma_{lb}\}$) which will be used later for solving the IBVP in (14) with a Galerkin method. Let us understand this by considering the corner Γ_{rt} and recall the DtN map over segment Γ_r from (23)

$$\partial_{x_1} u(x_1, x_2, t) = -e^{-i\pi/4} \partial_{\tau_1}^{1/2} \varphi(x_1, x_2, \tau_1, \tau_2) \Big|_{\tau_1=\tau_2=t}.$$

Applying ∂_{x_2} to obtain the additional constraints on the field at corners, we have

$$\partial_{x_2} \partial_{x_1} u(x_1, x_2, t) = -e^{-i\pi/4} \partial_{\tau_1}^{1/2} \partial_{x_2} \varphi(x_1, x_2, \tau_1, \tau_2) \Big|_{\tau_1=\tau_2=t}.$$

Now, plugging-in the value of $\partial_{x_2} \varphi(x_1, x_2, \tau_1, \tau_2)$ from (25) at the corner point Γ_{rt} , we obtain the following corner condition

$$\partial_{x_1} \partial_{x_2} u(x_1, x_2, t) = e^{-i\pi/4} e^{-i\pi/4} \partial_{\tau_1}^{1/2} \partial_{\tau_2}^{1/2} \varphi(x_1, x_2, \tau_1, \tau_2) \Big|_{\tau_1=\tau_2=t}. \quad (26)$$

2.2. Novel-Padé based approach

In this section, we would like to explore the Padé approximant based representation for the 1/2-order temporal derivative in (23) and its other ramifications. It is well-known that a rational approximation to the square-root function would allow one to obtain an effectively local approximation for the fractional derivative operator. We contrast this with the situation where the history grows with each time-step making it expensive computationally as well as from a storage point of view.

The diagonal Padé approximants for $\sqrt{1-z}$, with negative real axis as the branch-cut, can be used to obtain rational approximation $R_M(z)$ for the function \sqrt{z} as

$$R_M(z) = b_0 - \sum_{k=1}^M \frac{b_k}{z + \eta_k^2}, \quad \text{where} \quad \begin{cases} b_0 = 2M + 1, & b_k = \frac{2\eta_k^2(1 + \eta_k^2)}{2M + 1}, \\ \eta_k = \tan \theta_k, & \theta_k = \frac{k\pi}{2M + 1}, \quad k = 1, 2, \dots, M. \end{cases} \quad (27)$$

Here, the expression for the diagonal Padé approximant is taken from [24]. Let us start by introducing some compact notations for the auxiliary functions as:

$$\begin{aligned} \varphi_{a_1}(x_2, \tau_1, \tau_2) &= \varphi(x_{a_1}, x_2, \tau_1, \tau_2), & a_1 &\in \{l, r\}, \\ \varphi_{a_2}(x_1, \tau_1, \tau_2) &= \varphi(x_1, x_{a_2}, \tau_1, \tau_2), & a_2 &\in \{b, t\}. \end{aligned} \quad (28)$$

Let $z \in \mathbb{C}$, then the Laplace transform of the auxiliary function can be denoted as

$$\mathcal{L}_{\tau_1}[\varphi_{a_1}(x_2, \tau_1, \tau_2)] = \Phi_{a_1}(x_2, z, \tau_2), \quad \mathcal{L}_{\tau_2}[\varphi_{a_2}(x_1, \tau_1, \tau_2)] = \Phi_{a_2}(x_1, \tau_1, z). \quad (29)$$

The DtN maps described in (23) on the segments Γ_{a_1} and Γ_{a_2} can be restated as

$$\begin{aligned} \partial_{x_1} u(x_1, x_2, t) \pm e^{-i\pi/4} \mathcal{L}_z^{-1} \left[\sqrt{z} \Phi_{a_1}(x_2, z, \tau_2) \right] \Big|_{\tau_1=\tau_2=t} &= 0, \\ \partial_{x_2} u(x_1, x_2, t) \pm e^{-i\pi/4} \mathcal{L}_z^{-1} \left[\sqrt{z} \Phi_{a_2}(x_2, \tau_1, z) \right] \Big|_{\tau_1=\tau_2=t} &= 0. \end{aligned} \quad (30)$$

Inserting the rational approximation of order M for the function \sqrt{z} as

$$\begin{aligned} \partial_{x_1} u(x_1, x_2, t) \pm e^{-i\pi/4} \mathcal{L}_z^{-1} \left[R_M(z) \Phi_{a_1}(x_2, z, \tau_2) \right] \Big|_{\tau_1=\tau_2=t} &\approx 0, \\ \partial_{x_2} u(x_1, x_2, t) \pm e^{-i\pi/4} \mathcal{L}_z^{-1} \left[R_M(z) \Phi_{a_2}(x_2, \tau_1, z) \right] \Big|_{\tau_1=\tau_2=t} &\approx 0. \end{aligned} \quad (31)$$

The map expressed above is still nonlocal, however, the rational nature of the expression allows us to obtain an effectively local approximation for the DtN operation. Following Lindmann's approach [25], we introduce the auxiliary fields $\varphi_{k,a_1}(x_2, \tau_1, \tau_2)$ and $\varphi_{k,a_2}(x_1, \tau_1, \tau_2)$ at the boundary segments Γ_{a_1} and Γ_{a_2} , respectively, such that

$$\begin{aligned} (z + \eta_k^2)^{-1} \Phi_{a_1}(x_2, z, \tau_2) &= \Phi_{k,a_1}(x_2, z, \tau_2), \\ (z + \eta_k^2)^{-1} \Phi_{a_2}(x_1, \tau_1, z) &= \Phi_{k,a_2}(x_1, \tau_1, z), \end{aligned} \quad (32)$$

where $k = 1, 2, \dots, M$. In the physical space, every φ_{k,a_1} and φ_{k,a_2} satisfy the following ODEs:

$$\begin{aligned} (\partial_{\tau_1} + \eta_k^2) \varphi_{k,a_1}(x_2, \tau_1, \tau_2) &= \varphi_{a_1}(x_2, \tau_1, \tau_2), \\ (\partial_{\tau_2} + \eta_k^2) \varphi_{k,a_2}(x_1, \tau_1, \tau_2) &= \varphi_{a_2}(x_1, \tau_1, \tau_2), \end{aligned} \quad (33)$$

with the initial conditions assumed to be $\varphi_{k,a_1}(x_2, 0, \tau_2) = 0$ and $\varphi_{k,a_2}(x_1, \tau_1, 0) = 0$, respectively. The DtN maps for the interior problem present in (31) now reads as

$$\begin{aligned} \partial_{x_1} u(\mathbf{x}, t) \pm e^{-i\pi/4} \left[b_0 u(\mathbf{x}, t) - \sum_{k=1}^M b_k \varphi_{k,a_1}(x_2, t, t) \right] &\approx 0, \\ \partial_{x_2} u(\mathbf{x}, t) \pm e^{-i\pi/4} \left[b_0 u(\mathbf{x}, t) - \sum_{k=1}^M b_k \varphi_{k,a_2}(x_1, t, t) \right] &\approx 0. \end{aligned} \quad (34)$$

The solution to the ODEs (33) reads as

$$\begin{aligned}\varphi_{k,a_1}(x_2, \tau_1, \tau_2) &= \int_0^{\tau_1} e^{-\eta_k^2(\tau_1-s_1)} \varphi_{a_1}(x_2, s_1, \tau_2) ds_1, \quad a_1 \in \{l, r\}, \\ \varphi_{k,a_2}(x_1, \tau_1, \tau_2) &= \int_0^{\tau_2} e^{-\eta_k^2(\tau_2-s_2)} \varphi_{a_2}(x_1, \tau_1, s_2) ds_2, \quad a_2 \in \{t, b\}.\end{aligned}\tag{35}$$

It is straightforward to conclude that auxiliary fields satisfy the same IVPs which are satisfied by auxiliary functions

$$\begin{aligned}[i\partial_{\tau_2} + \partial_{x_2}^2] \varphi_{k,a_1}(x_2, \tau_1, \tau_2) &= 0, \quad (x_1, x_2) \in \Gamma_l \cup \Gamma_r, \quad \tau_2 \in (\tau_1, t], \\ [i\partial_{\tau_1} + \partial_{x_1}^2] \varphi_{k,a_2}(x_1, \tau_1, \tau_2) &= 0, \quad (x_1, x_2) \in \Gamma_t \cup \Gamma_b, \quad \tau_1 \in (\tau_2, t].\end{aligned}\tag{36}$$

The transparent boundary conditions for these IVPs can be written as:

$$\begin{aligned}\partial_{x_2} \varphi_{k,a_1}(x_b, \tau_1, \tau_2) - e^{-i\pi/4} \partial_{\tau_2}^{1/2} \varphi_{k,a_1}(x_b, \tau_1, \tau_2) &= 0, \\ \partial_{x_2} \varphi_{k,a_1}(x_t, \tau_1, \tau_2) + e^{-i\pi/4} \partial_{\tau_2}^{1/2} \varphi_{k,a_1}(x_t, \tau_1, \tau_2) &= 0, \\ \partial_{x_1} \varphi_{k,a_2}(x_l, \tau_1, \tau_2) - e^{-i\pi/4} \partial_{\tau_1}^{1/2} \varphi_{k,a_2}(x_l, \tau_1, \tau_2) &= 0, \\ \partial_{x_1} \varphi_{k,a_2}(x_r, \tau_1, \tau_2) + e^{-i\pi/4} \partial_{\tau_1}^{1/2} \varphi_{k,a_2}(x_r, \tau_1, \tau_2) &= 0.\end{aligned}\tag{37}$$

Once again, we use the Padé approximants based representation for the 1/2-order temporal derivative operator present in the TBCs for the auxiliary fields described in (37). Introducing the auxiliary fields $\psi_{k,k',a_1,a_2}(\tau_1, \tau_2)$ and $\psi_{k,k',a_2,a_1}(\tau_1, \tau_2)$ at the end points of the boundary segments Γ_{a_1} and Γ_{a_2} , respectively, such that

$$\begin{aligned}(z + \eta_{k'}^2)^{-1} \Phi_{k,a_1}(x_{a_2}, \tau_1, z) &= \Psi_{k,k',a_1,a_2}(\tau_1, z), \quad a_1 \in \{l, r\}, \\ (z + \eta_{k'}^2)^{-1} \Phi_{k,a_2}(x_{a_1}, \tau_2, z) &= \Psi_{k,k',a_2,a_1}(z, \tau_2), \quad a_2 \in \{b, t\}.\end{aligned}\tag{38}$$

In the physical space, every ψ_{k,k',a_1,a_2} and ψ_{k,k',a_2,a_1} satisfy the following ODEs:

$$\begin{aligned}(\partial_{\tau_2} + \eta_{k'}^2) \psi_{k,k',a_1,a_2}(\tau_1, \tau_2) &= \varphi_{k,a_1}(x_{a_2}, \tau_1, \tau_2), \\ (\partial_{\tau_1} + \eta_{k'}^2) \psi_{k,k',a_2,a_1}(\tau_1, \tau_2) &= \varphi_{k,a_2}(x_{a_1}, \tau_1, \tau_2),\end{aligned}\tag{39}$$

with the initial conditions assumed to be $\psi_{k,k',a_1,a_2}(\tau_1, 0) = 0$ and $\psi_{k,k',a_2,a_1}(0, \tau_2) = 0$, respectively. The DtN maps for the auxiliary fields (37) now reads as

$$\begin{aligned}\partial_{x_2} \varphi_{k,a_1}(x_{a_2}, \tau_1, \tau_2) \pm e^{-i\pi/4} \left[b_0 \varphi_{k,a_1}(x_{a_2}, \tau_1, \tau_2) - \sum_{k'=1}^M b_{k'} \psi_{k,k',a_1,a_2}(\tau_1, \tau_2) \right] &= 0, \\ \partial_{x_1} \varphi_{k,a_2}(x_{a_1}, \tau_1, \tau_2) \pm e^{-i\pi/4} \left[b_0 \varphi_{k,a_2}(x_{a_1}, \tau_1, \tau_2) - \sum_{k'=1}^M b_{k'} \psi_{k,k',a_2,a_1}(\tau_1, \tau_2) \right] &= 0.\end{aligned}\tag{40}$$

The solution to the ODEs (39) reads as

$$\begin{aligned}\psi_{k,k',a_1,a_2}(\tau_1, \tau_2) &= \int_0^{\tau_2} e^{-\eta_{k'}^2(\tau_2-s_2)} \varphi_{k,a_1}(x_{a_2}, \tau_1, s_2) ds_2, \\ \psi_{k,k',a_2,a_1}(\tau_1, \tau_2) &= \int_0^{\tau_1} e^{-\eta_{k'}^2(\tau_1-s_1)} \varphi_{k,a_2}(x_{a_1}, s_1, \tau_2) ds_1.\end{aligned}\tag{41}$$

Remark 1. It is interesting to note that fields $\psi_{k,k',a_1,a_2}(\tau_1, \tau_2)$ and $\psi_{k,k',a_2,a_1}(\tau_1, \tau_2)$ are transpose of each other. We

can verify it by inserting the value of auxiliary fields φ_{k,a_1} and φ_{k,a_2} from (35) as:

$$\begin{aligned}
\psi_{k,k',a_1,a_2}(\tau_1, \tau_2) &= \int_0^{\tau_2} e^{-\eta_{k'}^2(\tau_2-s_2)} \varphi_{k,a_1}(x_{a_2}, \tau_1, s_2) ds_2 \\
&= \int_0^{\tau_2} e^{-\eta_{k'}^2(\tau_2-s_2)} \int_0^{\tau_1} e^{-\eta_k^2(\tau_1-s_1)} \varphi(x_{a_1}, x_{a_2}, s_1, s_2) ds_1 ds_2 \\
&= \int_0^{\tau_1} e^{-\eta_k^2(\tau_1-s_1)} \int_0^{\tau_2} e^{-\eta_{k'}^2(\tau_2-s_2)} \varphi(x_{a_1}, x_{a_2}, s_1, s_2) ds_2 ds_1 \\
&= \int_0^{\tau_1} e^{-\eta_k^2(\tau_1-s_1)} \varphi_{k',a_2}(x_{a_1}, s_1, \tau_2) ds_1 = \psi_{k',k,a_2,a_1}(\tau_1, \tau_2).
\end{aligned} \tag{42}$$

This observation allows us to develop a rather efficient numerical scheme from a storage point of view.

In order to advance the auxiliary fields (ψ) from diagonal to diagonal point in (τ_1, τ_2) -plane, we need to establish the ODEs to advance the auxiliary fields in the directions orthogonal to those mentioned in (39). One can achieve that by observing

$$\begin{aligned}
[\partial_{\tau_1} + \eta_k^2] \psi_{k,k',a_1,a_2}(\tau_1, \tau_2) &= \int_0^{\tau_2} e^{-\eta_{k'}^2(\tau_2-s_2)} [\partial_{\tau_1} + \eta_k^2] \varphi_{k,a_1}(x_{a_2}, \tau_1, s_2) ds_2 \\
&= \int_0^{\tau_2} e^{-\eta_{k'}^2(\tau_2-s_2)} \varphi(x_{a_1}, x_{a_2}, \tau_1, s_2) ds_2 = \varphi_{k',a_2}(x_{a_1}, \tau_1, \tau_2), \\
[\partial_{\tau_2} + \eta_k^2] \psi_{k,k',a_2,a_1}(\tau_1, \tau_2) &= \int_0^{\tau_1} e^{-\eta_k^2(\tau_1-s_1)} [\partial_{\tau_2} + \eta_k^2] \varphi_{k,a_2}(x_{a_1}, s_1, \tau_2) ds_1 \\
&= \int_0^{\tau_1} e^{-\eta_k^2(\tau_1-s_1)} \varphi(x_{a_1}, x_{a_2}, s_1, \tau_2) ds_1 = \varphi_{k',a_1}(x_{a_1}, \tau_1, \tau_2).
\end{aligned} \tag{43}$$

These ODEs for the auxiliary fields can now be summarized as

$$\begin{aligned}
(\partial_{\tau_1} + \eta_k^2) \psi_{k,k',a_1,a_2}(\tau_1, \tau_2) &= \varphi_{k',a_2}(x_{a_1}, \tau_1, \tau_2), \\
(\partial_{\tau_2} + \eta_k^2) \psi_{k,k',a_2,a_1}(\tau_1, \tau_2) &= \varphi_{k',a_1}(x_{a_2}, \tau_1, \tau_2).
\end{aligned} \tag{44}$$

The evolution of the auxiliary fields $\varphi_{k,a_1}(x_2, \tau_1, \tau_2)$, $\varphi_{k,a_2}(x_1, \tau_1, \tau_2)$ and $\psi_{k,k',a_1,a_2}(\tau_1, \tau_2)$ in the (τ_1, τ_2) -plane can be understood with the help of the schematic shown in Fig. 3. In this schematic, Fig. 3(A) and Fig. 3(B) depict the evolution of the fields $\varphi_{k,a_2}(x_1, \tau_1, \tau_2)$ and $\varphi_{k,a_1}(x_2, \tau_1, \tau_2)$ on the boundary segments Γ_{a_2} and Γ_{a_1} , respectively. The diagonal to diagonal computation of the fields $\varphi_{k,a_1}(x_2, \tau_1, \tau_2)$ and $\varphi_{k,a_2}(x_1, \tau_1, \tau_2)$ consists of first advancing the fields using the IVPs established in (36) and then using the ODEs in (33) for the second movement. Our novel Padé approach makes the numerical scheme efficient from a storage point of view which is obvious from the schematic presented. Similarly, Fig. 3(C) depicts the evolution of the field $\psi_{k,k',a_1,a_2}(\tau_1, \tau_2)$ which can be achieved by moving either below or above the diagonal.

2.2.1. Corner conditions

With in the novel Padé approach, the constraints satisfied by the field at the corner can be obtained following a similar approach as that of the Sec. 2.1.1. Consider the corner Γ_{rt} and recall the DtN map over segment Γ_r from (34)

$$\partial_{x_1} u(\mathbf{x}, t) + e^{-i\pi/4} \left[b_0 u(\mathbf{x}, t) - \sum_{k=1}^M b_k \varphi_{k,a_1}(x_2, t, t) \right] = 0.$$

Applying ∂_{x_2} to obtain the additional constraints on the field at corners, we have

$$\partial_{x_2} \partial_{x_1} u(\mathbf{x}, t) + e^{-i\pi/4} \left[b_0 \partial_{x_2} u(\mathbf{x}, t) - \sum_{k=1}^M b_k \partial_{x_2} \varphi_{k,a_1}(x_2, t, t) \right] = 0.$$

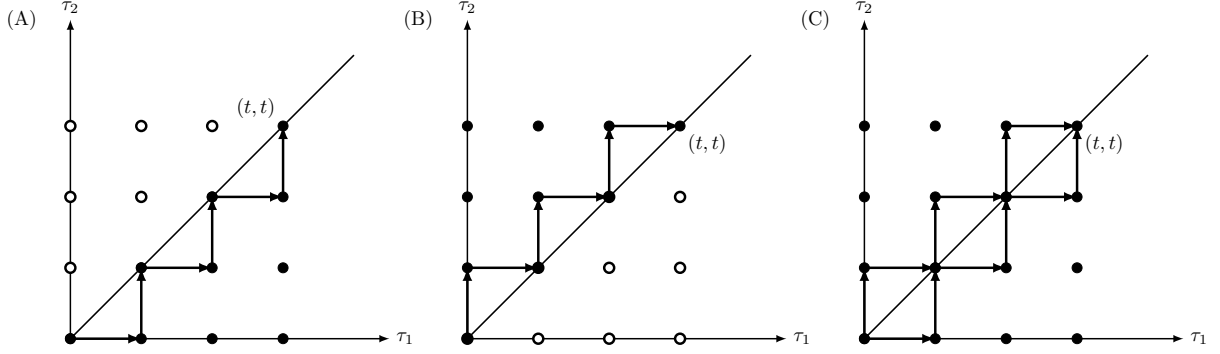


Figure 3: A schematic depiction of the evolution of the auxiliary fields $\varphi_{k,a_1}(x_2, \tau_1, \tau_2)$, $\varphi_{k,a_2}(x_1, \tau_1, \tau_2)$ and $\psi_{k,k',a_1,a_2}(\tau_1, \tau_2)$ in the (τ_1, τ_2) -plane is provided in this figure. The plots (A) and (B) depict the evolution of the fields $\varphi_{k,a_2}(x_1, \tau_1, \tau_2)$ and $\varphi_{k,a_1}(x_2, \tau_1, \tau_2)$ on the boundary segments Γ_{a_2} and Γ_{a_1} , respectively. The plot (C) depicts the evolution of the field $\psi_{k,k',a_1,a_2}(\tau_1, \tau_2)$ which can be achieved by moving either below or above the diagonal.

Plugging-in the value of $\partial_{x_2}\varphi_{k,a_1}(x_2, t, t)$ from (37) at corner point Γ_{rt} we get

$$\partial_{x_2}\partial_{x_1}u(\mathbf{x}, t) + e^{-i\pi/4}b_0\partial_{x_2}u(\mathbf{x}, t) + b_k e^{-i\pi/2} \sum_{k=1}^M \left[b_0\varphi_{k,a_1}(x_2, t, t) - \sum_{k'=1}^M b_{k'}\psi_{k,k',a_1,a_2}(t, t) \right] = 0.$$

The corner condition at Γ_{rt} becomes:

$$\partial_{x_2}\partial_{x_1}u(\mathbf{x}, t) + e^{-i\pi/4}b_0 \left[\partial_{x_2}u(\mathbf{x}, t) + \partial_{x_1}u(\mathbf{x}, t) + e^{-i\pi/4}b_0u(\mathbf{x}, t) \right] - e^{-i\pi/2} \sum_{k=1}^M \sum_{k'=1}^M b_k b_{k'} \psi_{k,k',a_1,a_2}(t, t) = 0. \quad (45)$$

2.3. Difficulty with conventional Padé based approach

Following Menza's approach [7], a Padé approximant based representation for the operators $(\partial_t - i\partial_{x_j}^2)^{1/2}$, $j = 1, 2$ can be developed by considering the rational function in (27). Using the Fourier representation in space and Laplace in time, we can write the DtN map on the segments Γ_{a_1} as

$$\partial_{x_1}u(x_1, x_2, t) \pm e^{-i\pi/4} \mathcal{L}_z^{-1} \mathcal{F}_{\zeta_2}^{-1} \left[R_M(z + i\zeta_2^2) \tilde{U}(x_1, \zeta_2, z) \right] = 0, \quad x_1 \in \{x_l, x_r\}. \quad (46)$$

Introducing the auxiliary fields $\{\varphi_{k,a_1}(x_2, t) \leftrightarrow \tilde{\Phi}_{k,a_1}(\zeta_2, z), z \in \mathbb{C}, \zeta_2 \in \mathbb{R}\}$ at the boundary segments denoted by Γ_{a_1} such that

$$(z + i\zeta_2^2 + \eta_k^2)^{-1} \tilde{U}(x_1, \zeta_2, z) = \tilde{\Phi}_{k,a_1}(\zeta_2, z), \quad k = 1, 2, \dots, M. \quad (47)$$

so that the DtN map becomes

$$\partial_{x_1}u(\mathbf{x}, t) \pm e^{-i\pi/4} \left[b_0 w(\mathbf{x}, t) - \sum_{k=1}^M b_k \varphi_{k,a_1}(x_2, t) \right] = 0, \quad (48)$$

and every φ_{k,a_1} satisfies the IVP given by

$$(i\partial_t + \partial_{x_2}^2 + i\eta_k^2)\varphi_{k,a_1}(x_2, t) = iu(x_1, x_2, t), \quad x_1 \in \{x_l, x_r\}, \quad (49)$$

with the initial conditions set to $\varphi_{k,a_1}(x_2, 0) = 0$. The equation above is a driven one-dimensional Schrödinger equation which can be handled in the standard way if $u(x_1, x_2, t)$ does not hit the end points of Γ_{a_1} . Under this assumption, the transparent boundary conditions at the end points are given by

$$\begin{aligned} \partial_{x_2}\varphi_{k,a_1}(x_l, t) + e^{-i\pi/4} e^{-\eta_k^2 t} \partial_t^{1/2} \left[e^{+\eta_k^2 t} \varphi_{k,a_1}(x_l, t) \right] &= 0, \\ \partial_{x_2}\varphi_{k,a_1}(x_r, t) - e^{-i\pi/4} e^{-\eta_k^2 t} \partial_t^{1/2} \left[e^{+\eta_k^2 t} \varphi_{k,a_1}(x_r, t) \right] &= 0. \end{aligned} \quad (50)$$

These conditions become inaccurate as soon as the support of $u(x_1, x_2, t)$ extends to the corners. While in principle, it is possible to remedy the problem here (irrespective of the computational cost), we do not pursue this line of investigation on account of the fact that the value of the field $u(x_1, x_2, t)$ is required outside of Ω_i in order to write the exact nonreflecting boundary conditions for φ_{k,a_1} .

3. Numerical Implementation

In this section, we address the complete numerical solution of the initial boundary-value problem (IBVP) stated in (14). In order to formulate the discrete linear system corresponding to the IBVP, we need to introduce temporal as well as spatial discretization of the problem. We first consider the temporal derivative which is discretized using one-step methods, namely, backward differentiation formula of order 1 (BDF1) and the trapezoidal rule (TR). Subsequently, a compatible temporal discretization scheme is developed for the boundary conditions where we strive to formulate the novel boundary maps at the time-discrete level as a Robin-type boundary condition for each time-step. Finally, the resulting semi-discrete partial differential equation is solved using a Legendre-Galerkin method where the boundary condition is enforced exactly by designing a boundary-adapted basis in terms of the Legendre polynomials followed by a boundary lifting process.

For the computational domain Ω_i , we introduce a reference domain $\Omega_i^{\text{ref.}} = \mathbb{I} \times \mathbb{I}$ keeping in view the typical domain of definition of the orthogonal polynomials being used. In order to describe the associated linear maps between the reference domain and the actual computational domain, we introduce the variables $y_1, y_2 \in \Omega_i^{\text{ref.}}$ such that

$$\begin{cases} x_1 = J_1 y_1 + \bar{x}_1, & J_1 = \frac{1}{2}(x_r - x_l), & \bar{x}_1 = \frac{1}{2}(x_l + x_r), & \beta_1 = J_1^{-2}, \\ x_2 = J_2 y_2 + \bar{x}_2, & J_2 = \frac{1}{2}(x_t - x_b), & \bar{x}_2 = \frac{1}{2}(x_b + x_t), & \beta_2 = J_2^{-2}. \end{cases} \quad (51)$$

Let Δt denote the time-step. In the rest of the section, with a slight abuse of notation, we switch to the variables $y_1 \in \mathbb{I}$ and $y_2 \in \mathbb{I}$ for all the discrete approximations of the dependent variables. For instance, $u^j(\mathbf{y})$ is taken to approximate $u(\mathbf{x}, j\Delta t)$ for $j = 0, 1, 2, \dots, N_t - 1$. The temporal discretization of the interior problem using one-step methods is enumerated below:

- The BDF1 based discretization is given by

$$i \frac{u^{j+1} - u^j}{\Delta t} + \Delta u^{j+1} = 0 \implies (\beta_1 \partial_{y_1}^2 + \beta_2 \partial_{y_2}^2) u^{j+1} + i \rho u^{j+1} = i \rho u^j, \quad \rho = 1/\Delta t. \quad (52)$$

- The TR based discretization is given by

$$i \frac{u^{j+1} - u^j}{\Delta t} + \Delta u^{j+1/2} = 0 \implies (\beta_1 \partial_{y_1}^2 + \beta_2 \partial_{y_2}^2) v^{j+1} + i \rho v^{j+1} = i \rho u^j, \quad \rho = 2/\Delta t, \quad (53)$$

where we have used the staggered samples of the field defined as

$$v^{j+1} = u^{j+1/2} = \frac{u^{j+1} + u^j}{2}, \quad v^0 = 0. \quad (54)$$

The rest of this section is organized as follows: Sec. 3.1 addresses the temporal discretization of the boundary maps which is followed by a discussion of the resulting spatial problem in Sec. 3.2.

3.1. Discretizing the boundary conditions

As mentioned above, we seek a compatible temporal discretization of the novel boundary conditions discussed in earlier sections in order to solve the IBVP. To this end, we first discuss the convolution quadrature (CQ) based discretization of the 1/2-order time-fractional derivative present in the TBCs developed in Sec. 2.1 and its other ramifications. Here, we would like to emphasize that an unsuitable temporal discretization of the convolution operators may destroy the overall stability of the numerical scheme [19]. In order to avoid this, we try to match the time-stepping

methods in the CQ based discretization of the boundary conditions to that of the interior problem (namely, BDF1 and TR). Next, we discuss the temporal discretization of the boundary maps developed in Sec. 2.2 using Padé approximants based representation for the fractional operator present in the TBCs. This method is labelled as ‘NP’ which expands to novel Padé.

In order to facilitate the temporal discretization of the TBCs, we introduce the equispaced samples of the auxiliary function, $\varphi^{j,k}(y_1, y_2)$, to approximate $\varphi(x_1, x_2, j\Delta t, k\Delta t)$ for $j, k = 0, 1, \dots, N_t - 1$. It follows from the definition (20) that the diagonal values of the auxiliary function at the discrete level are determined by the interior field, i.e., $\varphi^{j,j}(y_1, y_2) = u^j(y_1, y_2)$.

3.1.1. CQ–BDF1

The discrete scheme for the boundary maps is said to be ‘CQ–BDF1’ if the underlying one-step method in the CQ scheme is BDF1. Let $(\omega_k)_{k \in \mathbb{N}_0}$ denote the corresponding quadrature weights, then

$$\omega_j = [(j - 3/2)/j] \omega_{j-1}, \quad j \geq 1, \quad \text{with} \quad \omega_0 = 1. \quad (55)$$

Here, the quadrature weights are obtained using semi-discrete formulation as discussed in [26]. The resulting discretization scheme for the DtN map described in (23) in terms of $\varphi^{j,k}(y_1, y_2)$ stated as a Robin-type boundary condition reads as

$$\begin{aligned} \partial_{y_1} u^{j+1} + \sqrt{\rho/\beta_1} e^{-i\pi/4} u^{j+1} &= -\sqrt{\rho/\beta_1} e^{-i\pi/4} \mathcal{B} \left[\{\varphi^{k,j+1}(y_r, y_2)\}_{k=0}^j \right], \\ \partial_{y_1} u^{j+1} - \sqrt{\rho/\beta_1} e^{-i\pi/4} u^{j+1} &= +\sqrt{\rho/\beta_1} e^{-i\pi/4} \mathcal{B} \left[\{\varphi^{k,j+1}(y_l, y_2)\}_{k=0}^j \right], \\ \partial_{y_2} u^{j+1} + \sqrt{\rho/\beta_2} e^{-i\pi/4} u^{j+1} &= -\sqrt{\rho/\beta_2} e^{-i\pi/4} \mathcal{B} \left[\{\varphi^{j+1,k}(y_1, y_t)\}_{k=0}^j \right], \\ \partial_{y_2} u^{j+1} - \sqrt{\rho/\beta_2} e^{-i\pi/4} u^{j+1} &= +\sqrt{\rho/\beta_2} e^{-i\pi/4} \mathcal{B} \left[\{\varphi^{j+1,k}(y_1, y_b)\}_{k=0}^j \right], \end{aligned} \quad (56)$$

where we have used the fact that $\varphi^{j+1,j+1}(y_1, y_2) = u^{j+1}(y_1, y_2)$ and

$$\begin{aligned} \mathcal{B}_{a_1}^{j+1}(y_2) &= \mathcal{B} \left[\{\varphi^{k,j+1}(y_{a_1}, y_2)\}_{k=0}^j \right] = \sum_{k=1}^{j+1} \omega_k \varphi^{j+1-k, j+1}(y_{a_1}, y_2), \quad a_1 \in \{r, l\}, \\ \mathcal{B}_{a_2}^{j+1}(y_1) &= \mathcal{B} \left[\{\varphi^{j+1,k}(y_1, y_{a_2})\}_{k=0}^j \right] = \sum_{k=1}^{j+1} \omega_k \varphi^{j+1, j+1-k}(y_1, y_{a_2}), \quad a_2 \in \{b, t\}. \end{aligned} \quad (57)$$

We may refer to these functions as the *history functions* on account of the fact that, for the latest time-step, they can be assumed to be determined by the quantities that are already determined in the previous time-steps. Set $\alpha_k = \sqrt{\rho/\beta_k} e^{-i\pi/4}$ for $k = 1, 2$, then the discretized maps take the form

$$\begin{aligned} \partial_{y_1} u^{j+1} + \alpha_1 u^{j+1} &= -\alpha_1 \mathcal{B}_r^{j+1}(y_2), & \partial_{y_2} u^{j+1} + \alpha_2 u^{j+1} &= -\alpha_2 \mathcal{B}_t^{j+1}(y_1), \\ \partial_{y_1} u^{j+1} - \alpha_1 u^{j+1} &= +\alpha_1 \mathcal{B}_l^{j+1}(y_2), & \partial_{y_2} u^{j+1} - \alpha_2 u^{j+1} &= +\alpha_2 \mathcal{B}_b^{j+1}(y_1). \end{aligned} \quad (58)$$

To obtain the history of the field $\varphi(y_1, y_2, \tau_1, \tau_2)$ needed to compute the history functions in (58), we employ a Legendre-Galerkin method to solve the IVPs listed in (24) by formulating the boundary conditions given in (25) as a Robin-type map. Let us start by introducing a compact notation obtained by restricting the auxiliary function in the following manner:

$$\varphi_{a_1}^{p,q}(y_2) = \varphi^{p,q}(y_{a_1}, y_2), \quad \varphi_{a_2}^{p,q}(y_1) = \varphi^{p,q}(y_1, y_{a_2}), \quad \varphi_{a_1 a_2}^{p,q} = \varphi^{p,q}(y_{a_1}, y_{a_2}), \quad a_1 \in \{l, r\}, \quad a_2 \in \{b, t\}. \quad (59)$$

The BDF1-based discretization of the IVPs (24) for the auxiliary functions read as follows:

$$\begin{aligned} (y_1, y_2) \in \Gamma_b^{\text{ref.}} \cup \Gamma_t^{\text{ref.}} : & \begin{cases} i \frac{\varphi_{a_2}^{p+1,q} - \varphi_{a_2}^{p,q}}{\Delta t} + \beta_1 \partial_{y_1}^2 \varphi_{a_2}^{p+1,q} = 0 \implies -\alpha_1^{-2} \partial_{y_1}^2 \varphi_{a_2}^{p+1,q} + \varphi_{a_2}^{p+1,q} = \varphi_{a_2}^{p,q}, \\ p = q, q+1, \dots, j, \quad q = 0, 1, \dots, j; \end{cases} \\ (y_1, y_2) \in \Gamma_l^{\text{ref.}} \cup \Gamma_r^{\text{ref.}} : & \begin{cases} i \frac{\varphi_{a_1}^{m,n+1} - \varphi_{a_1}^{m,n}}{\Delta t} + \beta_2 \partial_{y_2}^2 \varphi_{a_1}^{m,n+1} = 0 \implies -\alpha_2^{-2} \partial_{y_2}^2 \varphi_{a_1}^{m,n+1} + \varphi_{a_1}^{m,n+1} = \varphi_{a_1}^{m,n}, \\ n = m, m+1, \dots, j, \quad m = 0, 1, \dots, j. \end{cases} \end{aligned} \quad (60)$$

The BDF1-based discretization of the DtN map described in (25) stated as Robin-type boundary condition reads as:

$$\begin{aligned}
(\partial_{y_1} + \alpha_1)\varphi_{a_2}^{p+1,q}(y_1)\Big|_{y_1=y_r} &= -\alpha_1 \mathcal{B} \left[\{\varphi_{a_2}^{k,q}(y_r)\}_{k=0}^p \right], \\
(\partial_{y_1} - \alpha_1)\varphi_{a_2}^{p+1,q}(y_1)\Big|_{y_1=y_l} &= +\alpha_1 \mathcal{B} \left[\{\varphi_{a_2}^{k,q}(y_l)\}_{k=0}^p \right], \\
(\partial_{y_2} + \alpha_2)\varphi_{a_1}^{m,n+1}(y_2)\Big|_{y_2=y_r} &= -\alpha_2 \mathcal{B} \left[\{\varphi_{a_1}^{m,k}(y_r)\}_{k=0}^n \right], \\
(\partial_{y_2} - \alpha_2)\varphi_{a_1}^{m,n+1}(y_2)\Big|_{y_2=y_b} &= +\alpha_2 \mathcal{B} \left[\{\varphi_{a_1}^{m,k}(y_b)\}_{k=0}^n \right],
\end{aligned} \tag{61}$$

where

$$\begin{aligned}
\mathcal{B}_{a_2,a_1}^{p+1,q} &= \mathcal{B} \left[\{\varphi_{a_2}^{k,q}(y_{a_1})\}_{k=0}^p \right] = \sum_{k=1}^{p+1} \omega_k \varphi^{p+1-k,q}(y_{a_1}, y_{a_2}) = \sum_{k=1}^{p+1} \omega_k \varphi_{a_1 a_2}^{p+1-k,q}, \\
\mathcal{B}_{a_1,a_2}^{m,n+1} &= \mathcal{B} \left[\{\varphi_{a_1}^{m,k}(y_{a_2})\}_{k=0}^n \right] = \sum_{k=1}^{n+1} \omega_k \varphi^{m,n+1-k}(y_{a_1}, y_{a_2}) = \sum_{k=1}^{n+1} \omega_k \varphi_{a_1 a_2}^{m,n+1-k}.
\end{aligned} \tag{62}$$

The maps can now be expressed as

$$\begin{aligned}
(\partial_{y_1} + \alpha_1)\varphi_{a_2}^{p+1,q}(y_1)\Big|_{y_1=y_r} &= -\alpha_1 \mathcal{B}_{a_2,r}^{p+1,q}, & (\partial_{y_2} + \alpha_2)\varphi_{a_1}^{m,n+1}(y_2)\Big|_{y_2=y_r} &= -\alpha_2 \mathcal{B}_{a_1,t}^{m,n+1}, \\
(\partial_{y_1} - \alpha_1)\varphi_{a_2}^{p+1,q}(y_1)\Big|_{y_1=y_l} &= +\alpha_1 \mathcal{B}_{a_2,l}^{p+1,q}, & (\partial_{y_2} - \alpha_2)\varphi_{a_1}^{m,n+1}(y_2)\Big|_{y_2=y_b} &= +\alpha_2 \mathcal{B}_{a_1,b}^{m,n+1}.
\end{aligned} \tag{63}$$

Corner conditions—To solve the IBVP, we need to look at the discrete form of the corner conditions developed in Sec. 2.1.1. On the reference domain considered for the numerical implementation, we express the corner condition present in (26) as

$$\sqrt{\beta_1} \sqrt{\beta_2} \partial_{y_2} \partial_{y_1} u(x_1, x_2, t) = e^{-i\pi/4} e^{-i\pi/4} \partial_{\tau_1}^{1/2} \partial_{\tau_2}^{1/2} \varphi(x_1, x_2, \tau_1, \tau_2)\Big|_{\tau_1=\tau_2=t}. \tag{64}$$

At the discrete level, the corner condition at Γ_{rt} takes the form

$$\partial_{y_2} \partial_{y_1} u^{j+1} = \sqrt{\frac{\rho}{\beta_1}} e^{-i\pi/4} \sqrt{\frac{\rho}{\beta_2}} e^{-i\pi/4} \sum_{k=0}^{j+1} \omega_k \left[\sum_{k'=0}^{j+1} \omega_{k'} \varphi^{j+1-k,j+1-k'}(y_r, y_t) \right] = \alpha_1 \alpha_2 \sum_{k=0}^{j+1} \omega_k \left[\sum_{k'=0}^{j+1} \omega_{k'} \varphi^{j+1-k,j+1-k'}(y_r, y_t) \right].$$

In order to separate the current time-step value, we proceed in the following manner:

$$\begin{aligned}
\partial_{y_2} \partial_{y_1} u^{j+1} &= \alpha_1 \alpha_2 \sum_{k=0}^{j+1} \omega_k \left[\varphi^{j+1-k,j+1}(y_r, y_t) + \sum_{k'=1}^{j+1} \omega_{k'} \varphi^{j+1-k,j+1-k'}(y_r, y_t) \right] \\
&= \alpha_1 \alpha_2 \left[\sum_{k=0}^{j+1} \omega_k \varphi^{j+1-k,j+1}(y_r, y_t) + \sum_{k=0}^{j+1} \sum_{k'=1}^{j+1} \omega_k \omega_{k'} \varphi^{j+1-k,j+1-k'}(y_r, y_t) \right] \\
&= \alpha_1 \alpha_2 \left[\varphi^{j+1,j+1}(y_r, y_t) + \mathcal{B}_r^{j+1}(y_t) + \mathcal{B}_t^{j+1}(y_r) + \sum_{k=1}^{j+1} \sum_{k'=1}^{j+1} \omega_k \omega_{k'} \varphi^{j+1-k,j+1-k'}(y_r, y_t) \right].
\end{aligned} \tag{65}$$

Plugging-in the value for the history functions from (58) in the above equation, we obtain

$$\begin{aligned}
(\partial_{y_2} + \alpha_2)(\partial_{y_1} + \alpha_1)u^{j+1}\Big|_{(y_r,y_t)} &= +\alpha_1 \alpha_2 C_{rt}^{j+1}, & (\partial_{y_2} - \alpha_2)(\partial_{y_1} + \alpha_1)u^{j+1}\Big|_{(y_r,y_b)} &= -\alpha_1 \alpha_2 C_{br}^{j+1}, \\
(\partial_{y_2} + \alpha_2)(\partial_{y_1} - \alpha_1)u^{j+1}\Big|_{(y_l,y_t)} &= -\alpha_1 \alpha_2 C_{tl}^{j+1}, & (\partial_{y_2} - \alpha_2)(\partial_{y_1} - \alpha_1)u^{j+1}\Big|_{(y_l,y_b)} &= +\alpha_1 \alpha_2 C_{lb}^{j+1},
\end{aligned} \tag{66}$$

where

$$C_{a_1 a_2}^{j+1} = \sum_{k=1}^{j+1} \sum_{k'=1}^{j+1} \omega_k \omega_{k'} \varphi^{j+1-k,j+1-k'}(y_{a_1}, y_{a_2}), \quad a_1 \in \{r, l\}, \quad a_2 \in \{t, b\}.$$

3.1.2. CQ–TR

The discrete scheme is said to be ‘CQ–TR’ if the underlying one-step method in the CQ scheme is TR. Let $(\omega_k)_{k \in \mathbb{N}_0}$ denote the corresponding quadrature weights, then

$$\omega_j = \begin{cases} C_{j/2}, & j \text{ even,} \\ -C_{(j-1)/2}, & j \text{ odd,} \end{cases} \quad \text{where } C_n = \frac{1 \cdot 3 \cdots (2n-1)}{n!2^n}. \quad (67)$$

The quadrature weights can also be generated using the following recurrence relation [26]

$$(j+1)\omega_{j+1} = (j-1)\omega_{j-1} - \omega_j, \quad j \geq 1, \quad (68)$$

with $\omega_0 = 1, \omega_1 = -1$. The resulting discretization scheme for the DtN map described in (23) in terms of $\varphi^{j,k}(y_1, y_2)$ stated as a Robin-type boundary condition (consistent with the staggered samples of the interior field) reads as

$$\begin{aligned} \partial_{y_1} v^{j+1} + \alpha_1 v^{j+1} &= -\frac{\alpha_1}{2} \left(\mathcal{B} \left[\{\varphi^{k,j+1}(y_r, y_2)\}_{k=0}^j \right] + \mathcal{B} \left[\{\varphi^{k,j}(y_r, y_2)\}_{k=0}^{j-1} \right] \right), \\ \partial_{y_1} v^{j+1} - \alpha_1 v^{j+1} &= +\frac{\alpha_1}{2} \left(\mathcal{B} \left[\{\varphi^{k,j+1}(y_l, y_2)\}_{k=0}^j \right] + \mathcal{B} \left[\{\varphi^{k,j}(y_l, y_2)\}_{k=0}^{j-1} \right] \right), \\ \partial_{y_2} v^{j+1} + \alpha_2 v^{j+1} &= -\frac{\alpha_2}{2} \left(\mathcal{B} \left[\{\varphi^{k,j+1}(y_1, y_t)\}_{k=0}^j \right] + \mathcal{B} \left[\{\varphi^{k,j}(y_1, y_t)\}_{k=0}^{j-1} \right] \right), \\ \partial_{y_2} v^{j+1} - \alpha_2 v^{j+1} &= +\frac{\alpha_2}{2} \left(\mathcal{B} \left[\{\varphi^{k,j+1}(y_1, y_b)\}_{k=0}^j \right] + \mathcal{B} \left[\{\varphi^{k,j}(y_1, y_b)\}_{k=0}^{j-1} \right] \right), \end{aligned} \quad (69)$$

where the history operator \mathcal{B} is defined in the similar manner as in the case of BDF1. Let $\mathcal{B}^{j+1/2} = (\mathcal{B}^{j+1} + \mathcal{B}^j)/2$, then the maps can be compactly written as

$$\begin{aligned} \partial_{y_1} v^{j+1} + \alpha_1 v^{j+1} &= -\alpha_1 \mathcal{B}_r^{j+1/2}(y_2), & \partial_{y_2} v^{j+1} + \alpha_2 v^{j+1} &= -\alpha_2 \mathcal{B}_t^{j+1/2}(y_1), \\ \partial_{y_1} v^{j+1} - \alpha_1 v^{j+1} &= +\alpha_1 \mathcal{B}_l^{j+1/2}(y_2), & \partial_{y_2} v^{j+1} - \alpha_2 v^{j+1} &= +\alpha_2 \mathcal{B}_b^{j+1/2}(y_1). \end{aligned} \quad (70)$$

The TR-based discretization of the IVPs (24) for the auxiliary function reads as follows:

$$\begin{aligned} (y_1, y_2) \in \Gamma_b^{\text{ref.}} \cup \Gamma_t^{\text{ref.}} : & \begin{cases} i \frac{\varphi_{a_2}^{p+1,q} - \varphi_{a_2}^{p,q}}{\Delta t} + \beta_1 \partial_{y_1}^2 \frac{\varphi_{a_2}^{p+1,q} + \varphi_{a_2}^{p,q}}{2} = 0 \implies -\alpha_1^{-2} \partial_{y_1}^2 \varphi_{a_2}^{p+1/2,q} + \varphi_{a_2}^{p+1/2,q} = \varphi_{a_2}^{p,q}, \\ p = q, q+1, \dots, j, \quad q = 0, 1, \dots, j; \end{cases} \\ (y_1, y_2) \in \Gamma_l^{\text{ref.}} \cup \Gamma_r^{\text{ref.}} : & \begin{cases} i \frac{\varphi_{a_1}^{m,n+1} - \varphi_{a_1}^{m,n}}{\Delta t} + \beta_2 \partial_{y_2}^2 \frac{\varphi_{a_1}^{m,n+1} + \varphi_{a_1}^{m,n}}{2} = 0 \implies -\alpha_2^{-2} \partial_{y_2}^2 \varphi_{a_1}^{m,n+1/2} + \varphi_{a_1}^{m,n+1/2} = \varphi_{a_1}^{m,n}, \\ n = m, m+1, \dots, j, \quad m = 0, 1, \dots, j. \end{cases} \end{aligned} \quad (71)$$

The TR-based discretization of the DtN map described in (25) stated as Robin-type boundary condition reads as:

$$\begin{aligned} (\partial_{y_1} + \alpha_1) \varphi_{a_2}^{p+1/2,q}(y_1) \Big|_{y_1=y_r} &= -\frac{\alpha_1}{2} \left(\mathcal{B} \left[\{\varphi_{a_2}^{k,q}(y_r)\}_{k=0}^p \right] + \mathcal{B} \left[\{\varphi_{a_2}^{k,q}(y_r)\}_{k=0}^{p-1} \right] \right), \\ (\partial_{y_1} - \alpha_1) \varphi_{a_2}^{p+1/2,q}(y_1) \Big|_{y_1=y_l} &= +\frac{\alpha_1}{2} \left(\mathcal{B} \left[\{\varphi_{a_2}^{k,q}(y_l)\}_{k=0}^p \right] + \mathcal{B} \left[\{\varphi_{a_2}^{k,q}(y_l)\}_{k=0}^{p-1} \right] \right), \\ (\partial_{y_2} + \alpha_2) \varphi_{a_1}^{m,n+1/2}(y_2) \Big|_{y_2=y_t} &= -\frac{\alpha_2}{2} \left(\mathcal{B} \left[\{\varphi_{a_1}^{m,k}(y_t)\}_{k=0}^n \right] + \mathcal{B} \left[\{\varphi_{a_1}^{m,k}(y_t)\}_{k=0}^{n-1} \right] \right), \\ (\partial_{y_2} - \alpha_2) \varphi_{a_1}^{m,n+1/2}(y_2) \Big|_{y_2=y_b} &= +\frac{\alpha_2}{2} \left(\mathcal{B} \left[\{\varphi_{a_1}^{m,k}(y_b)\}_{k=0}^n \right] + \mathcal{B} \left[\{\varphi_{a_1}^{m,k}(y_b)\}_{k=0}^{n-1} \right] \right). \end{aligned} \quad (72)$$

where operator \mathcal{B} is defined as

$$\mathcal{B}_{a_2, a_1}^{p+1,q} = \mathcal{B} \left[\{\varphi_{a_2}^{k,q}(y_{a_1})\}_{k=0}^p \right] = \sum_{k=1}^{p+1} \omega_k \varphi_{a_1 a_2}^{p+1-k,q}, \quad \mathcal{B}_{a_1, a_2}^{m,n+1} = \mathcal{B} \left[\{\varphi_{a_1}^{m,k}(y_{a_2})\}_{k=0}^n \right] = \sum_{k=1}^{n+1} \omega_k \varphi_{a_1 a_2}^{m,n+1-k}. \quad (73)$$

so that the maps can now be expressed as

$$\begin{aligned} (\partial_{y_1} + \alpha_1)\varphi_{a_2}^{p+1/2,q}(y_1)\Big|_{y_1=y_r} &= -\alpha_1\mathcal{B}_{a_2,r}^{p+1/2,q}, & (\partial_{y_2} + \alpha_2)\varphi_{a_1}^{m,n+1/2}(y_2)\Big|_{y_1=y_r} &= -\alpha_2\mathcal{B}_{a_1,t}^{m,n+1/2}, \\ (\partial_{y_1} - \alpha_1)\varphi_{a_2}^{p+1/2,q}(y_1)\Big|_{y_1=y_l} &= +\alpha_1\mathcal{B}_{a_2,t}^{p+1/2,q}, & (\partial_{y_2} - \alpha_2)\varphi_{a_1}^{m,n+1/2}(y_2)\Big|_{y_1=y_b} &= +\alpha_2\mathcal{B}_{a_1,b}^{m,n+1/2}. \end{aligned} \quad (74)$$

Corner conditions—Following along the similar lines as that of BDF1, we can summarize the corner conditions consistent with staggered samples of the field as:

$$\begin{aligned} (\partial_{y_2} + \alpha_2)(\partial_{y_1} + \alpha_1)v^{j+1}\Big|_{(y_r,y_t)} &= +\alpha_1\alpha_2\mathcal{C}_{rt}^{j+1/2}, & (\partial_{y_2} - \alpha_2)(\partial_{y_1} + \alpha_1)v^{j+1}\Big|_{(y_r,y_b)} &= -\alpha_1\alpha_2\mathcal{C}_{br}^{j+1/2}, \\ (\partial_{y_2} + \alpha_2)(\partial_{y_1} - \alpha_1)v^{j+1}\Big|_{(y_l,y_t)} &= -\alpha_1\alpha_2\mathcal{C}_{tl}^{j+1/2}, & (\partial_{y_2} - \alpha_2)(\partial_{y_1} - \alpha_1)v^{j+1}\Big|_{(y_l,y_b)} &= +\alpha_1\alpha_2\mathcal{C}_{lb}^{j+1/2}, \end{aligned} \quad (75)$$

where

$$\mathcal{C}_{a_1a_2}^{j+1/2} = \frac{1}{2} \left[\sum_{k=1}^{j+1} \sum_{k'=1}^{j+1} \omega_k \omega_{k'} \varphi^{j+1-k,j+1-k'}(y_{a_1}, y_{a_2}) + \sum_{k=1}^j \sum_{k'=1}^j \omega_k \omega_{k'} \varphi^{j-k,j-k'}(y_{a_1}, y_{a_2}) \right].$$

3.1.3. NP-BDF1

The discrete scheme for the boundary maps is said to be ‘NP-BDF1’ if the temporal derivatives in the realization of the boundary maps, dubbed as ‘NP’, developed in Sec. 2.2 are discretized using the one-step method BDF1. To achieve this, we start by writing the time-discrete form of the DtN maps present in (34) in the reference domain as

$$\begin{aligned} \sqrt{\beta_1}\partial_{y_1}u^{j+1} \pm e^{-i\pi/4} \left[b_0u^{j+1} - \sum_{k=1}^M b_k\varphi_{k,a_1}^{j+1,j+1} \right] &= 0, \\ \sqrt{\beta_2}\partial_{y_2}u^{j+1} \pm e^{-i\pi/4} \left[b_0u^{j+1} - \sum_{k=1}^M b_k\varphi_{k,a_2}^{j+1,j+1} \right] &= 0, \end{aligned} \quad (76)$$

where we recall $a_1 \in \{r, l\}$ and $a_2 \in \{t, b\}$. In order to turn these equations into a Robin-type boundary condition, we need to compute the discrete samples $\varphi_{k,a_1}^{j+1,j+1}$ and $\varphi_{k,a_2}^{j+1,j+1}$ by considering the ODEs established for these auxiliary function earlier. For the temporal discretization of these ODEs, we try to match the time discretization scheme to that of the interior scheme to avoid any kind of instability as a result of incompatible discretization of the boundary maps. In the following, we discuss the BDF1-based discretization of (33): Setting $\rho = 1/\Delta t$ and for $k = 1, 2, \dots, M$, we have

$$\begin{cases} \frac{\varphi_{k,a_1}^{j+1,j+1} - \varphi_{k,a_1}^{j,j+1}}{\Delta t} + \eta_k^2\varphi_{k,a_1}^{j+1,j+1} = \varphi^{j+1,j+1} \implies \varphi_{k,a_1}^{j+1,j+1} = \frac{\rho}{(\rho + \eta_k^2)}\varphi_{k,a_1}^{j,j+1} + \frac{1}{(\rho + \eta_k^2)}u^{j+1}, \\ \frac{\varphi_{k,a_2}^{j+1,j+1} - \varphi_{k,a_2}^{j+1,j}}{\Delta t} + \eta_k^2\varphi_{k,a_2}^{j+1,j+1} = \varphi^{j+1,j+1} \implies \varphi_{k,a_2}^{j+1,j+1} = \frac{\rho}{(\rho + \eta_k^2)}\varphi_{k,a_2}^{j+1,j} + \frac{1}{(\rho + \eta_k^2)}u^{j+1}. \end{cases} \quad (77)$$

Introduce the scaling $\bar{\eta}_k = \eta_k/\sqrt{\rho}$ so that

$$\varphi_{k,a_1}^{j+1,j+1} = \frac{1}{(1 + \bar{\eta}_k^2)}\varphi_{k,a_1}^{j,j+1} + \frac{1/\rho}{(1 + \bar{\eta}_k^2)}u^{j+1}, \quad \varphi_{k,a_2}^{j+1,j+1} = \frac{1}{(1 + \bar{\eta}_k^2)}\varphi_{k,a_2}^{j+1,j} + \frac{1/\rho}{(1 + \bar{\eta}_k^2)}u^{j+1}. \quad (78)$$

Next, we plug-in the values of $\varphi_{k,a_1}^{j+1,j+1}$ and $\varphi_{k,a_2}^{j+1,j+1}$ in the boundary maps to obtain

$$\begin{aligned} \partial_{y_1}u^{j+1} \pm \alpha_1 \left[\bar{b}_0 + \frac{1}{\rho} \sum_{k=1}^M \Gamma_k \right] u^{j+1} &= \mp \alpha_1 \sum_{k=1}^M \Gamma_k \varphi_{k,a_1}^{j,j+1}, \\ \partial_{y_2}u^{j+1} \pm \alpha_2 \left[\bar{b}_0 + \frac{1}{\rho} \sum_{k=1}^M \Gamma_k \right] u^{j+1} &= \mp \alpha_2 \sum_{k=1}^M \Gamma_k \varphi_{k,a_2}^{j+1,j}, \end{aligned} \quad (79)$$

where

$$\Gamma_k = -\bar{b}_k/(1 + \bar{\eta}_k^2), \quad \bar{b}_0 = b_0/\sqrt{\rho}, \quad \bar{b}_k = b_k/\sqrt{\rho}, \quad k = 1, 2, \dots, M. \quad (80)$$

The maps can now be compactly written as a Robin-type boundary condition as

$$\partial_{y_1} u^{j+1} \pm \alpha_1 \varpi u^{j+1} = \mp \alpha_1 \mathcal{B}_{a_1}^{j+1}(y_2), \quad \partial_{y_2} u^{j+1} \pm \alpha_2 \varpi u^{j+1} = \mp \alpha_2 \mathcal{B}_{a_2}^{j+1}(y_1), \quad (81)$$

where

$$\varpi = \bar{b}_0 + \frac{1}{\rho} \sum_{k=1}^M \Gamma_k = \bar{b}_0 - \frac{1}{\rho} \sum_{k=1}^M \frac{\bar{b}_k}{1 + \bar{\eta}_k^2} = \sqrt{\rho} R_M(\rho), \quad (82)$$

and

$$\mathcal{B}_{a_1}^{j+1}(y_2) = \sum_{k=1}^M \Gamma_k \varphi_{k,a_1}^{j,j+1}, \quad \mathcal{B}_{a_2}^{j+1}(y_1) = \sum_{k=1}^M \Gamma_k \varphi_{k,a_2}^{j+1,j}, \quad (83)$$

are the so-called history functions in this setting. To obtain the discrete samples $\varphi_{k,a_1}^{j,j+1}$ and $\varphi_{k,a_2}^{j+1,j}$ needed to compute the history functions, we employ a Legendre-Galerkin method to solve the IVPs listed in (36) by formulating the boundary conditions present in (37) as a Robin-type boundary map. The BDF1 based discretization of the IVPs take the form

$$\begin{aligned} (y_1, y_2) \in \Gamma_b^{\text{ref.}} \cup \Gamma_t^{\text{ref.}} : \quad & i \frac{\varphi_{k,a_2}^{j+1,j} - \varphi_{k,a_2}^{j,j}}{\Delta t} + \beta_1 \partial_{y_1}^2 \varphi_{k,a_2}^{j,j} = 0 \implies -\alpha_1^{-2} \partial_{y_1}^2 \varphi_{k,a_2}^{j+1,j} + \varphi_{k,a_2}^{j+1,j} = \varphi_{k,a_2}^{j,j}, \\ (y_1, y_2) \in \Gamma_l^{\text{ref.}} \cup \Gamma_r^{\text{ref.}} : \quad & i \frac{\varphi_{k,a_1}^{j,j+1} - \varphi_{k,a_1}^{j,j}}{\Delta t} + \beta_1 \partial_{y_2}^2 \varphi_{k,a_1}^{j,j} = 0 \implies -\alpha_1^{-2} \partial_{y_2}^2 \varphi_{k,a_1}^{j,j+1} + \varphi_{k,a_1}^{j,j+1} = \varphi_{k,a_1}^{j,j}. \end{aligned} \quad (84)$$

The discrete form of the DtN maps (40) for these IVPs can be written as:

$$\begin{aligned} \sqrt{\beta_2} \partial_{y_2} \varphi_{k,a_1}^{j,j+1} \pm e^{-i\pi/4} \left[b_0 \varphi_{k,a_1}^{j,j+1} - \sum_{k'=1}^M b_{k'} \psi_{k,k',a_1,a_2}^{j,j+1} \right] &= 0, \\ \sqrt{\beta_1} \partial_{y_1} \varphi_{k,a_2}^{j+1,j} \pm e^{-i\pi/4} \left[b_0 \varphi_{k,a_2}^{j+1,j} - \sum_{k'=1}^M b_{k'} \psi_{k,k',a_2,a_1}^{j+1,j} \right] &= 0. \end{aligned} \quad (85)$$

In order to obtain the history functions, we invoke BDF1 based discretization of (39) and (44) to write

$$\begin{aligned} \frac{\psi_{k,k',a_1,a_2}^{j+1,j+1} - \psi_{k,k',a_1,a_2}^{j,j+1}}{\Delta t} + \bar{\eta}_k^2 \psi_{k,k',a_1,a_2}^{j+1,j+1} = \varphi_{k',a_2}^{j+1,j+1} \implies \psi_{k,k',a_1,a_2}^{j+1,j+1} &= \frac{1}{(1 + \bar{\eta}_k^2)} \psi_{k,k',a_1,a_2}^{j,j+1} + \frac{1/\rho}{(1 + \bar{\eta}_k^2)} \varphi_{k',a_2}^{j+1,j+1}, \\ \frac{\psi_{k,k',a_1,a_2}^{j,j+1} - \psi_{k,k',a_1,a_2}^{j,j}}{\Delta t} + \bar{\eta}_k^2 \psi_{k,k',a_1,a_2}^{j,j+1} = \varphi_{k,a_1}^{j,j+1} \implies \psi_{k,k',a_1,a_2}^{j,j+1} &= \frac{1}{(1 + \bar{\eta}_k^2)} \psi_{k,k',a_1,a_2}^{j,j} + \frac{1/\rho}{(1 + \bar{\eta}_k^2)} \varphi_{k,a_1}^{j,j+1}. \end{aligned} \quad (86)$$

Plugging-in the values of $\psi_{k,k',a_1,a_2}^{j,j+1}$ and $\psi_{k,k',a_2,a_1}^{j+1,j}$ in (85), we obtain

$$\begin{aligned} \partial_{y_2} \varphi_{k,a_1}^{j,j+1} \pm \alpha_2 \left[\bar{b}_0 + \frac{1}{\rho} \sum_{k'=1}^M \Gamma_{k'} \right] \varphi_{k,a_1}^{j,j+1} &= \mp \alpha_2 \sum_{k'=1}^M \Gamma_{k'} \psi_{k,k',a_1,a_2}^{j,j}, \\ \partial_{y_1} \varphi_{k,a_2}^{j+1,j} \pm \alpha_1 \left[\bar{b}_0 + \frac{1}{\rho} \sum_{k'=1}^M \Gamma_{k'} \right] \varphi_{k,a_2}^{j+1,j} &= \mp \alpha_1 \sum_{k'=1}^M \Gamma_{k'} \psi_{k,k',a_2,a_1}^{j+1,j}. \end{aligned} \quad (87)$$

Once again, we can express the maps compactly as

$$\partial_{y_2} \varphi_{k,a_1}^{j,j+1} \pm \alpha_2 \varpi \varphi_{k,a_1}^{j,j+1} = \mp \alpha_2 \mathcal{B}_{k,a_1,a_2}^{j+1}, \quad \partial_{y_1} \varphi_{k,a_2}^{j+1,j} \pm \alpha_1 \varpi \varphi_{k,a_2}^{j+1,j} = \mp \alpha_1 \mathcal{B}_{k,a_2,a_1}^{j+1}, \quad (88)$$

where the history functions in this setting are given by

$$\mathcal{B}_{k,a_1,a_2}^{j+1} = \sum_{k'=1}^M \Gamma_{k'} \psi_{k,k',a_1,a_2}^{j,j}, \quad \mathcal{B}_{k,a_2,a_1}^{j+1} = \sum_{k'=1}^M \Gamma_{k'} \psi_{k,k',a_2,a_1}^{j,j} = \sum_{k'=1}^M \Gamma_{k'} \psi_{k',k,a_1,a_2}^{j,j}. \quad (89)$$

Corner conditions–To solve the IBVP, we need to develop the discrete form of the corner conditions developed in Sec. 2.2. On the reference domain considered for the numerical implementation, we express the corner conditions present in (45) as

$$\left[\partial_{y_2} \partial_{y_1} + \alpha_2 \bar{b}_0 \partial_{y_1} + \alpha_1 \bar{b}_0 \partial_{y_2} + \alpha_1 \alpha_2 \bar{b}_0^2 \right] u(x_{a_1}, x_{a_2}, t) - \alpha_1 \alpha_2 \sum_{k=1}^M \sum_{k'=1}^M \bar{b}_k \bar{b}_{k'} \psi_{k,k',a_1,a_2}(t, t) = 0. \quad (90)$$

At the discrete level, the corner conditions take the form

$$\left[\partial_{y_2} \partial_{y_1} + \alpha_2 \bar{b}_0 \partial_{y_1} + \alpha_1 \bar{b}_0 \partial_{y_2} + \alpha_1 \alpha_2 \bar{b}_0^2 \right] u^{j+1} - \alpha_1 \alpha_2 \sum_{k=1}^M \sum_{k'=1}^M \bar{b}_k \bar{b}_{k'} \psi_{k,k',a_1,a_2}^{j+1,j+1} = 0. \quad (91)$$

The diagonal-to-diagonal update of auxiliary fields ψ is already computed in (86) which can be simplified as

$$\begin{aligned} \psi_{k,k',a_1,a_2}^{j+1,j+1} &= \frac{1}{(1 + \bar{\eta}_k^2)(1 + \bar{\eta}_{k'}^2)} \psi_{k,k',a_1,a_2}^{j,j} + \frac{(1/\rho)^2}{(1 + \bar{\eta}_k^2)(1 + \bar{\eta}_{k'}^2)} u^{j+1} \\ &\quad + \frac{1/\rho}{(1 + \bar{\eta}_k^2)(1 + \bar{\eta}_{k'}^2)} \varphi_{k,a_1}^{j,j+1} + \frac{1/\rho}{(1 + \bar{\eta}_k^2)(1 + \bar{\eta}_{k'}^2)} \varphi_{k',a_2}^{j+1,j}. \end{aligned} \quad (92)$$

The last term in (91) can be expressed in terms of boundary sums as

$$\begin{aligned} \sum_k \sum_{k'} \bar{b}_k \bar{b}_{k'} \psi_{k,k',a_1,a_2}^{j+1,j+1} &= \sum_k \sum_{k'} \left[\frac{\bar{b}_k \bar{b}_{k'}}{(1 + \bar{\eta}_k^2)(1 + \bar{\eta}_{k'}^2)} \psi_{k,k',a_1,a_2}^{j,j} \right] \\ &\quad + \frac{1}{\rho} \left[\sum_k \Gamma_k \right] \mathcal{B}_{a_1}^{j+1}(y_2) + \frac{1}{\rho} \left[\sum_k \Gamma_k \right] \mathcal{B}_{a_2}^{j+1}(y_1) + \frac{1}{\rho^2} \left[\sum_k \Gamma_k \right]^2 u^{j+1}. \end{aligned} \quad (93)$$

Plugging-in the value of $\psi_{k,k',a_1,a_2}^{j+1,j+1}$ in (91) and collecting all the terms at $(j+1)$ -th time-step on the left hand side, we arrive at the expression

$$\begin{aligned} &\left[\partial_{y_2} \partial_{y_1} + \alpha_2 \varpi \partial_{y_1} + \alpha_1 \varpi \partial_{y_2} + \alpha_1 \alpha_2 \bar{b}_0^2 \right] u^{j+1} + \alpha_1 \alpha_2 [2\varpi(\varpi - \bar{b}_0) - (\varpi - \bar{b}_0)^2] u^{j+1} \\ &= \left[\partial_{y_2} \partial_{y_1} + \alpha_2 \varpi \partial_{y_1} + \alpha_1 \varpi \partial_{y_2} + \alpha_1 \alpha_2 \bar{b}_0^2 \right] u^{j+1} + \alpha_1 \alpha_2 [\varpi^2 - \bar{b}_0^2] u^{j+1} \\ &= (\partial_{y_2} + \alpha_2 \varpi)(\partial_{y_1} + \alpha_1 \varpi) u^{j+1}. \end{aligned} \quad (94)$$

With this observation, the corner conditions turns out to be

$$\begin{aligned} (\partial_{y_2} + \alpha_2 \varpi)(\partial_{y_1} + \alpha_1 \varpi) u^{j+1} \Big|_{(y_r, y_t)} &= +\alpha_1 \alpha_2 C_{rt}^{j+1}, & (\partial_{y_2} - \alpha_2 \varpi)(\partial_{y_1} + \alpha_1 \varpi) u^{j+1} \Big|_{(y_r, y_b)} &= -\alpha_1 \alpha_2 C_{br}^{j+1}, \\ (\partial_{y_2} + \alpha_2 \varpi)(\partial_{y_1} - \alpha_1 \varpi) u^{j+1} \Big|_{(y_l, y_t)} &= -\alpha_1 \alpha_2 C_{tl}^{j+1}, & (\partial_{y_2} - \alpha_2 \varpi)(\partial_{y_1} - \alpha_1 \varpi) u^{j+1} \Big|_{(y_l, y_b)} &= +\alpha_1 \alpha_2 C_{lb}^{j+1}, \end{aligned} \quad (95)$$

where

$$C_{a_1 a_2}^{j+1} = \sum_k \sum_{k'} \left[\frac{\bar{b}_k \bar{b}_{k'}}{(1 + \bar{\eta}_k^2)(1 + \bar{\eta}_{k'}^2)} \psi_{k,k',a_1,a_2}^{j,j} \right], \quad a_1 \in \{r, l\}, \quad a_2 \in \{t, b\}.$$

3.1.4. NP-TR

The discrete scheme for the boundary maps is said to be ‘NP-TR’ if the temporal derivatives in the realization of the boundary maps, dubbed as ‘NP’, developed in Sec. 2.2 are discretized using the one-step method TR. The time-discrete form of DtN maps consistent with the staggered samples of field present in (34) on the reference domain reads as

$$\begin{aligned} \sqrt{\beta_1} \partial_{y_1} v^{j+1} \pm e^{-i\pi/4} \left[b_0 v^{j+1} - \sum_{k=1}^M b_k \varphi_{k,a_1}^{j+1/2,j+1/2} \right] &= 0, \\ \sqrt{\beta_2} \partial_{y_2} v^{j+1} \pm e^{-i\pi/4} \left[b_0 v^{j+1} - \sum_{k=1}^M b_k \varphi_{k,a_2}^{j+1/2,j+1/2} \right] &= 0. \end{aligned} \quad (96)$$

In order to obtain a Robin-type boundary condition, we need to compute the discrete values of $\varphi_{k,a_1}^{j+1/2,j+1/2}$ and $\varphi_{k,a_2}^{j+1/2,j+1/2}$ as in the last section. The TR-based discretization of (33) reads as

$$\begin{aligned} \frac{\varphi_{k,a_1}^{j+1,j+1} - \varphi_{k,a_1}^{j,j+1}}{\Delta t} + \eta_k^2 \frac{\varphi_{k,a_1}^{j+1,j+1} + \varphi_{k,a_1}^{j,j+1}}{2} &= \frac{\varphi_{a_1}^{j+1,j+1} + \varphi_{a_1}^{j,j+1}}{2}, \\ \frac{\varphi_{k,a_2}^{j+1,j+1} - \varphi_{k,a_2}^{j+1,j}}{\Delta t} + \eta_k^2 \frac{\varphi_{k,a_2}^{j+1,j+1} + \varphi_{k,a_2}^{j+1,j}}{2} &= \frac{\varphi_{a_2}^{j+1,j+1} + \varphi_{a_2}^{j+1,j}}{2}, \end{aligned} \quad (97)$$

which simplifies to

$$\begin{aligned} \varphi_{k,a_1}^{j+1,j+1} &= \left(\frac{1 - \bar{\eta}_k^2}{1 + \bar{\eta}_k^2} \right) \varphi_{k,a_1}^{j,j+1} + \frac{2/\rho}{(1 + \bar{\eta}_k^2)} \left[v_{a_1}^{j+1} + \frac{\varphi_{a_1}^{j,j+1} - \varphi_{a_1}^{j,j}}{2} \right], \\ \varphi_{k,a_2}^{j+1,j+1} &= \left(\frac{1 - \bar{\eta}_k^2}{1 + \bar{\eta}_k^2} \right) \varphi_{k,a_2}^{j+1,j} + \frac{2/\rho}{(1 + \bar{\eta}_k^2)} \left[v_{a_2}^{j+1} + \frac{\varphi_{a_2}^{j+1,j} - \varphi_{a_2}^{j,j}}{2} \right]. \end{aligned} \quad (98)$$

The staggered samples then work out to be

$$\begin{aligned} \varphi_{k,a_1}^{j+1/2,j+1/2} &= \frac{1}{2} \left[\left(\frac{1 - \bar{\eta}_k^2}{1 + \bar{\eta}_k^2} \right) \varphi_{k,a_1}^{j,j+1} + \varphi_{k,a_1}^{j,j} \right] + \frac{1/\rho}{(1 + \bar{\eta}_k^2)} \left[v_{a_1}^{j+1} + \frac{\varphi_{a_1}^{j,j+1} - \varphi_{a_1}^{j,j}}{2} \right], \\ \varphi_{k,a_2}^{j+1/2,j+1/2} &= \frac{1}{2} \left[\left(\frac{1 - \bar{\eta}_k^2}{1 + \bar{\eta}_k^2} \right) \varphi_{k,a_2}^{j+1,j} + \varphi_{k,a_2}^{j,j} \right] + \frac{1/\rho}{(1 + \bar{\eta}_k^2)} \left[v_{a_2}^{j+1} + \frac{\varphi_{a_2}^{j+1,j} - \varphi_{a_2}^{j,j}}{2} \right]. \end{aligned} \quad (99)$$

Plugging-in the values of $\varphi_{k,a_1}^{j+1/2,j+1/2}$ and $\varphi_{k,a_2}^{j+1/2,j+1/2}$, the maps can be compactly written as

$$\partial_{y_1} v^{j+1} \pm \alpha_1 \varpi v^{j+1} = \mp \alpha_1 \mathcal{B}_{a_1}^{j+1/2}(y_2), \quad \partial_{y_2} v^{j+1} \pm \alpha_2 \varpi v^{j+1} = \mp \alpha_2 \mathcal{B}_{a_2}^{j+1/2}(y_1), \quad (100)$$

where the history functions in this setting are given by

$$\begin{aligned} \mathcal{B}_{a_1}^{j+1/2}(y_2) &= \sum_{k=1}^M \left(\frac{-\bar{b}_k}{2} \left[\left(\frac{1 - \bar{\eta}_k^2}{1 + \bar{\eta}_k^2} \right) \varphi_{k,a_1}^{j,j+1} + \varphi_{k,a_1}^{j,j} \right] + \frac{\Gamma_k}{\rho} \left[\frac{\varphi_{a_1}^{j,j+1} - u_{a_1}^{j,j}}{2} \right] \right), \\ \mathcal{B}_{a_2}^{j+1/2}(y_1) &= \sum_{k=1}^M \left(\frac{-\bar{b}_k}{2} \left[\left(\frac{1 - \bar{\eta}_k^2}{1 + \bar{\eta}_k^2} \right) \varphi_{k,a_2}^{j+1,j} + \varphi_{k,a_2}^{j,j} \right] + \frac{\Gamma_k}{\rho} \left[\frac{\varphi_{a_2}^{j+1,j} - u_{a_1}^{j,j}}{2} \right] \right). \end{aligned} \quad (101)$$

To obtain the discrete samples $\varphi_{k,a_1}^{j+1,j}$ and $\varphi_{k,a_2}^{j+1,j}$ needed to compute the history functions, we employ a Legendre-Galerkin method to solve the IVPs (36) using a TR-based discretization as

$$\begin{aligned} (y_1, y_2) \in \Gamma_b^{\text{ref.}} \cup \Gamma_t^{\text{ref.}} : \quad i \frac{\varphi_{k,a_2}^{j+1,j} - \varphi_{k,a_2}^{j,j}}{\Delta t} + \beta_1 \partial_{y_1}^2 \varphi_{k,a_2}^{j+1/2,j} &= 0 \implies -\alpha_1^{-2} \partial_{y_1}^2 \varphi_{k,a_2}^{j+1/2,j} + \varphi_{k,a_2}^{j+1/2,j} = \varphi_{k,a_2}^{j,j}, \\ (y_1, y_2) \in \Gamma_l^{\text{ref.}} \cup \Gamma_r^{\text{ref.}} : \quad i \frac{\varphi_{k,a_1}^{j,j+1} - \varphi_{k,a_1}^{j,j}}{\Delta t} + \beta_1 \partial_{y_2}^2 \varphi_{k,a_1}^{j,j+1/2} &= 0 \implies -\alpha_1^{-2} \partial_{y_2}^2 \varphi_{k,a_1}^{j,j+1/2} + \varphi_{k,a_1}^{j,j+1/2} = \varphi_{k,a_1}^{j,j}. \end{aligned} \quad (102)$$

The discrete form of the DtN maps (40) for these IVPs can be written as:

$$\begin{aligned} \sqrt{\beta_2} \partial_{y_2} \varphi_{k,a_1}^{j,j+1/2} \pm e^{-i\pi/4} \left[b_0 \varphi_{k,a_1}^{j,j+1/2} - \sum_{k'=1}^M b_{k'} \psi_{k,k',a_1,a_2}^{j,j+1/2} \right] &= 0, \\ \sqrt{\beta_1} \partial_{y_1} \varphi_{k,a_2}^{j+1/2,j} \pm e^{-i\pi/4} \left[b_0 \varphi_{k,a_2}^{j+1/2,j} - \sum_{k'=1}^M b_{k'} \psi_{k,k',a_2,a_1}^{j+1/2,j} \right] &= 0. \end{aligned} \quad (103)$$

In order to arrive at the Robin-type boundary conditions, we invoke TR-based discretization of (39) to write

$$\begin{aligned} \frac{\psi_{k,k',a_1,a_2}^{j,j+1} - \psi_{k,k',a_1,a_2}^{j,j}}{\Delta t} + \eta_{k'}^2 \psi_{k,k',a_1,a_2}^{j,j+1/2} = \varphi_{k,a_1}^{j,j+1/2} &\implies \psi_{k,k',a_1,a_2}^{j,j+1} = \frac{(1 - \bar{\eta}_{k'}^2)}{(1 + \bar{\eta}_{k'}^2)} \psi_{k,k',a_1,a_2}^{j,j} + \frac{2/\rho}{(1 + \bar{\eta}_{k'}^2)} \varphi_{k,a_1}^{j,j+1/2}, \\ \frac{\psi_{k,k',a_2,a_1}^{j+1,j} - \psi_{k,k',a_2,a_1}^{j,j}}{\Delta t} + \eta_{k'}^2 \psi_{k,k',a_2,a_1}^{j+1/2,j} = \varphi_{k,a_2}^{j+1/2,j} &\implies \psi_{k,k',a_2,a_1}^{j+1,j} = \frac{(1 - \bar{\eta}_{k'}^2)}{(1 + \bar{\eta}_{k'}^2)} \psi_{k,k',a_2,a_1}^{j,j} + \frac{2/\rho}{(1 + \bar{\eta}_{k'}^2)} \varphi_{k,a_2}^{j+1/2,j}, \end{aligned} \quad (104)$$

so that the staggered samples work out to be

$$\psi_{k,k',a_1,a_2}^{j,j+1/2} = \frac{1}{(1 + \bar{\eta}_{k'}^2)} \psi_{k,k',a_1,a_2}^{j,j} + \frac{1/\rho}{(1 + \bar{\eta}_{k'}^2)} \varphi_{k,a_1}^{j,j+1/2}, \quad \psi_{k,k',a_2,a_1}^{j+1/2,j} = \frac{1}{(1 + \bar{\eta}_{k'}^2)} \psi_{k,k',a_2,a_1}^{j,j} + \frac{1/\rho}{(1 + \bar{\eta}_{k'}^2)} \varphi_{k,a_2}^{j+1/2,j}. \quad (105)$$

Plugging-in the values of $\psi_{k,k',a_1,a_2}^{j,j+1/2}$ and $\psi_{k,k',a_2,a_1}^{j+1/2,j}$ in (103), we get

$$\begin{aligned} \partial_{y_2} \varphi_{k,a_1}^{j,j+1/2} \pm \alpha_2 \left[\bar{b}_0 + \frac{1}{\rho} \sum_{k'=1}^M \Gamma_{k'} \right] \varphi_{k,a_1}^{j,j+1/2} &= \mp \alpha_2 \sum_{k'=1}^M \Gamma_{k'} \psi_{k,k',a_1,a_2}^{j,j}, \\ \partial_{y_1} \varphi_{k,a_2}^{j+1/2,j} \pm \alpha_1 \left[\bar{b}_0 + \frac{1}{\rho} \sum_{k'=1}^M \Gamma_{k'} \right] \varphi_{k,a_2}^{j+1/2,j} &= \mp \alpha_1 \sum_{k'=1}^M \Gamma_{k'} \psi_{k,k',a_2,a_1}^{j,j}. \end{aligned} \quad (106)$$

Finally, we can express these maps compactly as

$$\partial_{y_2} \varphi_{k,a_1}^{j,j+1/2} \pm \alpha_2 \varpi \varphi_{k,a_1}^{j,j+1/2} = \mp \alpha_2 \mathcal{B}_{k,a_1,a_2}^{j+1}, \quad \partial_{y_1} \varphi_{k,a_2}^{j+1/2,j} \pm \alpha_1 \varpi \varphi_{k,a_2}^{j+1/2,j} = \mp \alpha_1 \mathcal{B}_{k,a_2,a_1}^{j+1}. \quad (107)$$

where the history functions are given by

$$\mathcal{B}_{k,a_1,a_2}^{j+1} = \sum_{k'=1}^M \Gamma_{k'} \psi_{k,k',a_1,a_2}^{j,j}, \quad \mathcal{B}_{k,a_2,a_1}^{j+1} = \sum_{k'=1}^M \Gamma_{k'} \psi_{k,k',a_2,a_1}^{j,j} = \sum_{k'=1}^M \Gamma_{k'} \psi_{k',k,a_1,a_2}^{j,j}, \quad (108)$$

where the second result uses the fact that $\psi_{k,k',a_2,a_1}^{j,j} = \psi_{k',k,a_1,a_2}^{j,j}$ (see Remark 1).

Addressing the diagonal-to-diagonal update for the ψ -function in the order $\psi_{k,k',a_1,a_2}^{j,j} \rightarrow \psi_{k,k',a_1,a_2}^{j,j+1} \rightarrow \psi_{k,k',a_1,a_2}^{j+1,j+1}$, we use (104) and the discrete version of (44) which reads as

$$\begin{aligned} \frac{\psi_{k,k',a_1,a_2}^{j+1,j+1} - \psi_{k,k',a_1,a_2}^{j,j+1}}{\Delta t} + \eta_{k'}^2 \psi_{k,k',a_1,a_2}^{j+1/2,j+1} &= \varphi_{k',a_2}^{j+1/2,j+1}, \\ \psi_{k,k',a_1,a_2}^{j+1,j+1} &= \frac{(1 - \bar{\eta}_{k'}^2)}{(1 + \bar{\eta}_{k'}^2)} \psi_{k,k',a_1,a_2}^{j,j+1} + \frac{2/\rho}{(1 + \bar{\eta}_{k'}^2)} \left[\frac{\varphi_{k',a_2}^{j+1,j+1} + \varphi_{k',a_2}^{j,j+1}}{2} \right]. \end{aligned} \quad (109)$$

To obtain the discrete samples $\varphi_{a_1}^{j,j+1}$ and $\varphi_{a_2}^{j+1,j}$ needed to compute the history functions in (101), we employ a Legendre-Galerkin method to solve the IVPs listed in (24) using a TR-based discretization as

$$\begin{aligned} (y_1, y_2) \in \Gamma_b^{\text{ref.}} \cup \Gamma_t^{\text{ref.}} : \quad i \frac{\varphi_{a_2}^{j+1,j} - \varphi_{a_2}^{j,j}}{\Delta t} + \beta_1 \partial_{y_1}^2 \varphi_{a_2}^{j+1/2,j} &= 0 \implies -\alpha_1^{-2} \partial_{y_1}^2 \varphi_{a_2}^{j+1/2,j} + \varphi_{a_2}^{j+1/2,j} = \varphi_{a_2}^{j,j}, \\ (y_1, y_2) \in \Gamma_l^{\text{ref.}} \cup \Gamma_r^{\text{ref.}} : \quad i \frac{\varphi_{a_1}^{j,j+1} - \varphi_{a_1}^{j,j}}{\Delta t} + \beta_1 \partial_{y_2}^2 \varphi_{a_1}^{j,j+1/2} &= 0 \implies -\alpha_1^{-2} \partial_{y_2}^2 \varphi_{a_1}^{j,j+1/2} + \varphi_{a_1}^{j,j+1/2} = \varphi_{a_1}^{j,j}. \end{aligned} \quad (110)$$

The DtN maps for the IVPs above are given in (25) where we approximate the fractional derivative according to the novel Padé scheme as discussed in Sec. 2.2. To this end, let us introduce the auxiliary functions $\psi_{k,a_2a_1}(\tau_1, \tau_2)$ and $\psi_{k,a_1a_2}(\tau_1, \tau_2)$ such that

$$(\partial_{\tau_1} + \eta_k^2)\psi_{k,a_2a_1}(\tau_1, \tau_2) = \varphi_{a_2}(x_1, \tau_1, \tau_2), \quad (\partial_{\tau_2} + \eta_k^2)\psi_{k,a_1a_2}(\tau_1, \tau_2) = \varphi_{a_1}(x_2, \tau_1, \tau_2). \quad (111)$$

As it turns out, the auxiliary functions, $\psi_{k,a_2a_1}(\tau_1, \tau_2)$ and $\psi_{k,a_1a_2}(\tau_1, \tau_2)$ become identical to $\varphi_{k,a_1}(x_2, \tau_1, \tau_2)$ and $\varphi_{k,a_2}(x_1, \tau_1, \tau_2)$, respectively (see Remark 2). Following along the similar lines as above, we can write the discrete Robin-type boundary conditions for these IVPs as

$$\partial_{y_2}\varphi_{a_1}^{j,j+1/2} \pm \alpha_2\varpi\varphi_{a_1}^{j,j+1/2} = \mp\alpha_2\mathcal{B}_{a_1,a_2}^{j+1}, \quad \partial_{y_1}\varphi_{a_2}^{j+1/2,j} \pm \alpha_1\varpi\varphi_{a_2}^{j+1/2,j} = \mp\alpha_1\mathcal{B}_{a_2,a_1}^{j+1}, \quad (112)$$

where the history functions are given by

$$\mathcal{B}_{a_1,a_2}^{j+1} = \sum_{k=1}^M \Gamma_k \phi_{k,a_2}^{j,j}(y_{a_1}), \quad \mathcal{B}_{a_2,a_1}^{j+1} = \sum_{k=1}^M \Gamma_k \phi_{k,a_1}^{j,j}(y_{a_2}). \quad (113)$$

Remark 2. From the definition of $\psi_{k,a_2a_1}(\tau_1, \tau_2)$ and $\psi_{k,a_1a_2}(\tau_1, \tau_2)$ it follows that

$$\begin{aligned} \psi_{k,a_2a_1}(\tau_1, \tau_2) &= \int_0^{\tau_1} e^{-\eta_k^2(\tau_1-s)} \varphi(x_1, x_2, \tau_2, s) ds = \varphi_{k,a_1}(x_{a_2}, \tau_1, \tau_2), \quad a_2 \in \{b, t\}, \\ \psi_{k,a_1a_2}(\tau_1, \tau_2) &= \int_0^{\tau_2} e^{-\eta_k^2(\tau_2-s)} \varphi(x_1, x_2, s, \tau_1) ds = \varphi_{k,a_2}(x_{a_1}, \tau_1, \tau_2), \quad a_1 \in \{l, r\}. \end{aligned} \quad (114)$$

Note that the discrete samples of the auxiliary functions $\varphi_{k,a_1}(x_2, \tau_1, \tau_2)$ and $\varphi_{k,a_2}(x_1, \tau_1, \tau_2)$ are already being computed in connection with the Robin-type boundary condition for the interior field.

Corner conditions—Following along the similar lines as discussed in the case of NP–BDF1, we can formulate the time-discrete corner conditions for NP–TR as well. At the discrete level, we write the corner conditions consistent with staggered samples of the field present in (45) as

$$\left[\partial_{y_2}\partial_{y_1} + \alpha_2\bar{b}_0\partial_{y_1} + \alpha_1\bar{b}_0\partial_{y_2} + \alpha_1\alpha_2\bar{b}_0^2 \right] v^{j+1} - \alpha_1\alpha_2 \sum_{k=1}^M \sum_{k'=1}^M \bar{b}_k\bar{b}_{k'} \psi_{k,k',a_1,a_2}^{j+1/2,j+1/2} = 0. \quad (115)$$

The diagonal-to-diagonal update of auxiliary fields ψ is already computed in (105) which can be simplified as

$$\begin{aligned} \psi_{k,k',a_1a_2}^{j+1,j+1} &= \frac{(1-\bar{\eta}_k^2)(1-\bar{\eta}_{k'}^2)}{(1+\bar{\eta}_k^2)(1+\bar{\eta}_{k'}^2)} \psi_{k,k',a_1a_2}^{j,j} \\ &+ \frac{(1-\bar{\eta}_k^2)}{(1+\bar{\eta}_k^2)} \frac{1/\rho}{(1+\bar{\eta}_{k'}^2)} [\varphi_{k,a_1}^{j,j+1} + \varphi_{k,a_1}^{j,j}] + \frac{1/\rho}{(1+\bar{\eta}_k^2)} \left(\frac{1-\bar{\eta}_{k'}^2}{1+\bar{\eta}_{k'}^2} \right) [\varphi_{k',a_2}^{j+1,j} + \varphi_{k',a_2}^{j,j}], \\ &+ \frac{1/\rho}{(1+\bar{\eta}_k^2)} \frac{1/\rho}{(1+\bar{\eta}_{k'}^2)} [u^{j+1} + u^j + \varphi_{a_2}^{j+1,j} + \varphi_{a_2}^{j,j+1}]. \end{aligned} \quad (116)$$

The last term in (115) can be expressed in terms of the history functions (101) to obtain

$$\begin{aligned} \sum_k \sum_{k'} \bar{b}_k\bar{b}_{k'} \psi_{k,k',a_1a_2}^{j+1/2,j+1/2} &= \sum_k \sum_{k'} \frac{1}{2} \bar{b}_k\bar{b}_{k'} \left[\left(\frac{1-\bar{\eta}_k^2}{1+\bar{\eta}_k^2} \right) \left(\frac{1-\bar{\eta}_{k'}^2}{1+\bar{\eta}_{k'}^2} \right) \psi_{k,k',a_1a_2}^{j,j} + \psi_{k,k',a_1a_2}^{j,j} \right] \\ &- \frac{1}{\rho} \left[\sum_k \Gamma_k \right] \sum_k \bar{b}_k \left(\frac{-\bar{\eta}_k^2}{1+\bar{\eta}_k^2} \right) [\varphi_{k,a_1}^{j,j} + \varphi_{k,a_2}^{j,j}] + \frac{1}{\rho^2} \left[\sum_k \Gamma_k \right]^2 u^j \\ &+ \frac{1}{\rho} \left[\sum_k \Gamma_k \right] \mathcal{B}_{a_1}^{j+1/2}(y_2) + \frac{1}{\rho} \left[\sum_k \Gamma_k \right] \mathcal{B}_{a_2}^{j+1/2}(y_1) + \frac{1}{\rho^2} \left[\sum_k \Gamma_k \right]^2 v^{j+1}. \end{aligned} \quad (117)$$

Plugging-in the value of $\psi_{k,k',a_1,a_2}^{j+1/2,j+1/2}$ in (115) and collecting all the terms at $(j+1)$ -th time-step on the left hand side, we arrive at the expression

$$\begin{aligned} & \left[\partial_{y_2} \partial_{y_1} + \alpha_2 \varpi \partial_{y_1} + \alpha_1 \varpi \partial_{y_2} + \alpha_1 \alpha_2 \bar{b}_0^{-2} \right] v^{j+1} + \alpha_1 \alpha_2 [2\varpi(\varpi - \bar{b}_0) - (\varpi - \bar{b}_0)^2] v^{j+1} \\ &= \left[\partial_{y_2} \partial_{y_1} + \alpha_2 \varpi \partial_{y_1} + \alpha_1 \varpi \partial_{y_2} + \alpha_1 \alpha_2 \bar{b}_0^{-2} \right] v^{j+1} + \alpha_1 \alpha_2 [\varpi^2 - \bar{b}_0^2] v^{j+1} \\ &= (\partial_{y_2} + \alpha_2 \varpi)(\partial_{y_1} + \alpha_1 \varpi) v^{j+1}. \end{aligned} \quad (118)$$

With this observation, the corner conditions turns out to be

$$\begin{aligned} (\partial_{y_2} + \alpha_2 \varpi)(\partial_{y_1} + \alpha_1 \varpi) v^{j+1} \Big|_{(y_r, y_t)} &= +\alpha_1 \alpha_2 C_{rt}^{j+1/2}, & (\partial_{y_2} - \alpha_2 \varpi)(\partial_{y_1} + \alpha_1 \varpi) v^{j+1} \Big|_{(y_r, y_b)} &= -\alpha_1 \alpha_2 C_{br}^{j+1/2}, \\ (\partial_{y_2} + \alpha_2 \varpi)(\partial_{y_1} - \alpha_1 \varpi) v^{j+1} \Big|_{(y_l, y_t)} &= -\alpha_1 \alpha_2 C_{tl}^{j+1/2}, & (\partial_{y_2} - \alpha_2 \varpi)(\partial_{y_1} - \alpha_1 \varpi) v^{j+1} \Big|_{(y_l, y_b)} &= +\alpha_1 \alpha_2 C_{lb}^{j+1/2}, \end{aligned} \quad (119)$$

where

$$\begin{aligned} C_{a_1 a_2}^{j+1/2} &= \alpha_1 \alpha_2 \sum_k \sum_{k'} \frac{1}{2} \bar{b}_k \bar{b}_{k'} \left[\left(\frac{1 - \bar{\eta}_k^2}{1 + \bar{\eta}_k^2} \right) \left(\frac{1 - \bar{\eta}_{k'}^2}{1 + \bar{\eta}_{k'}^2} \right) \psi_{k,k',a_1 a_2}^{j,j} + \psi_{k,k',a_1 a_2}^{j,j} \right] \\ &\quad - \alpha_1 \alpha_2 \frac{1}{\rho} \left[\sum_k \Gamma_k \right] \sum_k \frac{1}{2} \bar{b}_k \left(\frac{1 - \bar{\eta}_k^2}{1 + \bar{\eta}_k^2} - 1 \right) [\varphi_{k,a_1}^{j,j} + \varphi_{k,a_2}^{j,j}] + \alpha_1 \alpha_2 \frac{1}{\rho^2} \left[\sum_k \Gamma_k \right]^2 u^j, \end{aligned} \quad (120)$$

for $a_1 \in \{r, l\}$ and $a_2 \in \{t, b\}$.

3.2. Numerical solution of the IBVP

So far, we achieved the temporal discretization of the novel boundary conditions developed in this work together with the temporal discretization of the interior problem using one step time-stepping methods namely, BDF1 and TR. For the spatial discretization, we use a Legendre-Galerkin spectral method where we develop a new basis, referred to as the boundary adapted basis [16], in terms of the Legendre polynomials to arrive at a banded linear system. Recall that the Robin-type formulation of boundary maps discussed in this work turns out to be non-homogeneous in nature. The formulation of the linear system using a Legendre-Galerkin method requires us to convert the TBCs from non-homogeneous to homogeneous form which is achieved by using a boundary lifting procedure. Further, we will first address the boundary lifting on the segments followed by the discussion on the rectangular computational domain Ω_i . Set $\mathbb{I} = (-1, 1)$ and let $L_n(y)$ denote the Legendre polynomial of degree n . Define the polynomial space

$$\mathbf{P}_N = \text{Span} \{ L_p(y) \mid p = 0, 1, \dots, N, y \in \mathbb{I} \}. \quad (121)$$

3.2.1. Linear system: 1D

We observed that in order to implement the DtN maps for the interior field, we needed to solve a one-dimensional Schrödinger equation in terms of certain auxiliary functions with boundary segments as the underlying spatial domain together with the accompanying transparent boundary conditions. The recipe comprised two time-like variables, namely, τ_1 and τ_2 , which played the role of the temporal dimension one at a time depending on the boundary segment involved. Therefore, it is worthwhile to consider a model IVP corresponding to the Schrödinger equation in 1D to represent each of the IVPs involved at the boundary segments.

Let $\mathbb{S}_i = (x_-, x_+)$ denote the interior domain in this section. Let us state our model IVP in 1D with transparent boundary conditions as follows:

$$\begin{cases} i\partial_t u + \partial_x^2 u = 0, & (x, t) \in \mathbb{S}_i \times \mathbb{R}_+, \\ u(x, 0) = u_0(x) \in L^2(\mathbb{S}_i), & \text{supp } u_0 \subset \mathbb{S}_i, \\ \partial_n u + e^{-i\pi/4} \partial_t^{1/2} u = 0, & x \in \{x_-, x_+\}, \quad t > 0. \end{cases} \quad (122)$$

For the computational domain \mathbb{S}_i , the reference domain is \mathbb{I} . Let $y \in \mathbb{I}$ such that

$$x = Jy + \bar{x}, \quad J = \frac{1}{2}(x_+ - x_-), \quad \bar{x} = \frac{1}{2}(x_- + x_+), \quad \beta = J^{-2}. \quad (123)$$

Let Δt denote the time-step. Following the earlier convention, $u^j(y)$ is taken to approximate $u(x, j\Delta t)$ for $j = 0, 1, 2, \dots, N_t - 1$ for the sake of brevity of presentation. Also, we formulate the linear system in context of BDF1 time-stepping for the interior problem as well as for discretizing the boundary conditions. The results can be easily extended to the case of TR. Setting $\rho = 1/\Delta t$ and $\alpha = \sqrt{\rho/\beta}e^{-i\pi/4}$, then the BDF1 based discretization of (122) becomes

$$\alpha^{-2}\partial_y^2 u^{j+1} + u^{j+1} = u^j, \quad (\partial_y - \kappa)u^{j+1}\big|_{y=-1} = +\alpha\mathcal{B}_-^{j+1}, \quad (\partial_y + \kappa)u^{j+1}\big|_{y=+1} = -\alpha\mathcal{B}_+^{j+1}, \quad (124)$$

where κ and history functions, \mathcal{B}_\pm^{j+1} , in the Robin-type boundary condition are specific to the method chosen, namely, CQ and NP, for discretizing the boundary conditions. In order to enforce the boundary conditions exactly, we introduce the space of boundary adapted basis functions given by

$$\mathbf{X}_N = \left\{ u \in \mathbf{P}_N \left| \begin{array}{l} (\partial_y - \kappa)u(y)\big|_{y=-1} = 0, \\ (\partial_y + \kappa)u(y)\big|_{y=+1} = 0 \end{array} \right. \right\}. \quad (125)$$

Let the index set $\{0, 1, \dots, N-2\}$ be denoted by \mathbb{J} . Next, we introduce a function χ to convert the discrete TBCs to a homogeneous form by stating the original field as $u^j = w^j + \chi^j(y)$ where $w^j \in \mathbf{X}_N$ so that

$$\alpha^{-2}\partial_y^2 w^{j+1} + w^{j+1} = u^j - \chi^{j+1}, \quad (\partial_y - \kappa)w^{j+1}\big|_{y=-1} = 0, \quad (\partial_y + \kappa)w^{j+1}\big|_{y=+1} = 0, \quad (126)$$

and the field $\chi^j(y)$ is forced to satisfy the constraints below

$$(\partial_y - \kappa)\chi^j(y)\big|_{y=-1} = +\alpha\mathcal{B}_-^j, \quad (\partial_y + \kappa)\chi^j(y)\big|_{y=+1} = -\alpha\mathcal{B}_+^j. \quad (127)$$

The form of the equations suggest the use of an ansatz of the form $\chi^j(y) = c_-^j\chi_- + c_+^j\chi_+$ with $c_-^j = \alpha\mathcal{B}_-^j$ and $c_+^j = -\alpha\mathcal{B}_+^j$ so that the lifting functions satisfy

$$(\partial_y - \kappa) \begin{pmatrix} \chi_- \\ \chi_+ \end{pmatrix} \bigg|_{y=-1} = \begin{pmatrix} 1 \\ 0 \end{pmatrix}, \quad (\partial_y + \kappa) \begin{pmatrix} \chi_- \\ \chi_+ \end{pmatrix} \bigg|_{y=+1} = \begin{pmatrix} 0 \\ 1 \end{pmatrix}. \quad (128)$$

From here, the degree of the lifting functions χ_\pm can be inferred to be utmost 1. Exploiting the fact that we can expand them in terms of Legendre polynomials, we have

$$\begin{pmatrix} \chi_-(y) \\ \chi_+(y) \end{pmatrix} = A_0 \begin{pmatrix} L_0(y) \\ L_1(y) \end{pmatrix}, \quad (129)$$

where A_0 is the unknown transformation matrix. Solving the linear system for A_0 yields

$$\begin{cases} \chi_-(y) = -\frac{1}{2\kappa}L_0(y) + \frac{1}{2(\kappa+1)}L_1(y), \\ \chi_+(y) = +\frac{1}{2\kappa}L_0(y) + \frac{1}{2(\kappa+1)}L_1(y). \end{cases} \quad (130)$$

The lifted field then takes the form

$$u^j(y) = w^j(y) - \frac{\alpha}{2\kappa} [\mathcal{B}_+^j + \mathcal{B}_-^j] L_0(y) - \frac{\alpha}{2(1+\kappa)} [\mathcal{B}_+^j - \mathcal{B}_-^j] L_1(y). \quad (131)$$

Next, we address the construction a basis $\{\phi_p | p \in \mathbb{J}\}$ for \mathbf{X}_N using the ansatz $\phi_p(y) = L_p(y) + a_p L_{p+1}(y) + b_p L_{p+2}(y)$. Imposing the boundary conditions in the definition of \mathbf{X}_N , the sequences $(a_p)_{p \in \mathbb{J}}$ and $(b_p)_{p \in \mathbb{J}}$ work out to be

$$a_p = 0, \quad b_p = -\frac{\kappa + \frac{1}{2}p(p+1)}{\kappa + \frac{1}{2}(p+2)(p+3)}, \quad p \in \mathbb{J}. \quad (132)$$

Invoking the orthogonality property of the Legendre polynomials, system matrices can be computed easily. Denoting the stiffness matrix and the mass matrix for the boundary adapted Legendre basis by $S = (s_{j,k})_{j,k \in \mathbb{J}}$ and $M = (m_{j,k})_{j,k \in \mathbb{J}}$, respectively, where

$$s_{j,k} = -(\phi_j, \phi_k'')_{\mathbb{I}} = \begin{cases} -2(2k+3)b_k, & j = k, \\ 0, & \text{otherwise,} \end{cases} \quad m_{j,k} = (\phi_j, \phi_k)_{\mathbb{I}} = \begin{cases} \frac{2b_{k-2}}{2k+1}, & j = k-2, \\ \frac{2}{2k+1} + \frac{2b_k^2}{2k+5}, & j = k, \\ \frac{2b_k}{2k+5}, & j = k+2, \\ 0 & \text{otherwise,} \end{cases} \quad (133)$$

Therefore, it is evident that the mass matrix is a pentadiagonal symmetric matrix while the stiffness matrix is diagonal.

Within the variational formulation, our goal is to find the approximate solution $u_N \in X_N$ to (124) such that

$$\alpha^{-2}(\partial_y^2 u_N^{j+1}, \phi_p)_{\mathbb{I}} + (u_N^{j+1}, \phi_p)_{\mathbb{I}} = (u_N^j, \phi_p)_{\mathbb{I}}, \quad \phi_p \in X_N, \quad p \in \mathbb{J}, \quad (134)$$

where $(u, \phi)_{\mathbb{I}} = \int_{\mathbb{I}} u \phi dy$ is the scalar product in $L^2(\mathbb{I})$. We approximate u by polynomial interpolation over the Legendre-Gauss-Lobatto (LGL) nodes in the context of discrete Legendre transforms. The variational formulation (134) in terms of the unknown field w^{j+1} (dropping the subscript 'N' for the sake of brevity) can now be stated as

$$-\alpha^{-2}(\partial_y^2 w^{j+1}, \phi_p)_{\mathbb{I}} + (w^{j+1}, \phi_p)_{\mathbb{I}} = (u^j, \phi_p)_{\mathbb{I}} + \alpha (\mathcal{B}_+^{j+1} \chi_+ - \mathcal{B}_-^{j+1} \chi_-, \phi_p)_{\mathbb{I}} \quad (135)$$

Let \tilde{u}_p denote the expansion coefficients of the field in Legendre basis and \widehat{w}_p denote the expansion coefficients in the boundary adapted basis

$$w^{j+1}(y) = \sum_{p' \in \mathbb{J}} \widehat{w}_{p'}^{j+1} \phi_{p'}(y), \quad u^{j+1}(y) = \sum_{p'=0}^N \tilde{u}_{p'}^{j+1} L_{p'}(y). \quad (136)$$

where $\tilde{\mathbf{u}} = (\tilde{u}_0, \tilde{u}_1, \dots, \tilde{u}_N)^\top$ and $\widehat{\mathbf{w}} = (\widehat{w}_0, \widehat{w}_1, \dots, \widehat{w}_{N-2})^\top$. We can compute the inner product terms on LHS in (135) as

$$-(\partial_y^2 w^{j+1}, \phi_p)_{\mathbb{I}} = \sum_{p'} s_{pp'} \widehat{w}_{p'}^{j+1} = (S \widehat{\mathbf{w}}^{j+1})_p, \quad (w^{j+1}, \phi_p)_{\mathbb{I}} = \sum_{p'} m_{pp'} \widehat{w}_{p'}^{j+1} = (M \widehat{\mathbf{w}}^{j+1})_p \quad (137)$$

where M and S denote the mass and stiffness matrices, respectively, defined in (133). In matrix form, the expansion coefficients for the fields in Legendre basis satisfy

$$\tilde{\mathbf{u}}^j = \tilde{\mathbf{w}}^j - \frac{\alpha}{2\kappa} [\mathcal{B}_+^j + \mathcal{B}_-^j] \mathbf{e}_0 - \frac{\alpha}{2(1+\kappa)} [\mathcal{B}_+^j - \mathcal{B}_-^j] \mathbf{e}_1, \quad (138)$$

where $\mathbf{e}_0 = (1, 0, \dots, 0) \in \mathbb{R}^{(N+1) \times 1}$ and $\mathbf{e}_1 = (0, 1, \dots, 0) \in \mathbb{R}^{(N+1) \times 1}$. We seek to further simplify the expression for the linear system by collecting the right hand side of (135) into one term. To this end, let $f^j(y)$ be such that

$$(u^j, \phi_p)_{\mathbb{I}} + \alpha [\mathcal{B}_+^{j+1} (\chi_+, \phi_p)_{\mathbb{I}} - \mathcal{B}_-^{j+1} (\chi_-, \phi_p)_{\mathbb{I}}] = (f^j, \phi_p)_{\mathbb{I}}, \quad (139)$$

then it follows that

$$f^j(y) = u^j(y) + \frac{\alpha}{2\kappa} (\mathcal{B}_+^{j+1} + \mathcal{B}_-^{j+1}) + \frac{\alpha}{2(1+\kappa)} (\mathcal{B}_+^{j+1} - \mathcal{B}_-^{j+1}). \quad (140)$$

In matrix form, the expansion coefficients for the function $f^j(y)$ in the Legendre basis satisfy

$$\tilde{\mathbf{f}}^j = \tilde{\mathbf{u}}^j + \frac{\alpha}{2\kappa} [\mathcal{B}_+^{j+1} + \mathcal{B}_-^{j+1}] \mathbf{e}_0 + \frac{\alpha}{2(1+\kappa)} [\mathcal{B}_+^{j+1} - \mathcal{B}_-^{j+1}] \mathbf{e}_1.$$

Introducing the normalization factors $\gamma_k = \|L_k\|_2^2 = 2/(2k+1)$, $k \in \mathbb{N}_0$, we define the normalization matrix as $\Gamma = \text{diag}(\gamma_0, \gamma_1, \dots, \gamma_N)$. The inner product $(f^j, \phi_p)_{\mathbb{I}}$ can be computed from the knowledge of the Legendre coefficient

\tilde{f}^j using the specific form of the boundary adapted basis. In [Appendix B](#), it is shown that the aforementioned operation can be achieved via a *quadrature matrix* (Q) given by

$$Q = \begin{pmatrix} 1 & 0 & b_0 & & & \\ & 1 & 0 & b_1 & & \\ & & 1 & 0 & b_2 & \\ & & & \ddots & \ddots & \ddots \\ & & & & 1 & 0 & b_{N-2} \end{pmatrix} \in \mathbb{C}^{(N-1) \times (N+1)} \quad \text{such that} \quad (f^j, \phi_p)_{\mathbb{I}} = \left(Q \Gamma \tilde{f}^j \right)_p. \quad (141)$$

The linear system for (135) then becomes

$$\alpha^{-2} S \widehat{w}^{j+1} + M \widehat{w}^{j+1} = Q \Gamma \tilde{f}^j. \quad (142)$$

In our implementation, we have found that, for the space depended variables, it is convenient to store them as samples over the LGL-nodes or as coefficients of their discrete Legendre transform. It is easy to work out that the transpose of the quadrature matrix which transforms Legendre coefficients to that of the boundary adapted basis (see [Appendix B](#)), therefore, storage in terms of the latter is not necessary. This linear system is then solved using LU-decomposition method. The matrix $\alpha^{-2} S + M$ is pentadiagonal. The LU decomposition of this matrix inherits its bandedness provided pivoting is not required [27] and the resulting complexity of solving the linear system becomes $\mathcal{O}(N)$. A thorough study of this issue is beyond the scope of this paper. Let us note that, in the realization of the TBCs, the linear system considered here plays a significant role. For a range of values of Δt , we note that MATLAB arrives at a banded L and U matrix consistent with lack of pivoting.

3.2.2. Linear system: 2D

We formulate the linear system for solving the IBVP (14) in the context of the BDF1 time-stepping for the interior problem as well as for temporal discretization of the boundary conditions. The results can be easily extended to the case of TR. For the 2D problem, we consider the tensor product space $\mathbb{P}_{N_1} \otimes \mathbb{P}_{N_2}$ of the Legendre polynomial spaces \mathbb{P}_{N_j} , $j = 1, 2$. In order to enforce the boundary conditions exactly, we introduce the space of boundary adapted basis given by

$$\mathbb{X}_{N_1} \otimes \mathbb{X}_{N_2} = \left\{ u \in \mathbb{P}_{N_1} \otimes \mathbb{P}_{N_2} \left| \begin{array}{l} (\partial_{y_1} - \kappa_1)u(y_1, y_2) \Big|_{y_1=-1} = 0, \\ (\partial_{y_1} + \kappa_1)u(y_1, y_2) \Big|_{y_1=+1} = 0, \\ (\partial_{y_2} - \kappa_2)u(y_1, y_2) \Big|_{y_2=-1} = 0, \\ (\partial_{y_2} + \kappa_2)u(y_1, y_2) \Big|_{y_2=+1} = 0 \end{array} \right. \right\},$$

where κ_1 and κ_2 are determined by the Robin-type formulation of TBCs specific to the cases, CQ and NP, for temporal discretization of the boundary conditions.

Remark 3. *The form of κ follows from the Robin-type formulation of the discretized version of the DtN-maps as discussed in Sec. 3.1. For CQ methods $\kappa_j = \alpha_j = \sqrt{\rho/\beta_j} \exp(-i\pi/4)$ while for the NP methods, we have $\kappa_j = \alpha_j \varpi$ where $\varpi = \sqrt{\rho} R_M(\rho)$ as defined in (82) for $j = 1, 2$.*

Let the index set $\{0, 1, \dots, N_j - 2\}$ be denoted by \mathbb{J}_j for $j = 1, 2$. We once again introduce a function χ in order to homogenize the Robin-type formulation of the discrete TBCs such that $u^{j+1} = w^{j+1} + \chi^{j+1}(y_1, y_2)$ where $w^j \in \mathbb{X}_{N_1} \otimes \mathbb{X}_{N_2}$ so that the interior problem in (52) reads as

$$-\left(\alpha_1^{-2} \partial_{y_1}^2 + \alpha_2^{-2} \partial_{y_2}^2 \right) w^{j+1} + w^{j+1} = u^j - \chi^{j+1} + \left(\alpha_1^{-2} \partial_{y_1}^2 + \alpha_2^{-2} \partial_{y_2}^2 \right) \chi^{j+1}, \quad (143)$$

now with the homogeneous TBCs given by

$$\begin{aligned} (\partial_{y_1} - \kappa_1)w^{j+1}(y_1, y_2) \Big|_{y_1=-1} &= 0, & (\partial_{y_2} - \kappa_2)w^{j+1}(y_1, y_2) \Big|_{y_2=-1} &= 0, \\ (\partial_{y_1} + \kappa_1)w^{j+1}(y_1, y_2) \Big|_{y_1=+1} &= 0, & (\partial_{y_2} + \kappa_2)w^{j+1}(y_1, y_2) \Big|_{y_2=+1} &= 0. \end{aligned} \quad (144)$$

The field $\chi^{j+1}(y_1, y_2)$ is forced to satisfy the following constraints on the segments

$$\begin{aligned} (\partial_{y_1} + \kappa_1)\chi^{j+1}(y_1, y_2)\Big|_{y_1=y_r} &= -\alpha_1\mathcal{B}_r^{j+1}(y_2), & (\partial_{y_2} + \kappa_2)\chi^{j+1}(y_1, y_2)\Big|_{y_2=y_t} &= -\alpha_2\mathcal{B}_t^{j+1}(y_1), \\ (\partial_{y_1} - \kappa_1)\chi^{j+1}(y_1, y_2)\Big|_{y_1=y_l} &= +\alpha_1\mathcal{B}_l^{j+1}(y_2), & (\partial_{y_2} - \kappa_2)\chi^{j+1}(y_1, y_2)\Big|_{y_2=y_b} &= +\alpha_2\mathcal{B}_b^{j+1}(y_1), \end{aligned} \quad (145)$$

together with the constraints on the corners below

$$\begin{aligned} (\partial_{y_1} + \kappa_1)(\partial_{y_2} + \kappa_2)\chi^{j+1}(y_1, y_2)\Big|_{(y_r, y_t)} &= +\alpha_1\alpha_2\mathcal{C}_{rt}^{j+1}, & (\partial_{y_1} - \kappa_1)(\partial_{y_2} - \kappa_2)\chi^{j+1}(y_1, y_2)\Big|_{(y_l, y_b)} &= +\alpha_1\alpha_2\mathcal{C}_{lb}^{j+1}, \\ (\partial_{y_1} + \kappa_1)(\partial_{y_2} - \kappa_2)\chi^{j+1}(y_1, y_2)\Big|_{(y_r, y_b)} &= -\alpha_1\alpha_2\mathcal{C}_{rb}^{j+1}, & (\partial_{y_1} - \kappa_1)(\partial_{y_2} + \kappa_2)\chi^{j+1}(y_1, y_2)\Big|_{(y_l, y_t)} &= -\alpha_1\alpha_2\mathcal{C}_{lt}^{j+1}. \end{aligned} \quad (146)$$

These boundary condition are taken from Sec. 3.1 where precise definition of the quantities are provided. We can express these operators compactly by introducing the notation $\partial_1^\pm \equiv (\partial_{y_1} \pm \alpha_1)$, $\partial_2^\pm \equiv (\partial_{y_2} \pm \alpha_2)$. Therefore,

$$\begin{aligned} \partial_1^+\partial_2^+\chi^{j+1}(y_1, y_2)\Big|_{(y_r, y_t)} &= +\alpha_1\alpha_2\mathcal{C}_{rt}^{j+1}, & \partial_1^-\partial_2^-\chi^{j+1}(y_1, y_2)\Big|_{(y_l, y_b)} &= +\alpha_1\alpha_2\mathcal{C}_{lb}^{j+1}, \\ \partial_1^+\partial_2^-\chi^{j+1}(y_1, y_2)\Big|_{(y_r, y_b)} &= -\alpha_1\alpha_2\mathcal{C}_{rb}^{j+1}, & \partial_1^-\partial_2^+\chi^{j+1}(y_1, y_2)\Big|_{(y_l, y_t)} &= -\alpha_1\alpha_2\mathcal{C}_{lt}^{j+1}. \end{aligned} \quad (147)$$

The form of the equations suggest an ansatz of the form

$$\chi^{j+1} = \eta^{j+1} + \alpha_1\alpha_2\mathcal{C}_{rt}^{j+1}\chi_{rt} + \alpha_1\alpha_2\mathcal{C}_{lb}^{j+1}\chi_{lb} - \alpha_1\alpha_2\mathcal{C}_{rb}^{j+1}\chi_{rb} - \alpha_1\alpha_2\mathcal{C}_{lt}^{j+1}\chi_{lt}, \quad (148)$$

where η^{j+1} satisfy

$$\begin{aligned} \partial_1^+\partial_2^+\eta^{j+1}(y_1, y_2)\Big|_{(y_r, y_t)} &= 0, & \partial_1^-\partial_2^-\eta^{j+1}(y_1, y_2)\Big|_{(y_l, y_b)} &= 0, \\ \partial_1^+\partial_2^-\eta^{j+1}(y_1, y_2)\Big|_{(y_r, y_b)} &= 0, & \partial_1^-\partial_2^+\eta^{j+1}(y_1, y_2)\Big|_{(y_l, y_t)} &= 0. \end{aligned} \quad (149)$$

Here, we suppress the temporal index j for the sake of brevity of presentation. Following along the similar lines as that of boundary lifting in 1D, we can set up the constraint equations for the lift functions as following:

$$\partial_1^+\partial_2^+\begin{pmatrix} \chi_{rt} \\ \chi_{lb} \\ \chi_{rb} \\ \chi_{lt} \end{pmatrix}\Big|_{(y_r, y_t)} = \begin{pmatrix} 1 \\ 0 \\ 0 \\ 0 \end{pmatrix}, \quad \partial_1^-\partial_2^-\begin{pmatrix} \chi_{rt} \\ \chi_{lb} \\ \chi_{rb} \\ \chi_{lt} \end{pmatrix}\Big|_{(y_l, y_b)} = \begin{pmatrix} 0 \\ 1 \\ 0 \\ 0 \end{pmatrix}, \quad \partial_1^+\partial_2^-\begin{pmatrix} \chi_{rt} \\ \chi_{lb} \\ \chi_{rb} \\ \chi_{lt} \end{pmatrix}\Big|_{(y_r, y_b)} = \begin{pmatrix} 0 \\ 0 \\ 1 \\ 0 \end{pmatrix}, \quad \partial_1^-\partial_2^+\begin{pmatrix} \chi_{rt} \\ \chi_{lb} \\ \chi_{rb} \\ \chi_{lt} \end{pmatrix}\Big|_{(y_l, y_t)} = \begin{pmatrix} 0 \\ 0 \\ 0 \\ 1 \end{pmatrix}. \quad (150)$$

From here, the degree of the lifting functions can be inferred to be utmost 1 in terms of each of the independent variables. Exploiting the fact that we can expand them in terms of Legendre polynomials, we have

$$\begin{pmatrix} \chi_{rt} \\ \chi_{lb} \\ \chi_{rb} \\ \chi_{lt} \end{pmatrix} = C \begin{pmatrix} L_0(y_1)L_0(y_2) \\ L_0(y_1)L_1(y_2) \\ L_1(y_1)L_0(y_2) \\ L_1(y_1)L_1(y_2) \end{pmatrix}, \quad (151)$$

where C is the unknown transformation matrix. Solving the linear system for C yields

$$\begin{aligned} \chi_{rt}(y_1, y_2) &= \chi_r(y_1)\chi_t(y_2), & \chi_{lb}(y_1, y_2) &= \chi_l(y_1)\chi_b(y_2), \\ \chi_{rb}(y_1, y_2) &= \chi_r(y_1)\chi_b(y_2), & \chi_{lt}(y_1, y_2) &= \chi_l(y_1)\chi_t(y_2), \end{aligned} \quad (152)$$

where

$$\begin{cases} \chi_r(y_1) = +\frac{1}{2\kappa_1}L_0(y_1) + \frac{1}{2(\kappa_1 + 1)}L_1(y_1), \\ \chi_l(y_1) = -\frac{1}{2\kappa_1}L_0(y_1) + \frac{1}{2(\kappa_1 + 1)}L_1(y_1), \end{cases} \quad \text{and} \quad \begin{cases} \chi_t(y_2) = +\frac{1}{2\kappa_2}L_0(y_2) + \frac{1}{2(\kappa_2 + 1)}L_1(y_2), \\ \chi_b(y_2) = -\frac{1}{2\kappa_2}L_0(y_2) + \frac{1}{2(\kappa_2 + 1)}L_1(y_2). \end{cases} \quad (153)$$

Plugging-in the form of χ in (145) and favouring η , we get

$$\begin{aligned}
\partial_1^+ \eta(y_1, y_2) \Big|_{y_1=y_r} &= -\alpha_1 [\mathcal{B}_r(y_2) - \alpha_2 C_{rb} \chi_b(y_2) + \alpha_2 C_{rt} \chi_t(y_2)], \\
\partial_1^- \eta(y_1, y_2) \Big|_{y_1=y_l} &= +\alpha_1 [\mathcal{B}_l(y_2) - \alpha_2 C_{lb} \chi_b(y_2) + \alpha_2 C_{lt} \chi_t(y_2)], \\
\partial_2^+ \eta(y_1, y_2) \Big|_{y_2=y_l} &= -\alpha_2 [\mathcal{B}_l(y_1) - \alpha_1 C_{lt} \chi_l(y_1) + \alpha_1 C_{rt} \chi_r(y_1)], \\
\partial_2^- \eta(y_1, y_2) \Big|_{y_2=y_b} &= +\alpha_2 [\mathcal{B}_b(y_1) - \alpha_1 C_{lb} \chi_l(y_1) + \alpha_1 C_{rb} \chi_r(y_1)].
\end{aligned} \tag{154}$$

We can rewrite the set of equations above by identifying the RHS as:

$$\begin{aligned}
\partial_1^+ \eta(y_1, y_2) \Big|_{y_1=y_r} &= -\alpha_1 \check{\mathcal{B}}_r(y_2), & \partial_2^+ \eta(y_1, y_2) \Big|_{y_2=y_l} &= -\alpha_2 \check{\mathcal{B}}_l(y_1), \\
\partial_1^- \eta(y_1, y_2) \Big|_{y_1=y_l} &= +\alpha_1 \check{\mathcal{B}}_l(y_2), & \partial_2^- \eta(y_1, y_2) \Big|_{y_2=y_b} &= +\alpha_2 \check{\mathcal{B}}_b(y_1).
\end{aligned} \tag{155}$$

Restoring the superscripts, the system above can be solved in a similar manner as that of 1D case yielding

$$\eta^{j+1} = -\alpha_1 \chi_r(y_1) \check{\mathcal{B}}_r^{j+1}(y_2) + \alpha_1 \chi_l(y_1) \check{\mathcal{B}}_l^{j+1}(y_2) - \alpha_2 \check{\mathcal{B}}_l^{j+1}(y_1) \chi_t(y_2) + \alpha_2 \check{\mathcal{B}}_b^{j+1}(y_1) \chi_b(y_2). \tag{156}$$

The lifted field $u^{j+1} = w^{j+1} + \chi^{j+1}(y_1, y_2)$ now expands to

$$\begin{aligned}
u^{j+1} &= w^{j+1} - \alpha_1 \chi_r(y_1) \mathcal{B}_r^{j+1}(y_2) + \alpha_1 \chi_l(y_1) \mathcal{B}_l^{j+1}(y_2) - \alpha_2 \mathcal{B}_l^{j+1}(y_1) \chi_t(y_2) + \alpha_2 \mathcal{B}_b^{j+1}(y_1) \chi_b(y_2) \\
&\quad - \alpha_1 \alpha_2 C_{rt}^{j+1} \chi_r(y_1) \chi_t(y_2) - \alpha_1 \alpha_2 C_{lb}^{j+1} \chi_l(y_1) \chi_b(y_2) + \alpha_1 \alpha_2 C_{rb}^{j+1} \chi_r(y_1) \chi_b(y_2) + \alpha_1 \alpha_2 C_{lt}^{j+1} \chi_l(y_1) \chi_t(y_2).
\end{aligned} \tag{157}$$

Next, we address the construction of the basis for the boundary adapted space $\mathbb{X}_{N_1} \otimes \mathbb{X}_{N_2}$ by using the ansatz

$$\theta_{p_1, p_2}(y_1, y_2) = \phi_{p_1}^{(1)}(y_1) \phi_{p_2}^{(2)}(y_2), \tag{158}$$

where

$$\phi_{p_j}^{(j)}(y_j) = L_{p_j}(y_j) + a_{p_j}^{(j)} L_{p_j+1}(y_j) + b_{p_j}^{(j)} L_{p_j+2}(y_j), \quad p_1 \in \mathbb{J}_1, \quad p_2 \in \mathbb{J}_2. \tag{159}$$

Imposing the boundary conditions in the definition of $\mathbb{X}_{N_1} \otimes \mathbb{X}_{N_2}$, the sequences $\{a_{p_j}^{(j)}\}$ and $\{b_{p_j}^{(j)}\}$ work out to be

$$a_{p_j}^{(j)} = 0, \quad b_{p_j}^{(j)} = -\frac{\kappa_j + \frac{1}{2} p_j (p_j + 1)}{\kappa_j + \frac{1}{2} (p_j + 2)(p_j + 3)}, \quad p_j \in \mathbb{J}_j, \quad j = 1, 2. \tag{160}$$

The stiffness matrix and the mass matrix for the boundary adapted Legendre basis are denoted by $S_p = (\mathfrak{s}_{kj}^{(p)})_{k, j \in \mathbb{J}_p}$ and $M_p = (\mathfrak{m}_{kj}^{(p)})_{k, j \in \mathbb{J}_p}$, $p = 1, 2$, respectively, where

$$\mathfrak{s}_{jk}^{(p)} = -\left(\phi_j^{(p)}, \partial_{y_l}^2 \phi_k^{(p)}\right)_{\mathbb{I}} = \begin{cases} -2(2k+3)b_k^{(p)}, & j = k, \\ 0, & \text{otherwise,} \end{cases} \quad \mathfrak{m}_{jk}^{(p)} = \left(\phi_j^{(p)}, \phi_k^{(p)}\right)_{\mathbb{I}} = \begin{cases} \frac{2b_{k-2}^{(p)}}{2k+1}, & j = k-2, \\ \frac{2}{2k+1} + \frac{2(b_k^{(p)})^2}{2k+5}, & j = k, \\ \frac{2b_k^{(p)}}{2k+5}, & j = k+2, \\ 0 & \text{otherwise.} \end{cases} \tag{161}$$

It is interesting to note that mass matrices are pentadiagonal and stiffness matrices are simply diagonal.

Within the variational formulation, our goal is to find the approximate solution $u_{N_1, N_2} \in \mathbb{X}_{N_1} \otimes \mathbb{X}_{N_2}$ for the interior problem in (52):

$$-\alpha_1^{-2} \left(\partial_{y_1}^2 u_{N_1, N_2}^{j+1}, \theta_{p_1, p_2}\right)_{\Omega_{\text{ref}}} - \alpha_2^{-2} \left(\partial_{y_2}^2 u_{N_1, N_2}^{j+1}, \theta_{p_1, p_2}\right)_{\Omega_{\text{ref}}} + \left(u_{N_1, N_2}^{j+1}, \theta_{p_1, p_2}\right)_{\Omega_{\text{ref}}} = \left(u_{N_1, N_2}^j, \theta_{p_1, p_2}\right)_{\Omega_{\text{ref}}}, \quad \theta_{p_1, p_2} \in \mathbb{X}_{N_1} \otimes \mathbb{X}_{N_2}, \tag{162}$$

where $(u, \theta)_{\Omega_i^{\text{ref}}} = \int_{\Omega_i^{\text{ref}}} u \theta d^2 \mathbf{y}$ is the scalar product in $L^2(\Omega_i^{\text{ref}})$. The variational formulation defined above can be expressed in terms of unknown field w^{j+1} (dropping the subscripts ‘ N_1 ’ and ‘ N_2 ’ for the sake of brevity) as

$$\begin{aligned} & -\alpha_1^{-2} \left(\partial_{y_1}^2 w^{j+1}, \theta_{p_1, p_2} \right)_{\Omega_i^{\text{ref}}} - \alpha_2^{-2} \left(\partial_{y_2}^2 w^{j+1}, \theta_{p_1, p_2} \right)_{\Omega_i^{\text{ref}}} + \left(w^{j+1}, \theta_{p_1, p_2} \right)_{\Omega_i^{\text{ref}}} \\ & = \left(u^j - \chi^{j+1}, \theta_{p_1, p_2} \right)_{\Omega_i^{\text{ref}}} + \alpha_1^{-2} \left(\partial_{y_1}^2 \chi^{j+1}, \theta_{p_1, p_2} \right)_{\Omega_i^{\text{ref}}} + \alpha_2^{-2} \left(\partial_{y_2}^2 \chi^{j+1}, \theta_{p_1, p_2} \right)_{\Omega_i^{\text{ref}}}. \end{aligned} \quad (163)$$

Next, we simplify the second order derivative terms on the right hand side as:

$$\begin{aligned} \partial_{y_1}^2 \chi^{j+1} &= -\alpha_2 \partial_{y_1}^2 \mathcal{B}_t^{j+1}(y_1) \chi_t(y_2) + \alpha_2 \partial_{y_1}^2 \mathcal{B}_b^{j+1}(y_1) \chi_b(y_2), \\ \partial_{y_2}^2 \chi^{j+1} &= -\alpha_1 \partial_{y_2}^2 \mathcal{B}_r^{j+1}(y_2) \chi_r(y_1) + \alpha_1 \partial_{y_2}^2 \mathcal{B}_l^{j+1}(y_2) \chi_l(y_1). \end{aligned} \quad (164)$$

Let $\tilde{u}_{p, p'}$ denote the expansion coefficients of the field in Legendre basis and $\widehat{w}_{p, p'}$ denote the expansion coefficients in the boundary adapted basis as

$$u^{j+1}(y_1, y_2) = \sum_{p'=0}^{N_1} \sum_{q'=0}^{N_2} \tilde{u}_{p', q'}^{j+1} L_{p'}(y_1) L_{q'}(y_2), \quad \text{and} \quad w^{j+1}(y_1, y_2) = \sum_{p' \in \mathbb{J}_1} \sum_{q' \in \mathbb{J}_2} \widehat{w}_{p', q'}^{j+1} \phi_{p'}^{(1)}(y_1) \phi_{q'}^{(2)}(y_2), \quad (165)$$

respectively. Let us introduce the matrices $\widehat{W} = (\widehat{w}_{p', q'})_{p' \in \mathbb{J}_1, q' \in \mathbb{J}_2}$ and $\widetilde{U} = (\tilde{u}_{p', q'})_{0 \leq p' \leq N_1, 0 \leq q' \leq N_2}$ for convenience. In matrix form, the expansion coefficients for the fields introduced in (157) in the Legendre basis assume the form

$$\begin{aligned} \widetilde{U}^{j+1} &= \widetilde{W}^{j+1} - \frac{\alpha_1}{2\kappa_1} \mathbf{e}_0^{(1)} \otimes (\widetilde{\mathcal{B}}_r^{j+1} + \widetilde{\mathcal{B}}_l^{j+1})^\top - \frac{\alpha_1}{2(\kappa_1 + 1)} \mathbf{e}_1^{(1)} \otimes (\widetilde{\mathcal{B}}_r^{j+1} - \widetilde{\mathcal{B}}_l^{j+1})^\top \\ & - \frac{\alpha_2}{2\kappa_2} (\widetilde{\mathcal{B}}_t^{j+1} + \widetilde{\mathcal{B}}_b^{j+1}) \otimes (\mathbf{e}_0^{(2)})^\top - \frac{\alpha_2}{2(\kappa_2 + 1)} (\widetilde{\mathcal{B}}_t^{j+1} - \widetilde{\mathcal{B}}_b^{j+1}) \otimes (\mathbf{e}_1^{(2)})^\top \\ & - \frac{\alpha_1 \alpha_2}{4\kappa_1 \kappa_2} (C_{rt}^{j+1} + C_{lb}^{j+1} + C_{rb}^{j+1} + C_{lt}^{j+1}) \mathbf{e}_0^{(1)} \otimes (\mathbf{e}_0^{(2)})^\top \\ & - \frac{\alpha_1 \alpha_2}{4\kappa_1 (\kappa_2 + 1)} (C_{rt}^{j+1} - C_{lb}^{j+1} - C_{rb}^{j+1} + C_{lt}^{j+1}) \mathbf{e}_0^{(1)} \otimes (\mathbf{e}_1^{(2)})^\top \\ & - \frac{\alpha_1 \alpha_2}{4\kappa_2 (\kappa_1 + 1)} (C_{rt}^{j+1} - C_{lb}^{j+1} + C_{rb}^{j+1} - C_{lt}^{j+1}) \mathbf{e}_1^{(1)} \otimes (\mathbf{e}_0^{(2)})^\top \\ & - \frac{\alpha_1 \alpha_2}{4(\kappa_1 + 1)(\kappa_2 + 1)} (C_{rt}^{j+1} + C_{lb}^{j+1} - C_{rb}^{j+1} - C_{lt}^{j+1}) \mathbf{e}_1^{(1)} \otimes (\mathbf{e}_1^{(2)})^\top, \end{aligned} \quad (166)$$

where the hat and tilde convention is extended to other quantities as well. We seek to further simplify the expression for the linear system by collecting the right hand side of (163) into one term. To this end, let $f^j(y_1, y_2)$ be such that

$$(f^j, \theta_{p_1, p_2}) = (u^j - \chi^{j+1}, \theta_{p_1, p_2}) + \alpha_1^{-2} \left(\partial_{y_1}^2 \chi^{j+1}, \theta_{p_1, p_2} \right) + \alpha_2^{-2} \left(\partial_{y_2}^2 \chi^{j+1}, \theta_{p_1, p_2} \right). \quad (167)$$

In matrix form, the expansion coefficients for the function $f^j(y_1, y_2)$ in the Legendre basis satisfy

$$\begin{aligned} \widetilde{F}^j &= \widetilde{U}^j + \frac{\alpha_1}{2\kappa_1} \mathbf{e}_0^{(1)} \otimes (\widetilde{\mathcal{B}}_r^{j+1} + \widetilde{\mathcal{B}}_l^{j+1})^\top \mathcal{D}_2^\top + \frac{\alpha_1}{2(\kappa_1 + 1)} \mathbf{e}_1^{(1)} \otimes (\widetilde{\mathcal{B}}_r^{j+1} - \widetilde{\mathcal{B}}_l^{j+1})^\top \mathcal{D}_2^\top \\ & + \frac{\alpha_2}{2\kappa_2} \mathcal{D}_1 (\widetilde{\mathcal{B}}_t^{j+1} + \widetilde{\mathcal{B}}_b^{j+1}) \otimes (\mathbf{e}_0^{(2)})^\top + \frac{\alpha_2}{2(\kappa_2 + 1)} \mathcal{D}_1 (\widetilde{\mathcal{B}}_t^{j+1} - \widetilde{\mathcal{B}}_b^{j+1}) \otimes (\mathbf{e}_1^{(2)})^\top + \widetilde{G}^{j+1}, \end{aligned} \quad (168)$$

where $\mathcal{D}_k : 1 - \alpha_k^{-2} \partial_{y_k}^2$, $k = 1, 2$, are symbolic representations of the second order differential operators⁵ and

$$\widetilde{G}^{j+1} = (\widetilde{g}_{p_1, p_2}^{j+1}) = \begin{cases} \frac{\alpha_1 \alpha_2}{4\kappa_1 (\kappa_2 + 1)} (C_{rt}^{j+1} + C_{lb}^{j+1} + C_{rb}^{j+1} + C_{lt}^{j+1}), & p_1 = 0, p_2 = 0, \\ \frac{\alpha_1 \alpha_2}{4\kappa_1 (\kappa_2 + 1)} (C_{rt}^{j+1} - C_{lb}^{j+1} - C_{rb}^{j+1} + C_{lt}^{j+1}), & p_1 = 0, p_2 = 1, \\ \frac{\alpha_1 \alpha_2}{4\kappa_2 (\kappa_1 + 1)} (C_{rt}^{j+1} - C_{lb}^{j+1} + C_{rb}^{j+1} - C_{lt}^{j+1}), & p_1 = 1, p_2 = 0, \\ \frac{\alpha_1 \alpha_2}{4(\kappa_1 + 1)(\kappa_2 + 1)} (C_{rt}^{j+1} + C_{lb}^{j+1} - C_{rb}^{j+1} - C_{lt}^{j+1}), & p_1 = 1, p_2 = 1, \\ 0, & p_1 = 2, \dots, N_1, p_2 = 2, \dots, N_2, \end{cases} \quad (169)$$

⁵We would like to mention that the second order derivative of the history functions will be handled by first expanding them in the Legendre basis and then using the backward recursion in the frequency space to obtain the expansion coefficients for $\partial_{y_k}^2 \mathcal{B}^{j+1}(y_k)$, $k = 1, 2$. For more details the reader is referred to Shen [28, Chap. 3].

The variational formulation in (163) now takes the form

$$-\alpha_1^{-2} \left(\partial_{y_1}^2 w^{j+1}, \theta_{p_1, p_2} \right)_{\Omega_i^{\text{ref}}} - \alpha_2^{-2} \left(\partial_{y_2}^2 w^{j+1}, \theta_{p_1, p_2} \right)_{\Omega_i^{\text{ref}}} + \left(w^{j+1}, \theta_{p_1, p_2} \right)_{\Omega_i^{\text{ref}}} = \left(f^j, \theta_{p_1, p_2} \right)_{\Omega_i^{\text{ref}}}. \quad (170)$$

The inner product $(f^j, \theta_{p_1, p_2})_{\Omega_i^{\text{ref}}}$ can be computed from the knowledge of the Legendre coefficients \tilde{F}^j using the specific form of the boundary adapted basis. In Appendix B, it is shown that the aforementioned operation can be achieved via *quadrature matrices* (Q_j) given by

$$Q_j = B_j^T = \begin{pmatrix} 1 & 0 & b_0^{(j)} & & & & \\ & 1 & 0 & b_1^{(j)} & & & \\ & & 1 & 0 & b_2^{(j)} & & \\ & & & \ddots & \ddots & \ddots & \\ & & & & 1 & 0 & b_{N-2}^{(j)} \end{pmatrix} \in \mathbb{C}^{(N-1) \times (N+1)}, \quad j = 1, 2. \quad (171)$$

The linear system thus becomes

$$\begin{aligned} \alpha_1^{-2} S_1^T \widehat{W}^{j+1} M_2 + \alpha_2^{-2} M_1^T \widehat{W}^{j+1} S_2 + M_1^T \widehat{W}^{j+1} M_2 &= Q_1 \Gamma \tilde{F}^j \Gamma Q_2^T \equiv \widehat{F}, \\ \left(\alpha_1^{-2} M_2^T \otimes S_1^T + \alpha_2^{-2} S_2^T \otimes M_1^T + M_2^T \otimes M_1^T \right) \widehat{\mathbf{w}}^{j+1} &= \widehat{\mathbf{f}}^j, \end{aligned} \quad (172)$$

where \otimes denotes the tensor product and $\widehat{\mathbf{w}}$, $\widehat{\mathbf{f}}$ denote the column vectors obtained by stacking columns of matrices \widehat{W} , \widehat{F} , respectively, below one another. The mass and stiffness matrices are defined in (161) and the linear system is then solved using LU-decomposition method. In order to understand the sparsity pattern of the system matrix, we proceed as follows: Taking into account the symmetric nature of the mass matrices (noting stiffness matrices are already diagonal), we have

$$\left(\alpha_1^{-2} M_2^T \otimes S_1^T + \alpha_2^{-2} S_2^T \otimes M_1^T + M_2^T \otimes M_1^T \right) = \left(\alpha_2^{-2} S_2 + M_2 \right) \otimes \left(\alpha_1^{-2} S_1 + M_1 \right) - \alpha_2^{-2} \alpha_1^{-2} \left(S_2 \otimes S_1 \right). \quad (173)$$

From the property of Kronecker product, it follows that the system matrix is symmetric block pentadiagonal because the individual matrices in the Kronecker product are symmetric pentadiagonal in nature. The upper and lower bandwidth works out to be $2N_1$. The cost of LU decomposition can be worked out to be $\mathcal{O}(N_1^2 N_{\text{dim}})$ where $N_{\text{dim}} = (N_1 - 1)(N_2 - 1)$. The lower and upper triangular matrices inherit the bandedness of the system matrix provided pivoting is not required [27]. Under this assumption, the resulting complexity of solving the linear system (excluding the cost of LU decomposition) becomes $\mathcal{O}(N_1 N_{\text{dim}})$. A thorough study of this issue is beyond the scope of this paper. For a range of values of Δt , we note that MATLAB arrives at banded lower and upper triangular matrices which is consistent with lack of pivoting.

3.3. Algorithmic summary

In this section, we present a brief algorithmic summary for the CQ and NP methods in context of BDF1 based temporal discretization of the boundary maps and also the interior problem. For the TR case, the algorithmic steps are largely similar.

3.3.1. CQ-BDF1

Let us recall that, on the boundary segments Γ_{a_1} and Γ_{a_2} , the auxiliary function is denoted by $\varphi_{a_1}(y_2, \tau_1, \tau_2)$ and $\varphi_{a_2}(y_1, \tau_1, \tau_2)$, respectively, while the auxiliary function at the corners is denoted by $\varphi_{a_1 a_2}(\tau_1, \tau_2)$ where $a_1 \in \{l, r\}$, $a_2 \in \{b, t\}$. Let N be the number of spatial nodes along y_1 as well as y_2 , i.e., $N_1 = N_2 = N$. Let the number of time-steps be denoted by N_t . The temporal variables t , τ_1 and τ_2 are discretized with the same step-size Δt so that the maximum time $T = N_t \Delta t$. The storage of the auxiliary field on the boundary segments require four 3D-arrays of size $N \times N_t \times N_t$ and the storage of auxiliary field at corner points require four 2D-arrays of size $N_t \times N_t$ which corresponds to $\varphi_{a_1 a_2}(\tau_1, \tau_2)$. The algorithmic steps for the solving the IBVP are enumerated below.

Step 1: Advance the following IVPs corresponding to auxiliary functions by one-step, say, $j \rightarrow (j + 1)$ using the previously computed values of the auxiliary field on the segments (as described in Fig. 2):

$$\begin{aligned} -\alpha_1^{-2} \partial_{y_1}^2 \varphi_{a_2}^{j+1,q} + \varphi_{a_2}^{j+1,q} &= \varphi_{a_2}^{j,q}, \quad q = 0, 1, \dots, j, \\ -\alpha_2^{-2} \partial_{y_2}^2 \varphi_{a_1}^{m,j+1} + \varphi_{a_1}^{m,j+1} &= \varphi_{a_1}^{m,j}, \quad m = 0, 1, \dots, j, \end{aligned}$$

using the TBCs at the corner points given by

$$(\partial_{n_1} + \alpha_1) \varphi_{a_2}^{j+1,q}(y_{a_1}) = -\alpha_1 \mathcal{B}_{a_2, a_1}^{j+1,q}, \quad (\partial_{n_2} + \alpha_2) \varphi_{a_1}^{m,j+1}(y_{a_2}) = -\alpha_2 \mathcal{B}_{a_1, a_2}^{m,j+1},$$

where the history functions are computed as

$$\mathcal{B}_{a_2, a_1}^{j+1,q} = \sum_{k=1}^{j+1} \omega_k \varphi_{a_1 a_2}^{j+1-k,q}, \quad \mathcal{B}_{a_1, a_2}^{m,j+1} = \sum_{k=1}^{j+1} \omega_k \varphi_{a_1 a_2}^{m,j+1-k}.$$

Let the cost of solving the linear 1D system of the kind (142) be denoted by $\Theta_1(N_{\text{dim}})$ where the dimension is $N_{\text{dim}} = N - 1$. The cost of the steps outlined here works out to be $4(j+1)\Theta_1(N-1) + 4(j+1)^2$ where the second part is the cost of computing the history functions. The memory requirement is $4(j+1)^2 N + 4(j+1)^2$ size array. Therefore, the complexity scales with j . Moreover, for large number of time-steps, i.e., $N_t \gg N$, the term $(j+1)^2$ starts dominating after a point.

Step 2: Compute the history functions on the boundary segments of the domain Ω_i as

$$\mathcal{B}_{a_1}^{j+1}(y_2) = \sum_{k=1}^{j+1} \omega_k \varphi_{a_1}^{j+1-k,j+1}(y_2), \quad \mathcal{B}_{a_2}^{j+1}(y_1) = \sum_{k=1}^{j+1} \omega_k \varphi_{a_2}^{j+1,j+1-k}(y_1).$$

The cost of this step is $\mathcal{O}((j+1)N)$.

Step 3: Solve the linear system for the interior problem to compute the solution at $(j+1)$ -th time step

$$-\left(\alpha_1^{-2} \partial_{y_1}^2 + \alpha_2^{-2} \partial_{y_2}^2\right) u^{j+1} + u^{j+1} = u^j, \quad \rho = 1/\Delta t.$$

using the following Robin-type TBCs at discrete level

$$\partial_{n_1} u^{j+1} + \alpha_1 u^{j+1} = -\alpha_1 \mathcal{B}_{a_1}^{j+1}(y_2), \quad \partial_{n_2} u^{j+1} + \alpha_2 u^{j+1} = -\alpha_2 \mathcal{B}_{a_2}^{j+1}(y_1).$$

Let the cost of solving the linear 2D system of the kind (172) be denoted by $\Theta_2(N_{\text{dim}})$ where the dimension is $N_{\text{dim}} = (N-1)^2$. The cost of solving the linear system in this step works out to be $\Theta_2(N_{\text{dim}}) = \mathcal{O}(N^3)$ provided pivoting is not needed.

Step 4: Update the 2D and 3D arrays storing the values of the auxiliary field with the $(j+1)$ -th time step values using the fact that $\varphi^{j+1,j+1}(y_1, y_2) = u^{j+1}(y_1, y_2)$.

For moderate value of N_t , i.e., $N_t = \mathcal{O}(N)$, the cost of computation at each time-step is dominated by $\Theta_2(N_{\text{dim}}) = \mathcal{O}(N^3)$ which corresponds to the linear system for the interior problem. The memory requirement for the auxiliary functions in this case scales as $\mathcal{O}(N^3)$ which is quite prohibitive.

In the regime $N_t \gg N$, say, $N_t = \mathcal{O}(N^2)$, the cost of computation scales as $\mathcal{O}(N^4)$ which corresponds to cost of computing the history functions while the memory requirement scales as $\mathcal{O}(N^5)$.

3.3.2. NP-BDF1

Let us recall that, on the boundary segments Γ_{a_1} and Γ_{a_2} , the auxiliary fields are denoted by $\varphi_{k,a_1}(y_2, \tau_1, \tau_2)$ and $\varphi_{k,a_2}(y_1, \tau_1, \tau_2)$, respectively, while the auxiliary field at the corners is denoted by $\psi_{k,k',a_1,a_2}(\tau_1, \tau_2)$ where $a_1 \in \{l, r\}$, $a_2 \in \{b, t\}$ and $k, k' = 1, 2, \dots, M$. Let N be the number of spatial nodes along y_1 as well as y_2 , i.e., $N_1 = N_2 = N$. The storage of the auxiliary fields on the boundary segments require four 2D-arrays of size $M \times N$ and the storage of auxiliary field at corner points require four 2D-arrays of size $M \times M$ where $M(< N)$ is the order of the diagonal Padé approximants used in the NP method. The evolution of these fields are effectively local in time which circumvents the need to store the history of these fields in time. The algorithmic steps for the solving the IBVP are enumerated below.

Step 1: Advance the following IVPs corresponding to auxiliary fields by one step, say, $j \rightarrow (j+1)$ using the previously computed values of the auxiliary field on the segments (as described in Fig. 3):

$$-\alpha_1^{-2} \partial_{y_1}^2 \varphi_{k,a_2}^{j+1,j} + \varphi_{k,a_2}^{j+1,j} = \varphi_{k,a_2}^{j,j}, \quad -\alpha_1^{-2} \partial_{y_2}^2 \varphi_{k,a_1}^{j,j+1} + \varphi_{k,a_1}^{j,j+1} = \varphi_{k,a_1}^{j,j}, \quad k = 1, 2, \dots, M,$$

together with the boundary conditions

$$\partial_{n_2} \varphi_{k,a_1}^{j,j+1} + \alpha_2 \varpi \varphi_{k,a_1}^{j,j+1} = -\alpha_2 \mathcal{B}_{k,a_1,a_2}^{j+1}, \quad \partial_{n_1} \varphi_{k,a_2}^{j+1,j} + \alpha_1 \varpi \varphi_{k,a_2}^{j+1,j} = -\alpha_1 \mathcal{B}_{k,a_2,a_1}^{j+1},$$

where the history functions are given by

$$\mathcal{B}_{k,a_1,a_2}^{j+1} = \sum_{k'=1}^M \Gamma_{k'} \psi_{k,k',a_1,a_2}^{j,j}, \quad \mathcal{B}_{k,a_2,a_1}^{j+1} = \sum_{k'=1}^M \Gamma_{k'} \psi_{k,k',a_2,a_1}^{j,j} = \sum_{k'=1}^M \Gamma_{k'} \psi_{k',k,a_1,a_2}^{j,j}.$$

These boundary condition are taken from Sec. 3.1 where precise definition of the quantities are provided. The cost of the steps outlined here works out to be $4M\Theta_1(N-1) + 4M^2$ where the second part is the cost of computing the history functions. The memory requirement is $4MN + 4M^2$ size array.

Step 2: Compute the history functions on the boundary segments of the domain Ω_i as

$$\mathcal{B}_{a_1}^{j+1}(y_2) = \sum_{k=1}^M \Gamma_k \varphi_{k,a_1}^{j,j+1}, \quad \mathcal{B}_{a_2}^{j+1}(y_1) = \sum_{k=1}^M \Gamma_k \varphi_{k,a_2}^{j+1,j}.$$

The cost of this step is $\mathcal{O}(MN)$.

Step 3: Solve the linear system for the interior problem to compute the solution at $(j+1)$ -th time step

$$-(\alpha_1^{-2} \partial_{y_1}^2 + \alpha_2^{-2} \partial_{y_2}^2) u^{j+1} + u^{j+1} = u^j, \quad \rho = 1/\Delta t.$$

using the following Robin-type TBCs at discrete level

$$\partial_{n_1} u^{j+1} + \alpha_1 \varpi u^{j+1} = -\alpha_1 \mathcal{B}_{a_1}^{j+1}(y_2), \quad \partial_{n_2} u^{j+1} + \alpha_2 \varpi u^{j+1} = -\alpha_2 \mathcal{B}_{a_2}^{j+1}(y_1).$$

The cost of solving the linear system in this step works out to be $\Theta_2(N_{\text{dim}}) = \mathcal{O}(N^3)$ provided pivoting is not needed.

Step 4: Update the 2D arrays storing the values of the auxiliary fields with the $(j+1)$ -th time step values using the following update relations

$$\begin{cases} \varphi_{k,a_1}^{j+1,j+1} = \frac{1}{(1+\bar{\eta}_k^2)} \varphi_{k,a_1}^{j,j+1} + \frac{1/\rho}{(1+\bar{\eta}_k^2)} u^{j+1}, \\ \varphi_{k,a_2}^{j+1,j+1} = \frac{1}{(1+\bar{\eta}_k^2)} \varphi_{k,a_2}^{j+1,j} + \frac{1/\rho}{(1+\bar{\eta}_k^2)} u^{j+1}, \end{cases} \quad \text{and} \quad \begin{cases} \psi_{k,k',a_1,a_2}^{j,j+1} = \frac{1}{(1+\bar{\eta}_{k'}^2)} \psi_{k,k',a_1,a_2}^{j,j} + \frac{1/\rho}{(1+\bar{\eta}_{k'}^2)} \varphi_{k,a_1}^{j,j+1}, \\ \psi_{k,k',a_1,a_2}^{j+1,j+1} = \frac{1}{(1+\bar{\eta}_k^2)} \psi_{k,k',a_1,a_2}^{j,j+1} + \frac{1/\rho}{(1+\bar{\eta}_k^2)} \varphi_{k',a_2}^{j+1,j+1}. \end{cases}$$

From the discussion above, it is evident that the overall cost of computation is completely independent of the time-step and the DtN-maps get implemented at the cost of $\mathcal{O}(MN)$. The memory requirement for the auxiliary functions also remain independent of time-step with an estimate of $\mathcal{O}(MN)$. Therefore, the overall complexity is dominated by $\Theta_2(N_{\text{dim}}) = \mathcal{O}(N^3)$ which corresponds to the linear system for the interior problem.

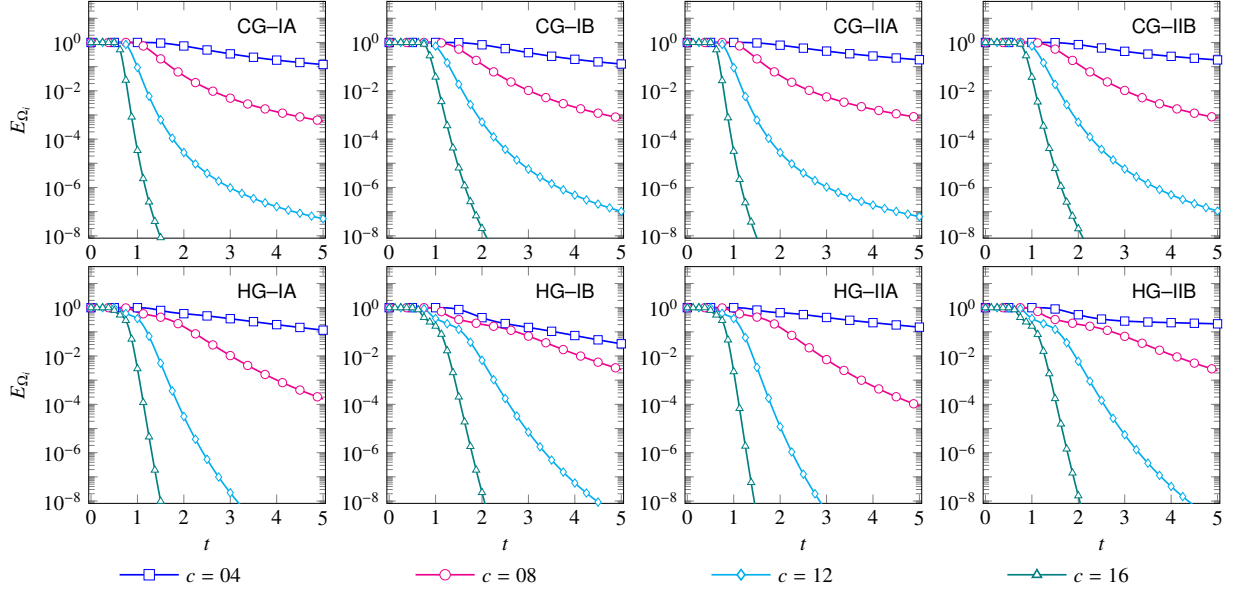


Figure 4: The figure shows the evolution of the relative energy content as defined in (177) of the chirped-Gaussian and the Hermite-Gaussian profiles considered in Table 1 and Table 2. Here the computational domain is $\Omega_i = (-10, 10)^2$.

4. Numerical Experiments

In this section, we will carry out the extensive numerical tests to showcase the accuracy of the numerical schemes developed in this work to solve the IBVP in (14). We start by analyzing the behaviour of the exact solutions for the IBVP under consideration followed by studying the error evolution behaviour and convergence analysis of the numerical schemes.

4.1. Exact solutions

The exact solutions admissible for our numerical experiments are such that the initial profile must be effectively supported within the computational domain. We primarily consider the wavepackets which are a modulation of a Gaussian envelop so that the requirement of effective initial support can be easily met. In this class of solutions, we consider the Chirped-Gaussian and the Hermite-Gaussian profiles.

Table 1: Chirped-Gaussian profile with $A_0 = 2$ and $c_0 \in \{4, 8, 12, 16\}$.

$$G(\mathbf{x}, t) = A_0 \sum_{j=1}^n G(\mathbf{x}, t; \mathbf{a}_j, \mathbf{b}_j, \mathbf{c}_j), \quad \mathbf{c}_j = c_0(\cos \theta_j, \sin \theta_j)$$

Type	n	$(\mathbf{a}_j \in \mathbb{R}^2)_{j=1}^n$	$(\mathbf{b}_j \in \mathbb{R}^2)_{j=1}^n$	$\boldsymbol{\theta} \in \mathbb{R}^n$
IA, IB	2	$\mathbf{a}_1 = (1/2.5, 1/2.4),$ $\mathbf{a}_2 = (1/2.3, 1/2.2)$	$\mathbf{b}_j = (1/2)\mathbf{1}$	IA: $\boldsymbol{\theta}_A = (0, \pi),$ IB: $\boldsymbol{\theta}_B = \boldsymbol{\theta}_A + (\pi/4)\mathbf{1}$
IIA, IIB	4	$\mathbf{a}_1 = (1/2.5, 1/2.4),$ $\mathbf{a}_2 = (1/2.3, 1/2.2),$ $\mathbf{a}_3 = (1/2.7, 1/2.6),$ $\mathbf{a}_4 = (1/2.2, 1/2.5)$	$\mathbf{b}_j = (1/2)\mathbf{1}$	IIA: $\boldsymbol{\theta}_A = (0, \pi/2, \pi, 3\pi/2),$ IIB: $\boldsymbol{\theta}_B = \boldsymbol{\theta}_A + (\pi/4)\mathbf{1}$

4.1.1. Chirped-Gaussian profile

Using the function defined by

$$\mathcal{G}(x, t; a, b) = \frac{1}{\sqrt{1 + 4i(a + ib)t}} \exp\left[-\frac{(a + ib)}{1 + 4i(a + ib)t} x^2\right], \quad a > 0, b \in \mathbb{R}, \quad (174)$$

one can define the family of solutions referred to as chirped-Gaussian profile by

$$G(\mathbf{x}, t; \mathbf{a}, \mathbf{b}, \mathbf{c}) = \mathcal{G}(x_1 - c_1 t, t; a_1, b_1) \mathcal{G}(x_2 - c_2 t, t; a_2, b_2) \exp\left(+i\frac{1}{2}\mathbf{c} \cdot \mathbf{x} - i\frac{1}{4}\mathbf{c} \cdot \mathbf{c} t\right), \quad (175)$$

where $\mathbf{a} \in \mathbb{R}_+^2$ determines the effective support of the profile at $t = 0$, $\mathbf{b} \in \mathbb{R}^2$ is the *chirp* parameter and $\mathbf{c} \in \mathbb{R}^2$ is the velocity of the profile. Using linear combination, one can further define a more general family of solutions with parameters $A_0, c_0 \in \mathbb{R}$, $\boldsymbol{\theta} \in \mathbb{R}^n$, $(\mathbf{a}_j \in \mathbb{R}_+^2)_{j=1}^n$ and $(\mathbf{b}_j \in \mathbb{R}^2)_{j=1}^n$ given by

$$G(\mathbf{x}, t; c_0, A_0; (\mathbf{a}_j)_{j=1}^n, (\mathbf{b}_j)_{j=1}^n, \boldsymbol{\theta}) = A_0 \sum_{j=1}^n G(\mathbf{x}, t; \mathbf{a}_j, \mathbf{b}_j, \mathbf{c}_j), \quad \mathbf{c}_j = c_0(\cos \theta_j, \sin \theta_j). \quad (176)$$

Let the constant vector $(1, 1, \dots) \in \mathbb{R}^n$ be denoted by $\mathbf{1}$, then the specific values of the parameters of the solutions used in the numerical experiments can be summarized as in Table 1. The energy content of the profile within the computational domain Ω_i over time is

$$E_{\Omega_i}(t) = \int_{\Omega_i} |G(\mathbf{x}, t)|^2 d^2 \mathbf{x} \Big/ \int_{\Omega_i} |G(\mathbf{x}, 0)|^2 d^2 \mathbf{x}, \quad t \geq 0. \quad (177)$$

The profiles are chosen with non-zero speed c_0 so that the field hits the boundary of Ω_i , In case of a square computational domain, the type ‘A’ class of solutions are directed to the segments of the boundary normally while type ‘B’ class of solutions are directed to the corners. The behaviour of the $E_{\Omega_i}(t)$ for $t \in [0, 5]$ is shown in Fig. 4.

Table 2: Hermite-Gaussian profile with $A_0 = 2$ and $c_0 \in \{4, 8, 12, 16\}$.

$G(\mathbf{x}, t) = A_0 \sum_{j=1}^n G(\mathbf{x}, t; \mathbf{m}_j, \mathbf{a}_j, \mathbf{c}_j), \quad \mathbf{c}_j = c_0(\cos \theta_j, \sin \theta_j)$				
Type	n	$(\mathbf{a}_j \in \mathbb{R}_+^2)_{j=1}^n$	$(\mathbf{m}_j \in \mathbb{N}_0^2)_{j=1}^n$	$\boldsymbol{\theta} \in \mathbb{R}^n$
IA, IB	2	$\mathbf{a}_1 = (1/2.5, 1/2.4),$ $\mathbf{a}_2 = (1/2.3, 1/2.2)$	$\mathbf{m}_1 = (1, 2),$ $\mathbf{m}_2 = (2, 1)$	$\boldsymbol{\theta}_A = (0, \pi),$ $\boldsymbol{\theta}_B = \boldsymbol{\theta}_A + (\pi/4)\mathbf{1}$
IIA, IIB	4	$\mathbf{a}_1 = (1/2.5, 1/2.4),$ $\mathbf{a}_2 = (1/2.3, 1/2.2),$ $\mathbf{a}_3 = (1/2.7, 1/2.6),$ $\mathbf{a}_4 = (1/2.2, 1/2.5)$	$\mathbf{m}_1 = (1, 2),$ $\mathbf{m}_2 = (2, 1),$ $\mathbf{m}_3 = (2, 1),$ $\mathbf{m}_4 = (1, 2)$	$\boldsymbol{\theta}_A = (0, \pi/2, \pi, 3\pi/2),$ $\boldsymbol{\theta}_B = \boldsymbol{\theta}_A + (\pi/4)\mathbf{1}$

4.1.2. Hermite-Gaussian profile

Consider the class of normalized Hermite-Gaussian functions defined by

$$\mathcal{G}_m(x, t; a) = \gamma_m^{-1} H_m\left(\frac{\sqrt{2a}x}{w(t)}\right) \sqrt{\frac{\mu(t)}{a}} \exp\left[-\mu(t)x^2 - im\theta(t)\right], \quad m \in \mathbb{N}_0 = \{0, 1, \dots\}, \quad (178)$$

where $a > 0$,

$$w(t) = \sqrt{1 + (4at)^2}, \quad \frac{1}{\mu(t)} = \frac{1}{a} + i4t = \frac{1}{a} w(t) \exp[i\theta(t)], \quad (179)$$

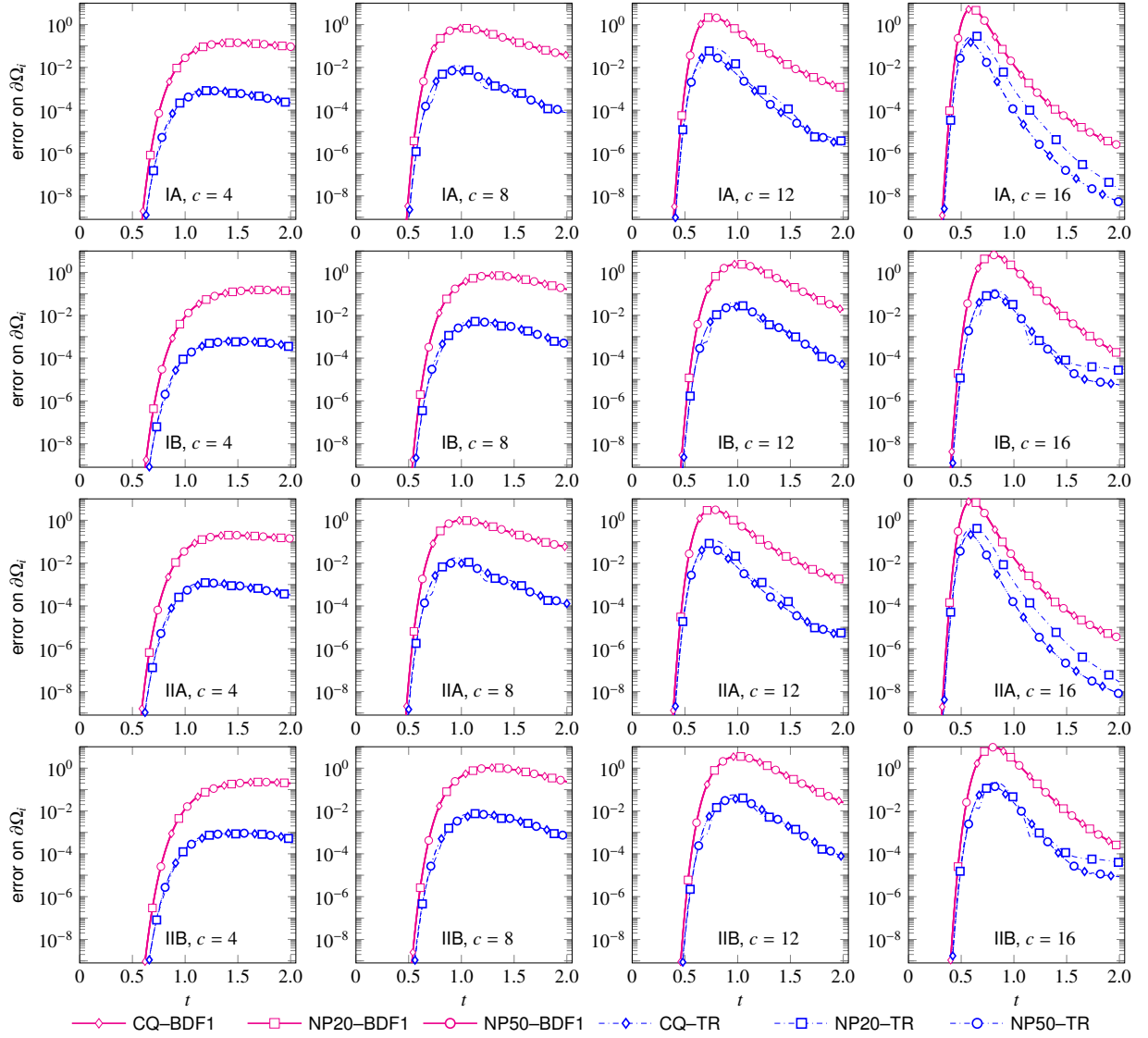


Figure 5: The figure shows the behaviour of error involved in the discretization of the boundary map alone for the chirped-Gaussian profile with different values of the speed ‘ c ’ (see Table 1). The numerical parameters and the labels are described in Sec. 4.2 where the error is quantified by (184).

and the normalization factor is given by $\gamma_m^2 = 2^m(m!) \sqrt{\pi}(2a)^{-1/2}$.

The Hermite polynomials are evaluated using the following relations

$$H_{n+1}(x) = 2xH_n(x) - 2nH_{n-1}(x), \quad H'_{n+1}(x) = 2(n+1)H_n(x), \quad (180)$$

with $H_0(x) = 1$ and $H_1(x) = 2x$. These relations can be used to compute the first spatial derivative of the Hermite-Gaussian functions:

$$\partial_x \mathcal{G}_m(x, t; a) = -\sqrt{(m+1)a} \mathcal{G}_{m+1}(x, t; a) + \sqrt{ma} \mathcal{G}_{m-1}(x, t; a), \quad m > 0, \quad (181)$$

with $\partial_x \mathcal{G}_0(x, t; a) = -\sqrt{a} \mathcal{G}_1(x, t; a)$. This is required for testing our Dirichlet-to-Neumann maps. Using these func-

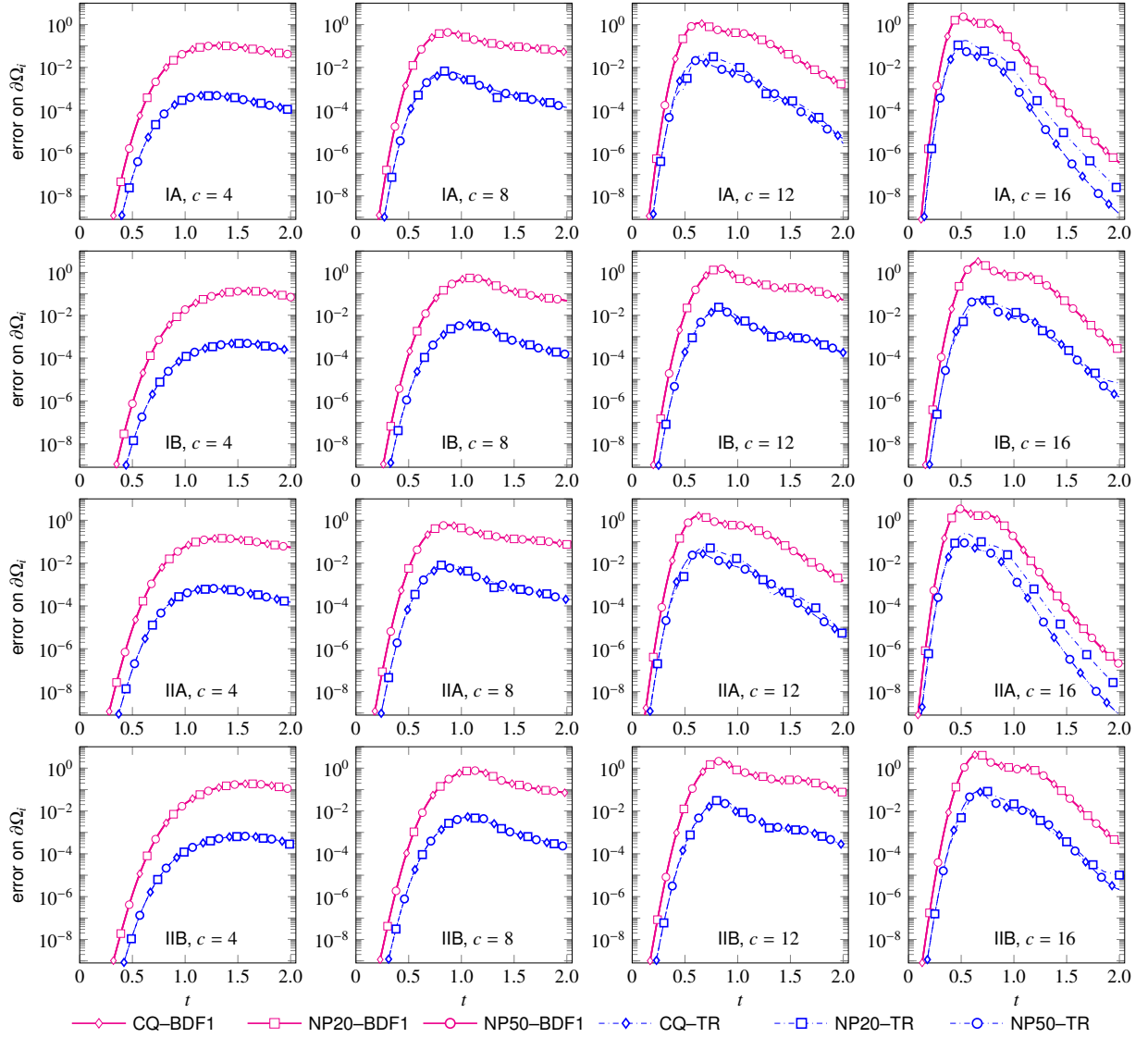


Figure 6: The figure shows the behaviour of error involved in the discretization of the boundary map alone for the Hermite-Gaussian profile with different values of the speed ‘ c ’ (see Table 2). The numerical parameters and the labels are described in Sec. 4.2 where the error is quantified by (184).

tions, we can define a family of solutions, referred to as Hermite-Gaussian profile by

$$G(\mathbf{x}, t; \mathbf{m}, \mathbf{a}, \mathbf{c}) = \mathcal{G}_{m_1}(x_1 - c_1 t, t; a_1) \mathcal{G}_{m_2}(x_2 - c_2 t, t; a_2) \exp\left(+i \frac{1}{2} \mathbf{c} \cdot \mathbf{x} - i \frac{1}{4} \mathbf{c} \cdot \mathbf{c} t\right), \quad (182)$$

where $\mathbf{m} \in \mathbb{N}_0^2$ is the order parameter, $\mathbf{a} \in \mathbb{R}_+^2$ determines the effective support of the profile at $t = 0$ and $\mathbf{c} \in \mathbb{R}^2$ is the velocity of the profile. Once again, using linear combination, one can further define a more general family of solutions with parameters $A_0, c_0 \in \mathbb{R}$, $\boldsymbol{\theta} \in \mathbb{R}^n$, $(\mathbf{m}_j \in \mathbb{N}_0^2)_{j=1}^n$ and $(\mathbf{a}_j \in \mathbb{R}_+^2)_{j=1}^n$ given by

$$G(\mathbf{x}, t; c_0, A_0; (\mathbf{m}_j)_{j=1}^n, (\mathbf{a}_j)_{j=1}^n, \boldsymbol{\theta}) = A_0 \sum_{j=1}^n G(\mathbf{x}, t; \mathbf{m}_j, \mathbf{a}_j, \mathbf{c}_j), \quad \mathbf{c}_j = c_0 (\cos \theta_j, \sin \theta_j). \quad (183)$$

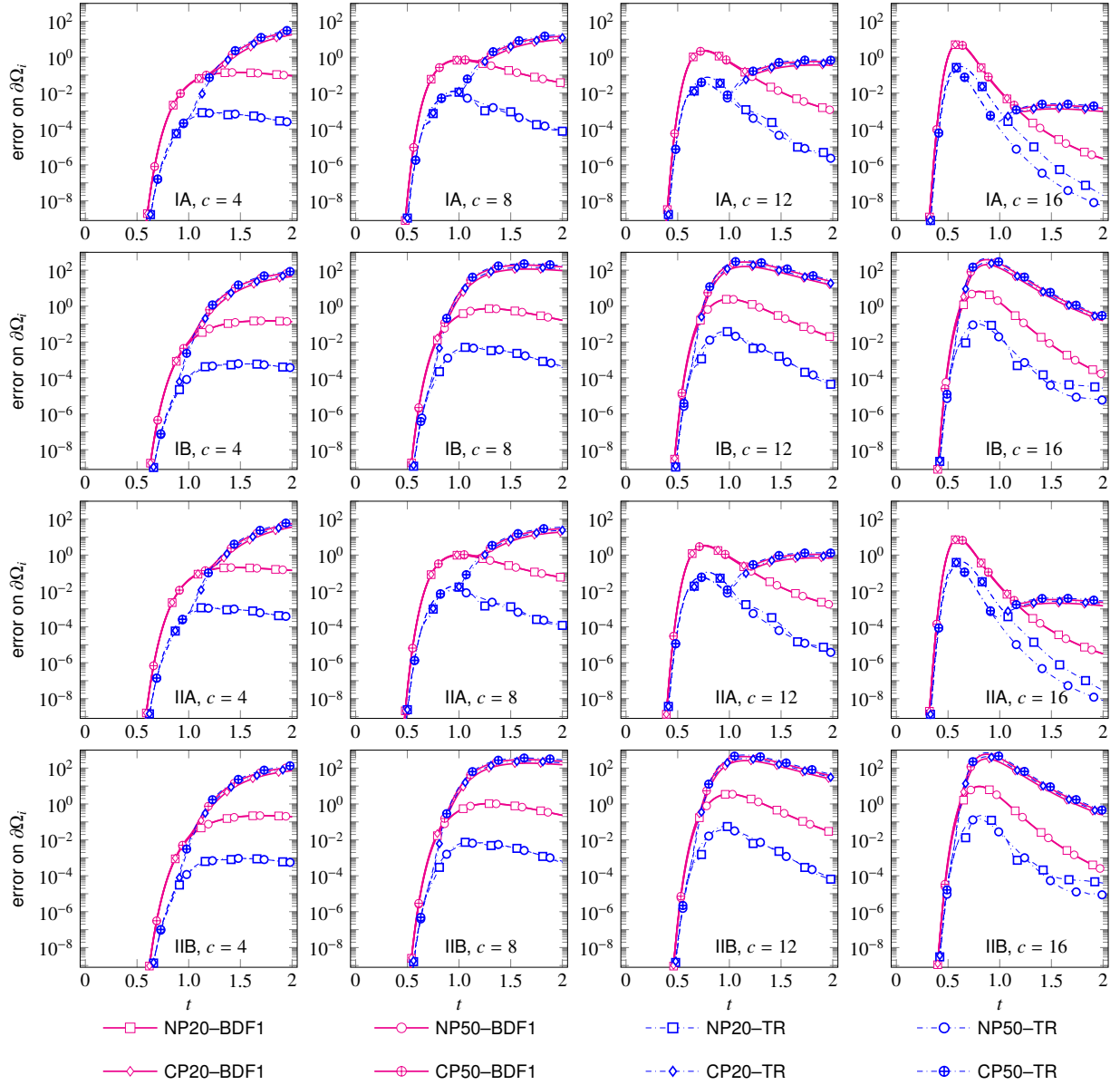


Figure 7: The figure shows a comparison of the novel Padé and Menza’s approach towards realizing the DtN maps for the chirped-Gaussian profile with different values of the speed ‘ c ’ (see Table 1). The numerical parameters and the labels are described in Sec. 4.2 where the error is quantified by (184).

As in the last case, we set $\mathbf{1} = (1, 1, \dots) \in \mathbb{R}^n$, then the specific values of the parameters of the solutions used in the numerical experiments can be summarized as in Table 2. The energy content of the profile within the computational domain Ω_i over time is $E_{\Omega_i}(t)$ as defined by (177) with the appropriate profile in the integrand. The profiles are chosen with non-zero speed c_0 so that the field hits the boundary of Ω_i . In case of a square computational domain, the type ‘A’ class of solutions are directed to the segments of the boundary normally while type ‘B’ class of solutions are directed to the corners. The behaviour of the $E_{\Omega_i}(t)$ for $t \in [0, 5]$ is shown in Fig. 4.

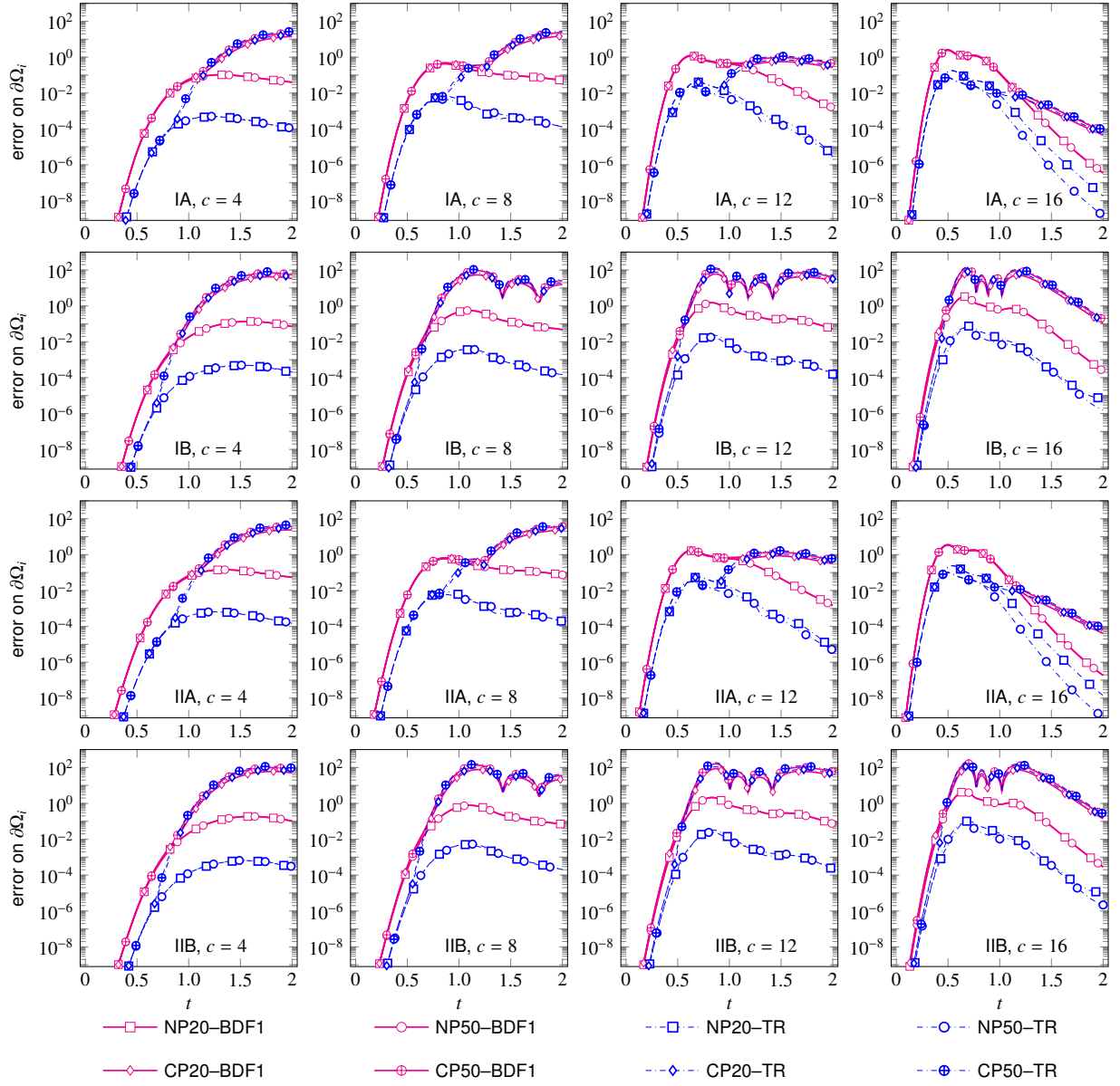


Figure 8: The figure shows a comparison of the novel Padé and Menza's approach towards realizing the DtN maps for the Hermite-Gaussian profile with different values of the speed 'c' (see Table 2). The numerical parameters and the labels are described in Sec. 4.2 where the error is quantified by (184).

4.2. Tests for DtN maps

Prior to the full implementation of the numerical scheme, one can test the accuracy of the DtN boundary maps where we quantify the error on $\partial\Omega_i$ by

$$e(t_j) = \left(\int_{\partial\Omega_i} |\partial_n u(\mathbf{x}, t_j) - [\partial_n u(\mathbf{x}, t_j)]_{\text{num.}}|^2 d\sigma(\mathbf{x}) \right)^{1/2}, \quad t_j \in [0, T_{\max}], \quad (184)$$

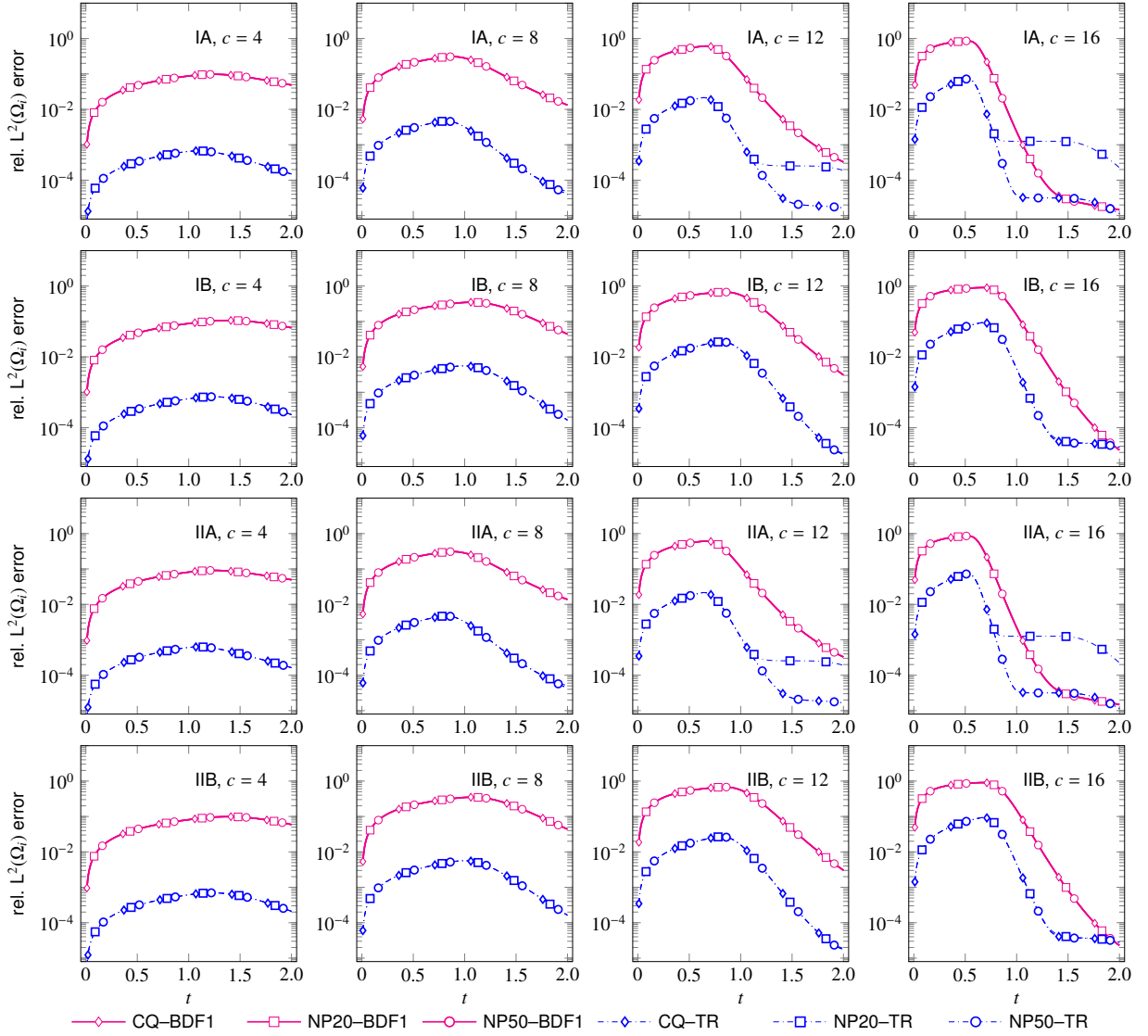


Figure 9: The figure shows a comparison of evolution of error in the numerical solution of the IBVP (14) with the various TBCs for the chirped-Gaussian profile with different values of the speed ‘c’ (see Table 1). The numerical parameters and the labels are described in Sec. 4.3 where the error is quantified by (185).

where $d\sigma(\mathbf{x})$ denotes the measure along the boundary of the computational domain Ω_i . Along the spatial dimension, the integral above will be approximated by Gauss quadrature over LGL-points⁶. The quantity $[\partial_n u(\mathbf{x}, t_j)]_{\text{num}}$ refers to the numerical approximation of the Neumann datum from the Dirichlet datum. All the intermediate quantities involved in this process is computed according to a numerical scheme developed as part of the numerical realization of the DtN map.

In this work, we have developed two discrete versions of the DtN maps, namely, CQ and NP. Each of these methods have a variant determined by the choice of one-step method used in the temporal discretization so that the complete list of methods to be tested can be labelled as CQ–BDF1, NP–BDF1 (corresponding to the one-step method BDF1),

⁶The quadrature nodes and the corresponding weights are computed using quad precision in order to avoid any numerical artifacts due to round-off errors.

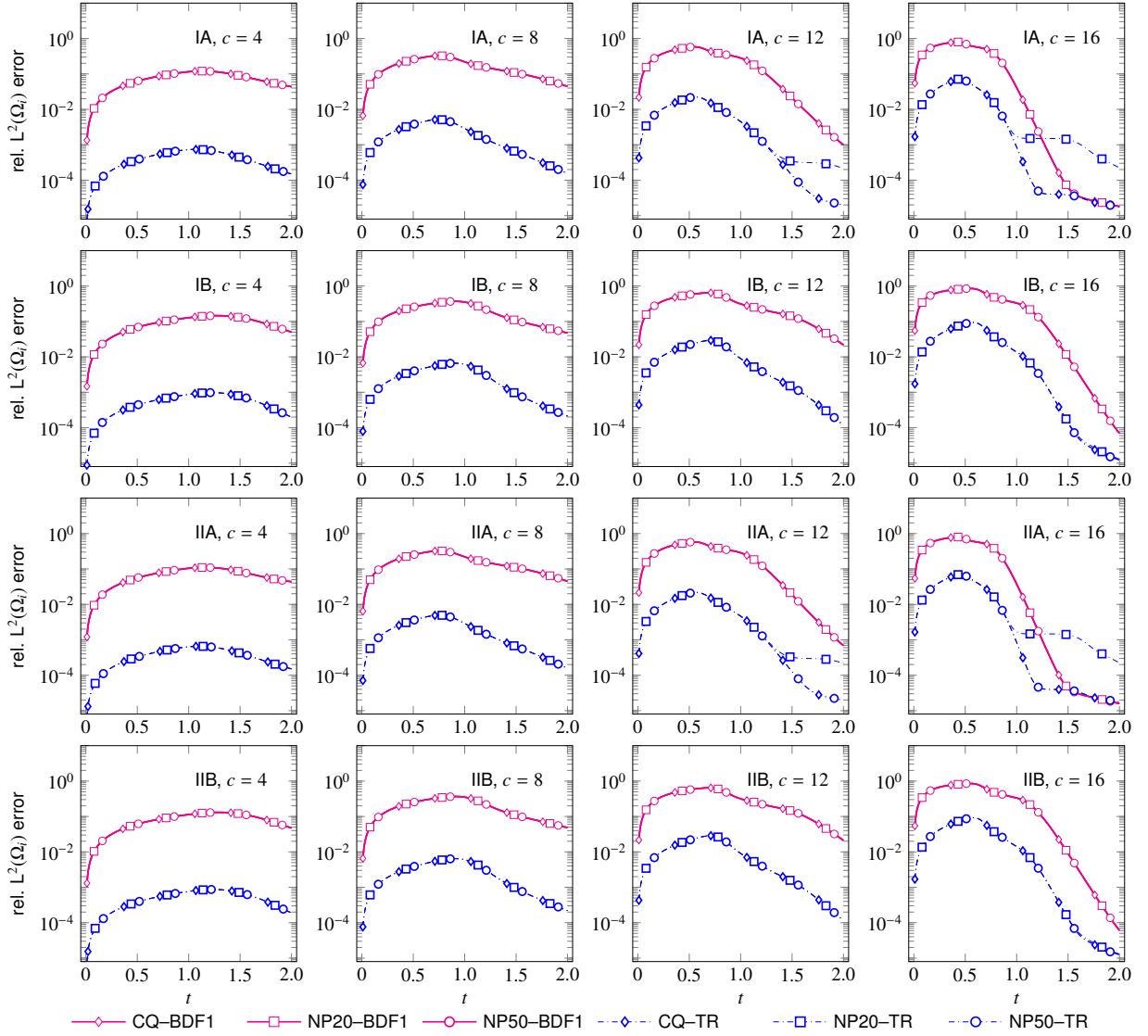


Figure 10: The figure shows a comparison of evolution of error in the numerical solution of the IBVP (14) with the various TBCs for the Hermite-Gaussian profile with different values of the speed ‘ c ’ (see Table 2). The numerical parameters and the labels are described in Sec. 4.3 where the error is quantified by (185).

and, CQ-TR, NP-TR (corresponding to the one-step method TR). For the Padé approximant based method ‘NP’, we distinguish the diagonal approximant of order 20 from that of 50 via the labels ‘NP20’ and ‘NP50’. The numerical parameters used in this section are summarized in Table 3. The exact solutions used are described in Sec. 4.1. Let us note that the accuracy of the DtN maps do not reflect the accuracy of the numerical solution computed with the TBCs on account of the fact that the interior problem together with the discretized DtN maps may turn out to be unstable.

The numerical results for error on $\partial\Omega_i$ corresponding to the chirped-Gaussian and the Hermite-Gaussian profiles are shown in Fig. 5 and Fig. 6, respectively. It can be seen that the diagonal Padé approximant based methods, namely, NP20 and NP50, perform equally well as compared to that of the convolution quadrature based method. Moreover, the TR methods perform better than the BDF1 methods which is clear from the error peaks in figures 5 and 6. The accuracy deteriorates with increase in the value of c . For faster moving profiles corresponding to IA and IIA type

Table 3: Numerical parameters for testing DtN maps

Computational domain (Ω_i)	$(-10, 10) \times (-10, 10)$
Maximum time (T_{max})	2
No. of time-steps (N_t)	1000 + 1
Time-step (Δt)	$2 \times 10^{-3} = T_{max}/(N_t - 1)$
Number of LGL-points ($N + 1$)	200

solutions, NP-20 becomes slightly less accurate compared to CQ and NP-50. There is no significant difference in the results for error on $\partial\Omega_i$ corresponding to the chirped-Gaussian profile and the Hermite-Gaussian profile.

Before concluding this section, we would like to present evidence of the phenomenon discussed in Sec. 2.3 with regard to deficiencies in the Menza’s approach. We can test the accuracy of the DtN boundary maps realized according to Menza’s approach using the error metric defined in (184). The discrete scheme for the boundary maps is labelled as ‘CP–’ followed by the time-stepping method used for temporal derivatives in the realization of the boundary maps. Here, Menza’s approach is labeled as ‘CP’ which stands for the conventional Padé approach. Moreover, we distinguish the diagonal Padé approximant of order 20 from that of 50 via the labels ‘CP20’ and ‘CP50’. The numerical results showing a comparison of the novel Padé and Menza’s approach corresponding to the chirped-Gaussian and the Hermite-Gaussian profiles are shown in Fig. 7 and Fig. 8, respectively. It can be seen that the NP methods perform superior to the CP methods which is clear from the error peaks in figures 7 and 8. Moreover, CP methods perform poorly in the case of IB and IIB type solutions where the profiles are directed towards the corners of the computational domain. This observation points towards the fact that Menza’s approach failed to handle corners of the domain adequately. For faster moving profiles corresponding to IA and IIA type solutions (directed towards the segments), error in the CP methods agree upto some extent with that of the NP methods. The error behaviour on $\partial\Omega_i$ with Menza’s approach becomes slightly oscillatory in case of the Hermite-Gaussian profile as evident in Fig. 8. On account of the poor accuracy of the Menza’s approach as demonstrated here, we do not consider the full implementation of the IBVP in (14) within the context of Menza’s approach.

4.3. Tests for evolution error

In this section, we consider the IBVP in (14) where the initial condition corresponds to the exact solutions described in Sec. 4.1. The numerical solution is labelled according to that of the boundary maps described in Sec. 4.2. The error in the evolution of the profile computed numerically is quantified by the relative $L^2(\Omega_i)$ -norm:

$$e(t_j) = \left(\int_{\Omega_i} |u(\mathbf{x}, t_j) - [u(\mathbf{x}, t_j)]_{\text{num.}}|^2 d^2\mathbf{x} \right)^{1/2} \left/ \left(\int_{\Omega_i} |u_0(\mathbf{x})|^2 d^2\mathbf{x} \right)^{1/2} \right., \quad (185)$$

for $t_j \in [0, T_{max}]$. The integral above will be approximated by Gauss quadrature over LGL-points.

For Padé based discretization (NP) of the DtN maps, it is possible to carry out evolution over larger number of time-steps. The Table 4 lists the numerical parameters for the NP20 and NP50 methods. The CQ based methods cannot be tested with the same parameters on account of the increasing memory requirements at each time-step. Therefore, we introduce a separate test-case for the sake of comparison with CQ methods by restricting $N_t = 1000 + 1$ and $T_{max} = 2$ while other parameters are same as that of Table 4.

The numerical results for the evolution error on Ω_i corresponding to the chirped-Gaussian and the Hermite-Gaussian profiles are shown in Fig. 9 and Fig. 10, respectively. It can be seen that the diagonal Padé approximants based method, namely, NP20 and NP50, perform equally well as compared to that of the convolution quadrature based method. Moreover, the TR methods perform better than the BDF1 methods which is clear from the error peaks in figures 9 and 10. The accuracy deteriorates with increase in the value of c . For faster moving profiles corresponding to IA and IIA type solutions, NP-20 becomes slightly less accurate compared to CQ and NP-50. There is no

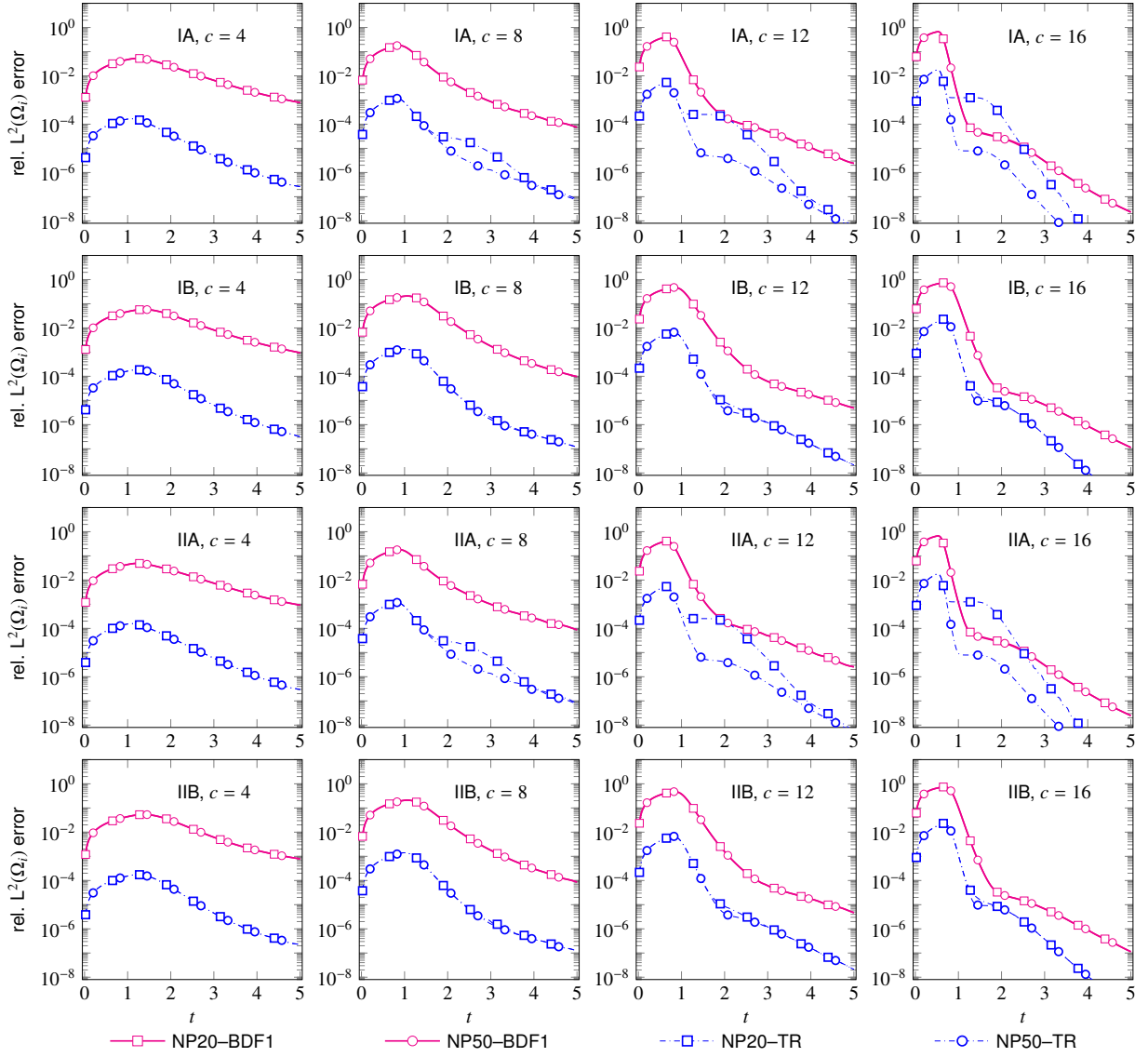


Figure 11: The figure shows a comparison of evolution of error in the numerical solution of the IBVP (14) with the TBCs developed using novel Padé approach for the chirped-Gaussian profile with different values of the speed ‘c’ (see Table 1). The numerical parameters and the labels are described in Sec. 4.3 where the error is quantified by (185).

significant difference in the results for evolution error on Ω_i corresponding to the chirped-Gaussian profile and the Hermite-Gaussian profile.

The numerical results for the evolution error on Ω_i particularly for NP methods corresponding to the chirped-Gaussian and Hermite-Gaussian profiles are shown in Fig. 11 and Fig. 12, respectively. Note that the results for NP are superior than that of CQ on account of the reduced size (Δt) of the time-step which was possible because increasing the number of time-steps did not significantly increase the computation time as well as memory requirements unlike that of CQ⁷.

⁷ Attempts to lower the step-size for the same maximum duration of time in case of CQ failed due to out-of-memory errors. We note that these problems may severely limit the practical utility of the CQ method.

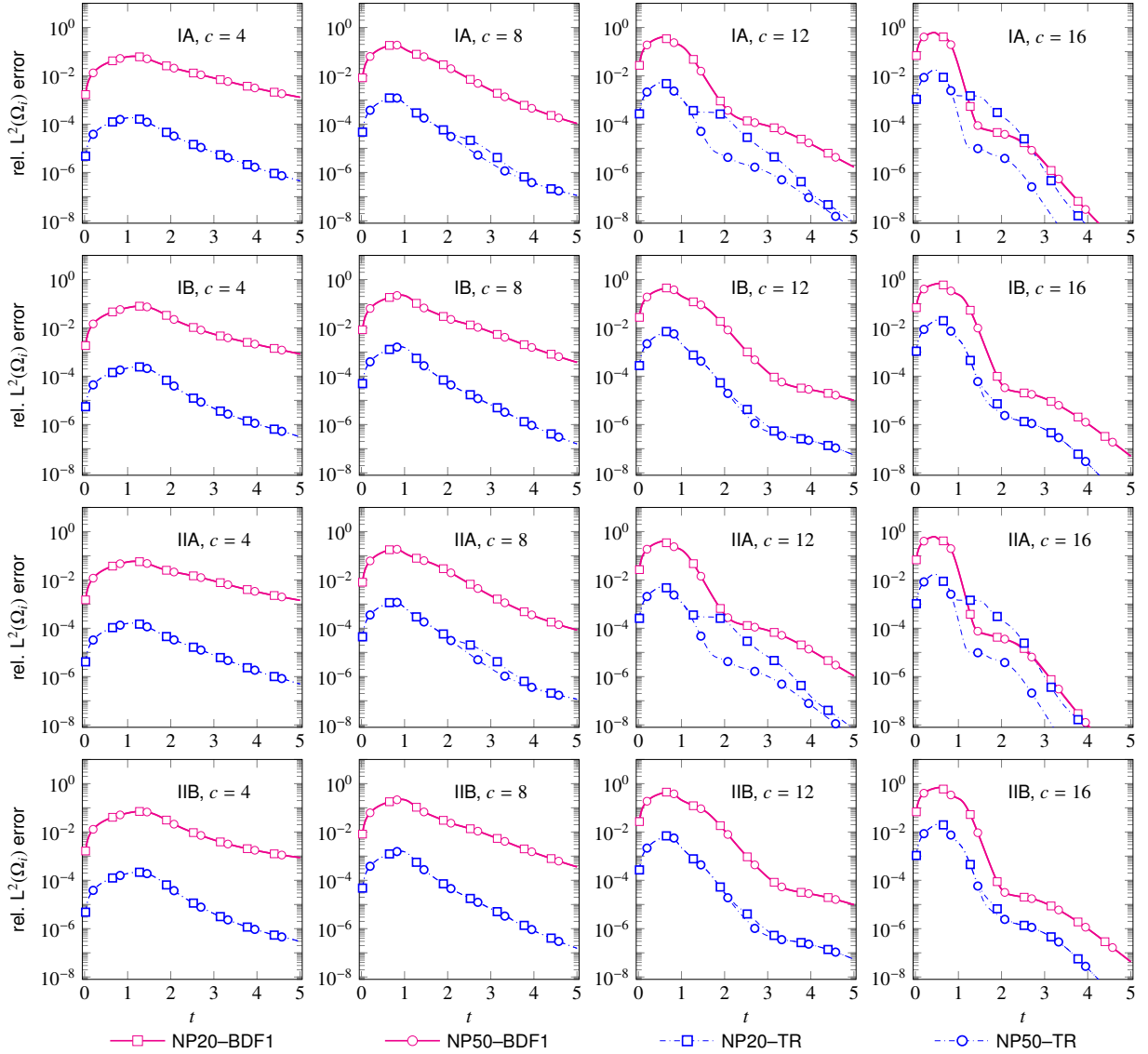


Figure 12: The figure shows a comparison of evolution of error in the numerical solution of the IBVP (14) with the TBCs developed using novel Padé approach for the Hermite-Gaussian profile with different values of the speed ‘c’ (see Table 2). The numerical parameters and the labels are described in Sec. 4.3 where the error is quantified by (185).

In order to visualize the reflections at the boundary, we resort to contour plots depicting the quantity $f_{\text{mag.}} \log_{10} |u(\mathbf{x}, t)|$ where the scalar quantity $f_{\text{mag.}}$ is adjusted to resolve the contour lines properly. The specific snapshots correspond to the equispaced energy levels in the logarithmic scale that is remaining in the computational domain. We restrict ourselves to presenting the contour plots only for the case of type IIB class of solutions which are directed towards the corners of the domain on account of being most complex among four different class of solutions. The contour plots depicting corresponding to the chirped-Gaussian ($f_{\text{mag.}} = 4$) and the Hermite-Gaussian ($f_{\text{mag.}} = 8$) profiles are shown in Fig. 15 and Fig. 16, respectively. The top row corresponds to the exact solution for reference. From these plots, we conclude that the results are similar for each of the types of solutions. There are minimal visible reflections in the contour plots proving the accuracy of the developed numerical schemes to implement the TBCs. Moreover, the TR based methods better resolve the contour levels in comparison to the BDF1 based methods.

Table 4: Numerical parameters for studying the evolution error for the NP methods

Computational domain (Ω_i)	$(-10, 10) \times (-10, 10)$
Maximum time (T_{max})	5
No. of time-steps (N_t)	5000 + 1
Time-step (Δt)	$10^{-3} = T_{max}/(N_t - 1)$
Number of LGL-points ($(N + 1) \times (N + 1)$)	200×200

Table 5: Numerical parameters for studying the convergence error for the NP methods

Computational domain (Ω_i)	$(-10, 10) \times (-10, 10)$
Maximum time (T_{max})	5
Set of no. of time-steps (\mathbb{N}_t)	$\{2^8, 2^9, \dots, 2^{18}\}$
Time-step	$\{\Delta t = T_{max}/(N_t - 1), N_t \in \mathbb{N}_t\}$
Number of LGL-points ($(N + 1) \times (N + 1)$)	200×200

4.4. Tests for convergence

In this section, we analyze the convergence behaviour of the numerical schemes for the IBVP in (14) where the initial condition corresponds to the exact solutions described in Sec. 4.1. The numerical solution is labelled according to that of the boundary maps described in Sec. 4.2.

The error used to study the convergence behaviour is quantified by the maximum relative $L^2(\Omega_i)$ -norm:

$$e = \max \{e(t_j) \mid j = 0, 1, \dots, N_t - 1\}, \quad (186)$$

for $t_j \in [0, T_{max}]$. For Padé based discretization (NP) of the DtN maps, it is possible to analyze the convergence behaviour over large number of time-steps. The Table 5 lists the numerical parameters for the NP20 and NP50 methods. The CQ based methods cannot be tested with the same parameters on account of the increasing memory requirements at each time-step.

The numerical results for the convergence behaviour on Ω_i corresponding to the chirped-Gaussian and the Hermite-Gaussian profiles are shown in Fig. 13 and Fig. 14, respectively. It can be seen that the diagonal Padé approximant based method, namely, NP20 and NP50, shows stable behaviour for the parameters specified in Table 5. In the log-log scale, we can clearly identify the error curve to be a straight line before it plateaus. The orders can be recovered from the slope which we found consistent with the order of the underlying one-step method. The TR methods perform better than the BDF1 methods which is obvious from the slope of the error curves in figures 13 and 14. We note that the error background increases with increase in the value of c . This is on account of the increased oscillatory behaviour of the solution in t as c increases and a method with higher order than 2 would be required to achieve the same accuracy as that of the slow moving profiles keeping the step-size same. Note that NP20 methods starts plateauing after a certain number of time-steps unlike NP50. This can be attributed to the approximate nature of the TBCs with a lower order of diagonal approximants chosen. Finally, let us observe that there is no significant difference in the results for convergence on Ω_i corresponding to the chirped-Gaussian profile and the Hermite-Gaussian profile.

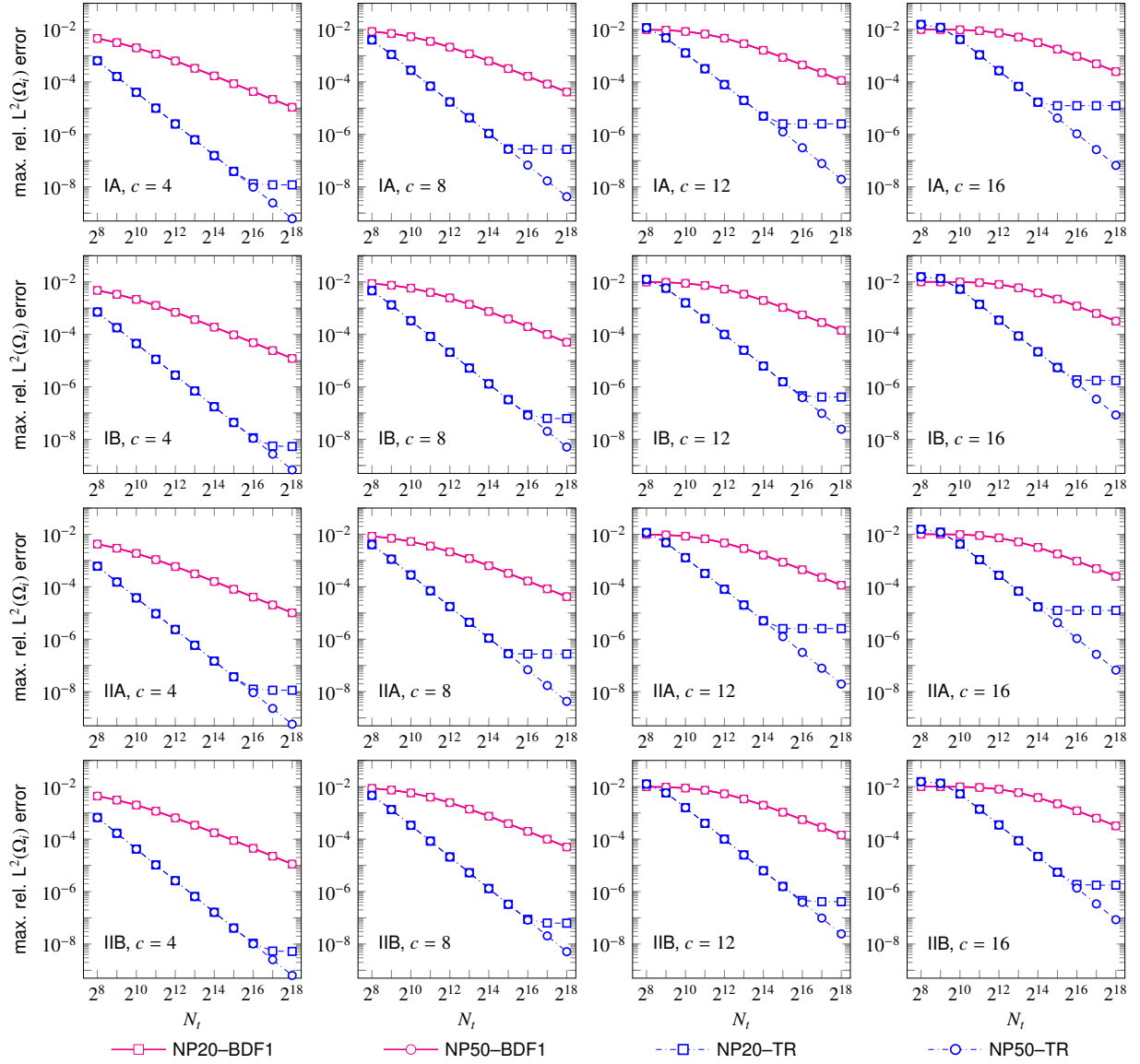


Figure 13: The figure depicts the convergence behaviour of the numerical solution of the IBVP (14) with the TBCs developed using novel Padé approach for the chirped-Gaussian profile with different values of the speed ‘c’ (see Table 1). The numerical parameters and the labels are described in Sec. 4.4 where the error is quantified by (186).

5. Conclusion

In this paper, we presented a new effectively local approximation for the numerical realization of the TBCs on a rectangular computational domain for the free Schrödinger equation in \mathbb{R}^2 . Our starting point was a numerically tractable formulation of the transparent boundary operator, $\sqrt{\partial_t - i\Delta_\Gamma}$, where Δ_Γ is the Laplace-Beltrami operator [4, 5], which is nonlocal in time as well as space. This formulation of the TBCs introduces an auxiliary function which happens to satisfy the one-dimensional Schrödinger equation along the boundary segments of the computational domain. It addressed the nonlocality in space, however, the nonlocality in time remained a serious bottleneck on account of the growing computational complexity with number of time-steps which becomes prohibitive after a point. To overcome this challenge, we developed a novel Padé approximant based rational approximation for the

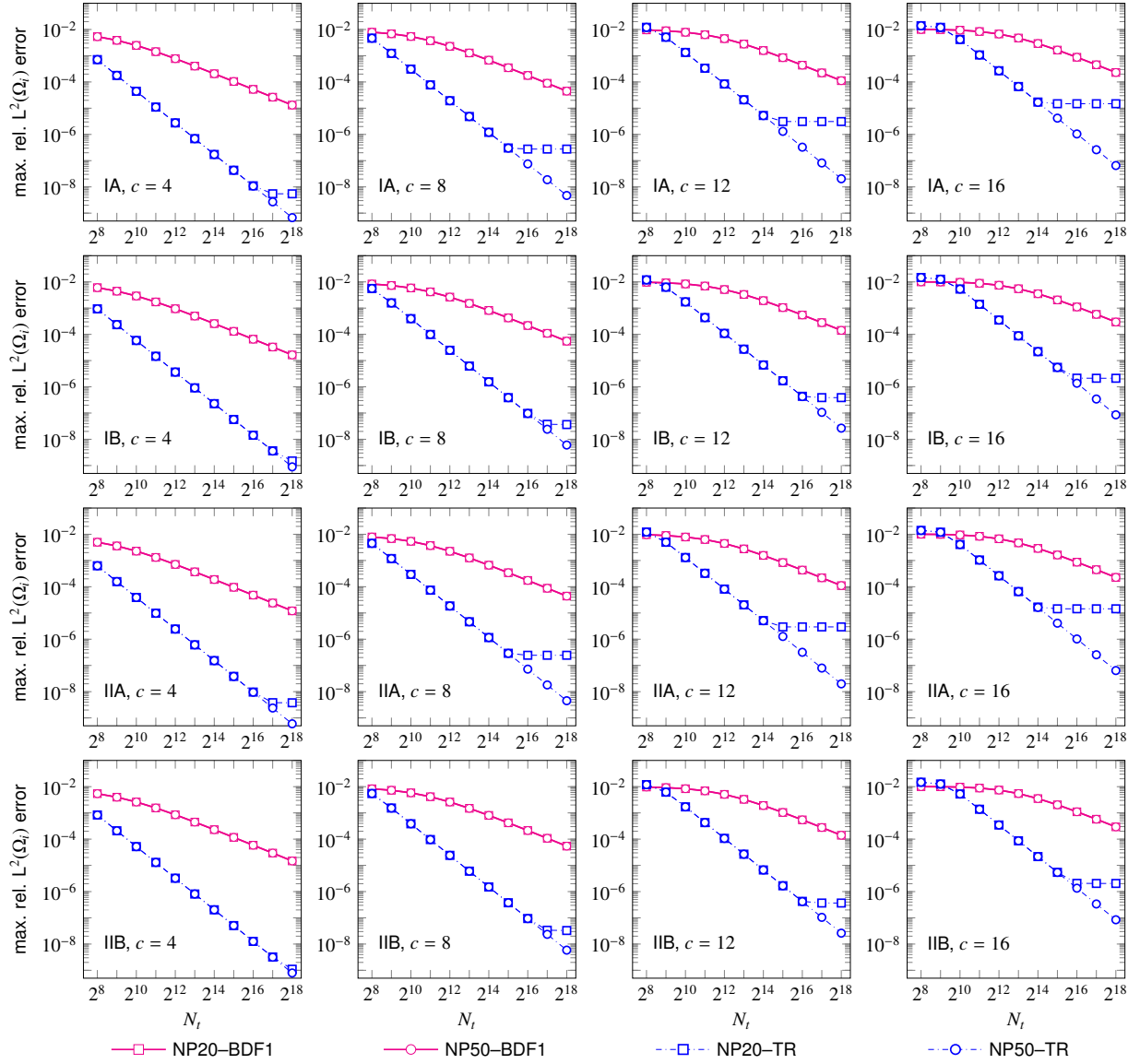


Figure 14: The figure depicts the convergence behaviour of the numerical solution of the IBVP (14) with the TBCs developed using novel Padé approach for the Hermite-Gaussian profile with different values of the speed ‘ c ’ (see Table 2). The numerical parameters and the labels are described in Sec. 4.4 where the error is quantified by (186).

1/2-order time-fractional derivative. This approach circumvents the need to store the entire history of the field on the boundary segments and allows us to achieve a computational complexity that remains independent of the number of time-steps. Let us emphasize that our approach is significantly different from that of Menza [7] which fails at the corners of the rectangular domain. Further, we also present a convolution quadrature based scheme which happens to be computationally expensive but it is well-known as a golden standard for 1D problems. As far as time marching is concerned, we note that one-step methods are best suited for our purpose and any higher-order method can be readily used to implement our algorithm. These aspects will be further explored in a future publication.

For the spatial discretization, we use a Legendre-Galerkin spectral method with a new boundary adapted basis which leads to a banded linear system for the 1D problems on the boundary segments as well as for the interior

problem. The time-discrete version of the boundary condition are formulated as a Robin-type condition in a manner reminiscent of the 1D problem [3]. A compatible boundary-lifting procedure to homogenize the Robin-type boundary conditions is also presented. In order to demonstrate the effectiveness of the methods developed, we carried out numerical tests to study the behaviour of evolution of error as well as to verify the order of convergence empirically. If the number of spatial grid points in every dimension is $\mathcal{O}(N)$, then the computational complexity of our novel Padé method for the DtN map scales as $\mathcal{O}(MN)$ where M is the order of the diagonal Padé approximant. Let us emphasize that this complexity is independent of the number of time-steps. The overall complexity thus becomes dominated by the cost of the linear solver for interior problem which is given by $\Theta_2(N_{\text{dim}}) = \mathcal{O}(N^3)$. A theoretical proof of the stability and convergence of the numerical scheme is beyond the scope of the paper. These issues are deferred to a future publication.

The ideas presented in this paper can be readily extended to three-dimensions. Feshchenko and Popov have already shown that the ideas in 2D [4] can be extended to 3D [29]. The formulation of the operator $\sqrt{\partial_t - i\Delta_\Gamma}$ on the boundary of a cuboidal computational domain can be obtained along the same lines as that presented in [5]. For all the cases discussed above, it remains to determine how competitive are PMLs. Such a comparison should however be made for a more general type of Schrödinger equation which is identical to the free Schrödinger on the exterior domain $\Omega_e = \mathbb{R}^d \setminus \Omega_i$, $d = 2, 3$.

Acknowledgements

The first author thanks CSIR India (grant no. 09/086(1431)/2019-EMR-I) for providing the financial assistance.

References

- [1] Y. S. Kivshar, G. P. Agrwal, *Optical Solitons: From Fibers to Photonic Crystals*, 1st Edition, Academic Press, San Diego, California, 2003.
- [2] D. Lee, S. T. McDaniel, *Ocean Acoustic Propagation by Finite Difference Methods*, Modern Applied Mathematics and Computer Science, Pergmon Press, New York, 1988.
- [3] X. Antoine, A. Arnold, C. Besse, M. Ehrhardt, A. Schädle, [A review of transparent and artificial boundary conditions techniques for linear and nonlinear Schrödinger equations](#), *Comm. Comput. Phys.* 4 (4) (2008) 729–796. URL <https://hal.archives-ouvertes.fr/hal-00347884>
- [4] R. M. Feshchenko, A. V. Popov, Exact transparent boundary condition for the parabolic equation in a rectangular computational domain, *J. Opt. Soc. Am. A* 28 (3) (2011) 373–380. doi:10.1364/JOSAA.28.000373.
- [5] V. Vaibhav, On the nonreflecting boundary operators for the general two dimensional Schrödinger equation, *J. Math. Phys.* 60 (1) (2019) 011509. doi:10.1063/1.5030875.
- [6] L. D. Menza, Absorbing boundary conditions on a hypersurface for the Schrödinger equation in a half-space, *Appl. Math. Lett.* 9 (4) (1996) 55–59. doi:10.1016/0893-9659(96)00051-1.
- [7] L. D. Menza, Transparent and absorbing boundary conditions for the Schrödinger equation in a bounded domain, *Numer. Funct. Anal. Optim.* 18 (7) (1997) 759–775. doi:10.1080/01630569708816790.
- [8] A. Schädle, Non-reflecting boundary conditions for the two-dimensional Schrödinger equation, *Wave Motion* 35 (2) (2002) 181–188. doi:10.1016/S0165-2125(01)00098-1.
- [9] H. Han, Z. Huang, [Exact artificial boundary conditions for Schrödinger equation in \$\mathbb{R}^2\$](#) , *Comm. Math. Sci.* 2 (1) (2004) 79–94. URL <https://projecteuclid.org/euclid.cms/1250880210>
- [10] S. Ji, Y. Yang, G. Pang, X. Antoine, Accurate artificial boundary conditions for the semi-discretized linear Schrödinger and heat equations on rectangular domains, *Comput. Phys. Commun.* 222 (2018) 84–93. doi:10.1016/j.cpc.2017.09.019.
- [11] X. Antoine, C. Besse, Construction, structure and asymptotic approximations of a microdifferential transparent boundary condition for the linear Schrödinger equation, *J. Math. Pures Appl.* 80 (7) (2001) 701–738. doi:10.1016/S0021-7824(01)01213-2.
- [12] J. Szeftel, Design of absorbing boundary conditions for Schrödinger equations in \mathbb{R}^d , *SIAM Journal on Numerical Analysis* 42 (4) (2005) 1527–1551.
- [13] X. Antoine, C. Besse, P. Klein, Absorbing boundary conditions for the two-dimensional Schrödinger equation with an exterior potential. Part I: Construction and a priori estimates, *Math. Models Methods Appl. Sci.* 22 (10) (2012) 1250026. doi:10.1142/S0218202512500261.
- [14] X. Antoine, C. Besse, P. Klein, Absorbing boundary conditions for the two-dimensional Schrödinger equation with an exterior potential. Part II: Discretization and numerical results, *Numer. Math.* 125 (2) (2013) 191–223. doi:10.1007/S00211-013-0542-8.
- [15] V. Vaibhav, Microlocal approach towards construction of nonreflecting boundary conditions, *J. Comput. Phys.* 272 (2014) 588–607. doi:10.1016/j.jcp.2014.04.050.
- [16] J. Shen, Efficient spectral-Galerkin method I. Direct solvers of second- and fourth-order equations using Legendre polynomials, *SIAM J. Sci. Comput.* 15 (6) (1994) 1489–1505. doi:10.1137/0915089.
- [17] C. Lubich, Discretized fractional calculus, *SIAM J. Math. Anal.* 17 (3) (1986) 704–719. doi:10.1137/0517050.
- [18] V. Baskakov, A. Popov, Implementation of transparent boundaries for numerical solution of the Schrödinger equation, *Wave Motion* 14 (2) (1991) 123–128. doi:10.1016/0165-2125(91)90053-Q.
- [19] B. Mayfield, Nonlocal boundary conditions for the Schrödinger equation, Ph.D. thesis, University of Rhodes Island, Providence, RI (1989).

- [20] C. Zheng, A perfectly matched layer approach to the nonlinear Schrödinger wave equations, *J. Comput. Phys.* 227 (1) (2007) 537–556. [doi:10.1016/j.jcp.2007.08.004](https://doi.org/10.1016/j.jcp.2007.08.004).
- [21] X. Antoine, C. Geuzaine, Q. Tang, Perfectly matched layer for computing the dynamics of nonlinear Schrödinger equations by pseudospectral methods. Application to rotating Bose-Einstein condensates, *Communications in Nonlinear Science and Numerical Simulation* 90 (2020) 105406. [doi:10.1016/j.cnsns.2020.105406](https://doi.org/10.1016/j.cnsns.2020.105406).
- [22] K. Miller, B. Ross, *An Introduction to the Fractional Calculus and Fractional Differential Equations*, 1st Edition, John Wiley and Sons Inc., 1993.
- [23] J. Mennemann, A. Jüngel, H. Kosina, Transient Schrödinger–Poisson simulations of a high-frequency resonant tunneling diode oscillator, *Journal of Computational Physics* 239 (2013) 187–205. [doi:10.1016/j.jcp.2012.12.009](https://doi.org/10.1016/j.jcp.2012.12.009).
- [24] V. Vaibhav, Artificial boundary conditions for certain evolution PDEs with cubic nonlinearity for noncompactly supported initial data, *J. Comput. Phys.* 230 (8) (2011) 3205–3229. [doi:10.1016/j.jcp.2011.01.024](https://doi.org/10.1016/j.jcp.2011.01.024).
- [25] E. Lindmann, Free-space boundary conditions for time dependant wave equation, *J. Compt. Phys.* 18 (1) (1975) 16–78. [doi:10.1016/0021-9991\(75\)90102-3](https://doi.org/10.1016/0021-9991(75)90102-3).
- [26] S. Yadav, V. Vaibhav, Nonreflecting boundary condition for the free Schrödinger equation in 2d, in: *2023 Photonics and Electromagnetics Research Symposium (PIERS)*, 2023, pp. 328–337. [doi:10.1109/PIERS59004.2023.10221299](https://doi.org/10.1109/PIERS59004.2023.10221299).
- [27] N. J. Higham, *Accuracy and Stability of Numerical Algorithms*, 2nd Edition, Society for Industrial and Applied Mathematics, Philadelphia, 2002. [doi:10.1137/1.9780898718027](https://doi.org/10.1137/1.9780898718027).
- [28] J. Shen, T. Tang, L. L. Wang, *Spectral Methods: Algorithms, Analysis and Applications*, 1st Edition, Springer Berlin Heidelberg, 2011.
- [29] R. M. Feshchenko, A. V. Popov, Exact transparent boundary condition for the three-dimensional Schrödinger equation in a rectangular cuboid computational domain, *Phys. Rev. E* 88 (2013) 053308. [doi:10.1103/PhysRevE.88.053308](https://doi.org/10.1103/PhysRevE.88.053308).

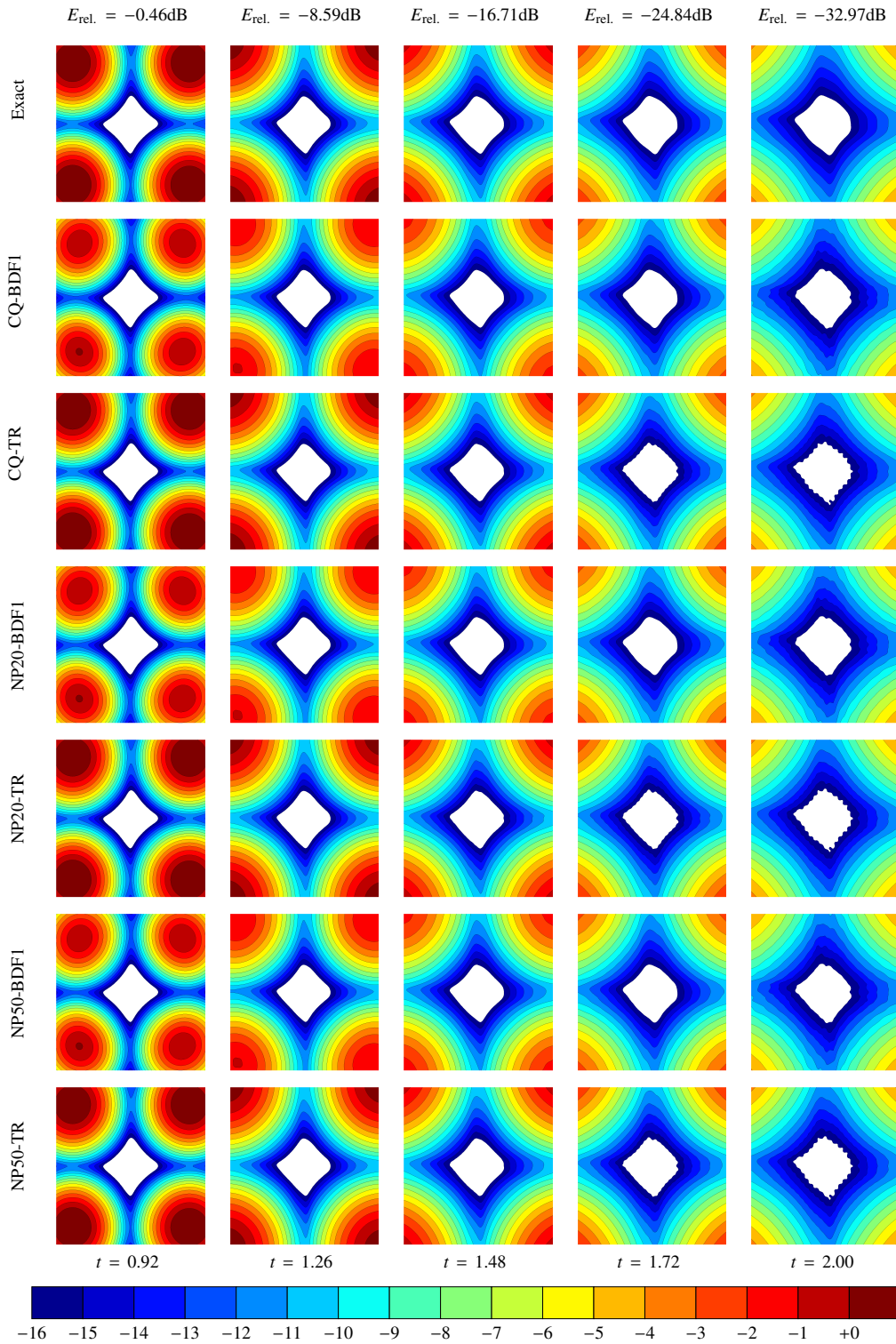


Figure 15: The figure shows contour plots of $4 \log_{10} |u(x, t)|$ with various TBCs for the IIB-type chirped-Gaussian profile (see Table 1) for $c = 12$ at different instants of time. The numerical parameters and the labels are described in Sec. 4.3.

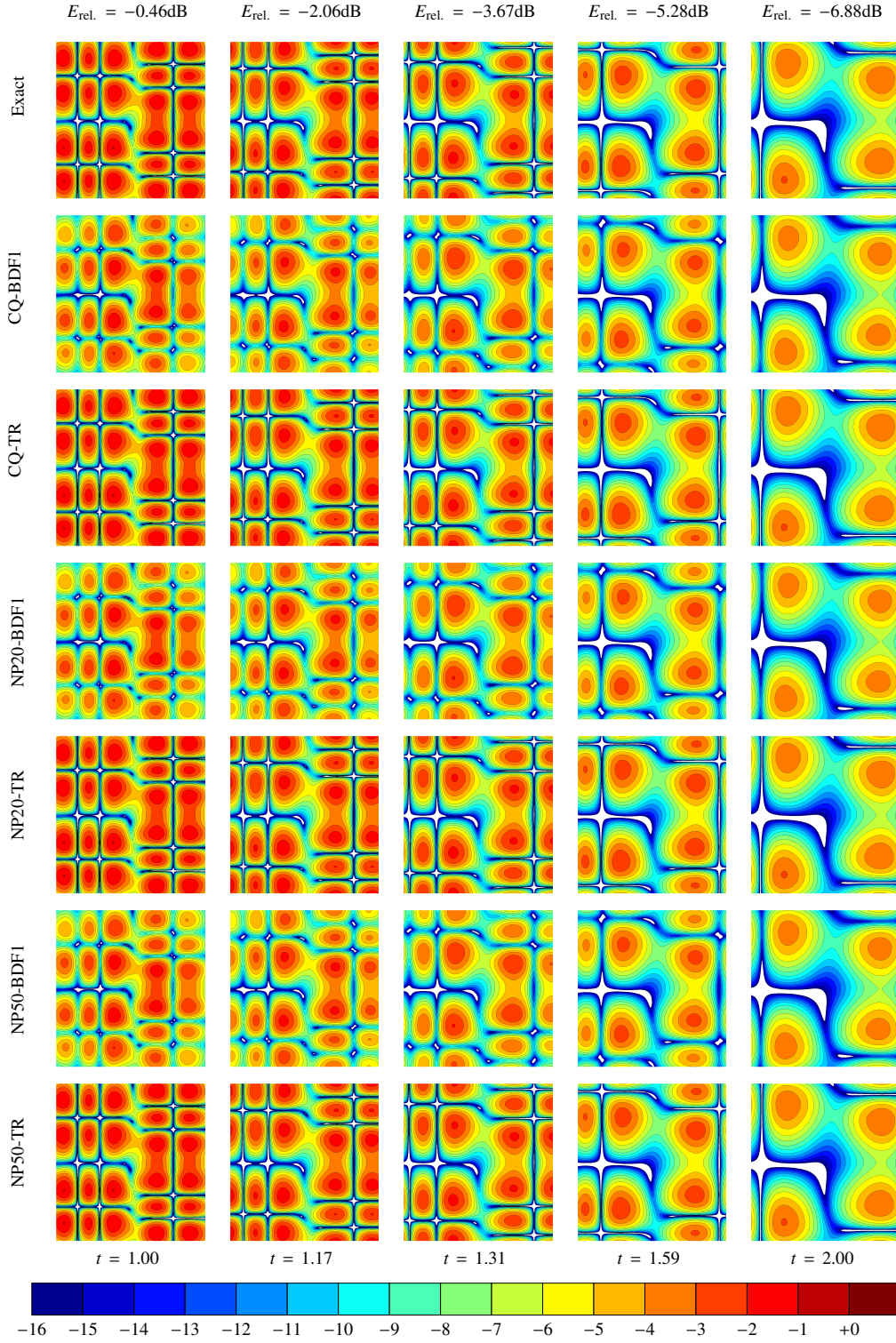


Figure 16: The figure shows contour plots of $8 \log_{10} |u(x, t)|$ with various TBCs for the IIB-type Hermite-Gaussian profile (see Table 2) for $c = 8$ at different instants of time. The numerical parameters and the labels are described in Sec. 4.3.

Appendix A. Fractional Operators

Definition 1 (Riemann-Liouville fractional integrals). Let $\alpha > 0$ and $f(t)$ be a piecewise continuous function on $(0, \infty)$, locally integrable on any finite subinterval of $[0, \infty)$. For $t > 0$, the Riemann-Liouville fractional integral of order α , denoted by $\partial_t^{-\alpha}$, is defined by

$$\partial_t^{-\alpha} f(t) = \frac{1}{\Gamma(\alpha)} \int_0^t (t-s)^{\alpha-1} f(s) ds. \quad (\text{A.1})$$

where Γ denotes the Euler's Gamma function.

Theorem 1 (Law of exponents). Let $f(t) \in C^\infty([0, \infty))$ and let $\mu, \nu > 0$, then the composition of two fractional integrals is given by

$$\partial_t^{-\nu}[\partial_t^{-\mu} f(t)] = \partial_t^{-(\mu+\nu)} f(t) = \partial_t^{-\mu}[\partial_t^{-\nu} f(t)], \quad \forall t \geq 0.$$

Definition 2 (Riemann-Liouville fractional derivatives). Let $f(t) \in C^\infty([0, \infty))$ and let $\mu > 0$. If p is the smallest integer greater than μ , then the fractional derivative of f of order μ is defined by

$$\partial_t^\mu f(t) = \partial_t^p[\partial_t^{-\nu} f(t)], \quad t > 0, \quad (\text{A.2})$$

where $\nu = p - \mu > 0$. For this fractional derivative to be defined at $t = 0$, the function $f(t)$ must have first $p - 1$ derivatives equal to zero at $t = 0$.

Appendix B. Boundary Adapted Basis Representation: Useful Results and Identities

In order to leverage the discrete Legendre transforms over Legendre-Gauss-Lobatto nodes, we choose to favour storage of space dependent variables in terms of their Legendre coefficients. As a result of this choice, all operations involving the boundary adapted basis must be implemented via the Legendre transform.

Let us recall the definitions: $L_n(y)$ denote the Legendre polynomial of degree n and the index set $\{0, 1, \dots, N-2\}$ is denoted by \mathbb{J} . The boundary adapted basis polynomials are given by

$$\phi_p(y) = L_p(y) + b_p L_{p+2}(y), \quad b_p = -\frac{\kappa + \frac{1}{2}p(p+1)}{\kappa + \frac{1}{2}(p+2)(p+3)}, \quad p \in \mathbb{J}, \quad (\text{B.1})$$

where $\kappa \in \mathbb{C}$. Let us briefly discuss the parameters that determine this quantity: We recall from Sec. 3.2.1 that $\beta = J^{-2}$ where $J = \partial_y x$ is the Jacobian corresponding to the transformation from the reference interval $\mathbb{I} = [-1, 1]$ to the actual domain $[x_-, x_+]$. We suppress the subscript which characterizes the axis along which the domain lies for the sake of brevity. The time-stepping schemes discussed in Sec. 3 dictate that either $\rho = 1/\Delta t$ (for BDF1) or $\rho = 2/\Delta t$ (for TR). The form of κ follows from the Robin-type formulation of the discretized version of the DtN-maps as discussed in Sec. 3.1. For CQ methods $\kappa = \alpha = \sqrt{\rho/\beta} \exp(-i\pi/4)$ while for the NP methods, we have $\kappa = \alpha\varpi$ where ϖ is defined in (82).

Any arbitrary function in $L^2(\mathbb{I})$ can be expanded in this basis as follows:

$$f(y) = \sum_{p=0}^{N-2} \hat{f}_p \phi_p(y) + \eta_0 L_0(y) + \eta_1 L_1(y) = \sum_{p'=0}^N \tilde{f}_{p'} L_{p'}(y). \quad (\text{B.2})$$

By virtue of linear independence of Legendre polynomials, we can equate their coefficients on both sides of the equality so that

$$\begin{cases} \tilde{f}_0 = \hat{f}_0 + \eta_0, \tilde{f}_1 = \hat{f}_1 + \eta_1, \\ \tilde{f}_p = \hat{f}_p + b_{p-2} \hat{f}_{p-2}, \quad p = 2, 3, \dots, N-2, \\ \tilde{f}_{N-1} = b_{N-3} \hat{f}_{N-3}, \tilde{f}_N = b_{N-2} \hat{f}_{N-2}. \end{cases} \quad (\text{B.3})$$

The linear system can be written as

$$\tilde{\mathbf{f}} = B\hat{\mathbf{f}} + \eta_0 \mathbf{e}_0 + \eta_1 \mathbf{e}_1 \quad (\text{B.4})$$

where

$$B_j = \begin{pmatrix} 1 & & & & & & & & & & \\ & 0 & 1 & & & & & & & & \\ & b_0^{(j)} & 0 & 1 & & & & & & & \\ & & b_1^{(j)} & 0 & 1 & & & & & & \\ & & & \ddots & \ddots & \ddots & & & & & \\ & & & & & & b_{N-4}^{(j)} & 0 & 1 & & \\ & & & & & & & b_{N-3}^{(j)} & 0 & & \\ & & & & & & & & & b_{N-2}^{(j)} & \end{pmatrix} \in \mathbb{C}^{(N+1) \times (N-1)}, \quad (\text{B.11})$$

The inner products of the form $g_{p_1, p_2} = (f, \phi_{p_1}^{(1)} \phi_{p_2}^{(2)})_{\Omega_{\text{ref}}}$ can be understood as

$$g_{p_1, p_2} = (f, \phi_{p_1}^{(1)} \phi_{p_2}^{(2)})_{\Omega_{\text{ref}}} = \gamma_{p_1} \gamma_{p_2} \tilde{f}_{p_1, p_2} + b_{p_1}^{(1)} \gamma_{p_1+2} \gamma_{p_2} \tilde{f}_{p_1+2, p_2} + b_{p_2}^{(2)} \gamma_{p_1} \gamma_{p_2+2} \tilde{f}_{p_1, p_2+2} + b_{p_1}^{(1)} b_{p_2}^{(2)} \gamma_{p_1+2} \gamma_{p_2+2} \tilde{f}_{p_1+2, p_2+2}. \quad (\text{B.12})$$

The relationship above can be compactly stated as $G = (g_{p_1, p_2}) = Q_1 \Gamma \tilde{F} \Gamma Q_2^T$ where $Q_j = B_j^T$ are referred to as the *quadrature matrices*.